This document was prepared for the ETI by third parties under contract to the ETI. The ETI is making these documents and data available to the public to inform the debate on low carbon energy innovation and deployment.

Programme Area: Marine

Project: PerAWAT

Title: Code Development in TELEMAC2D and TELEMAC3D in order to allow for the implementation of Parametric Characterization of Arrays

Abstract:

This study aims to build methodologies to simulate the wake of several turbines in a large basin using the Telemac2D and Telemac3D softwares.

Context:

The Performance Assessment of Wave and Tidal Array Systems (PerAWaT) project, launched in October 2009 with £8m of ETI investment. The project delivered validated, commercial software tools capable of significantly reducing the levels of uncertainty associated with predicting the energy yield of major wave and tidal stream energy arrays. It also produced information that will help reduce commercial risk of future large scale wave and tidal array developments.

Code development in TELEMAC2D and TELEMAC3D in order to allow for the implementation of parametric characterization of arrays.

Project	PerAWAT
Work package	WG3
Deliverable	WG3 WP3 D2 Code development
Responsible author	Marc Andreewsky (EDF)
Other authors	Pauline Bozonnet, Columbus Leonard (EDF)
Second reading	Vanessa Martin, Clarisse Fil, Antoine Joly, Clément Buvat (Jean-Michel Hervouet, Marta Nogaj) (EDF)
Circulation	Among all authors and readers
To be approved by	Robert Rawlinson-Smith (GH)
Date	
Issue	V1.0

Document revision history

Issue	Date	Summary
V0.1	31/10/2012	First draft
V0.2	21/03/2013	Second draft following comments by GH
V1.0	02/05/2013	All modifications in the second draft were accepted by GH

EXECUTIVE SUMMARY

This study aims to build methodologies to simulate the wake of several turbines in a large basin using the Telemac2D and Telemac3D softwares.

In order to have confidence in the simulations of tidal turbines in a large basin with Telemac2D, these steps were followed:
- First, we verify that the FORTRAN subroutine (DRAGFO) used to simulate a tidal turbine in Telemac2D produces the same results when launched with one processor as it does with several processors.
- Next, a simple flow than the wake downstream a tidal turbine is analyzed: this simple case is the wake of a flow around a cylinder, which is simulated for two models of turbulence in Telemac2D (k-epsilon model and constant viscosity model). The validated results from this analysis (mesh size, turbulence model ...) were used to get some guidance in our study which concerns the flow around the tidal turbines and not around cylinders.
- Third, the wake of a tidal turbine in a flume is simulated and validated in Telemac2D using laboratory measurements made by the LNHE department of EDF. The methodology for simulating one tidal turbine is defined, in particular a drag force is applied on a rectangular box in order to simulate the drag force due to the turbine.
- Once it was established that a single tidal turbine in a flume could be modeled, two varying alignments of tidal turbine arrays were simulated in Telemac2D using the same two models of turbulence. At this stage, two methodologies are defined: the first one for the method where a rectangular box is used for each turbine, and the second methodology for the global box containing all turbines method. In this second case, the methodology also explains how to calculate an equivalent drag coefficient to simulate a set of turbines in a large scale basin. In both methodologies, the way of choosing the mesh size (near and far from the rectangular box(es) and in the transition area ranging from a fine mesh to a larger mesh), the turbulence model, the drag coefficient, and the limitations are given.
With these methodologies, we have the ability to accurately simulate several turbines on a large basin with Telemac2D.

The same approach can be done in three dimensions and the following steps were followed with Telemac3d to develop the methodology:
-First, it is verified that the subroutine (SOURCE) used to simulate a tidal turbine in Telemac3D produces the same results when launched with one processor as it does with several processors.
-Second, a tidal turbine in a flume is simulated with Telemac3D. The simulations are compared to the EDF LNHE measurements to adjust the parameters in order to obtain realistic simulations.
-Then, numerical analysis shows that the Telemac2D approach is transferable to Telemac3D. This lays the groundwork for defining the methodology to be used to simulate multiple turbines in a large maritime area with Telemac3D (particularly, the methodology for calculating a drag coefficient equivalent to a set of turbines for large-scale basin applications). This methodology defines also the choice of the mesh size (near and far from the horizontal cylinder(s)), the turbulence model, the drag coefficient, and the limitations.

Finally, methodologies which enable the simulation of a tidal array in a coastal basin scale model have been set up for both 2D and 3D. It is built on the step-by-step process which had been used for the validation task, which increases confidence in the ability of the developed routines to assess large scale effects of tidal energy extraction at basin scale. It consists in running simulations at a local scale with individual devices, in extracting the equivalent array drag coefficient from these, and in inserting that piece of information in the large basin scale model.

Telemac2D and Telemac3D are now capable of assessing the impact of any array layouts on large scale hydrodynamics effects, as the software user has the opportunity of combining the use of the DRAGFO and SOURCE routines with an appropriate methodology.

TABLE OF CONTENT

1 INTRODUCTION

1.1 Scope of this document

This study aims to simulate the wake of several turbines in a large basin using the Telemac2D and Telemac3D softwares. Methodologies are proposed to assist, for example, the choice of the mesh size, both near and far from the turbines, adjust various parameters (associated with the representation of turbines), and guide the choice of turbulence model in order to simulate in a most accurate way the wake of the tidal turbines in a large basin. Limitations or sensitivity issues are also discussed in this study.

1.2 Approach followed

In order to have confidence in the simulations of tidal turbines in a large basin with Telemac2D, these four steps were followed:

-First, we verify that the FORTRAN subroutine (DRAGFO) used to simulate a tidal turbine in Telemac2D produces the same results when launched with one processor as it does with several processors. In particular, an identical energy loss is verified across the two methods. This confirms that our methods are sound, computationally speaking.

-Next, a simple flow than the wake downstream a tidal turbine is analyzed: this simple case is the wake of a flow around a cylinder, which is simulated for two models of turbulence in Telemac2D (k-epsilon model and constant viscosity model). Two kinds of meshes are also investigated, structured and unstructured. Mesh convergence and time step convergence are analyzed for each turbulence model. Note that, with Telemac2D (or Telemac3D) the mesh convergence and time step convergence analysis should always be done for any kind of study. The validated results from this analysis (mesh size, turbulence model ...) were used to get some guidance in our study which concerns the flow around the tidal turbines and not around cylinders.

-Third, the wake of a tidal turbine in a flume is simulated and validated in Telemac2D using laboratory measurements made by the LNHE department of EDF. Note that, at this step, the tidal turbine is not represented by a vertical cylinder but with a rectangular box containing nodes where a drag force is applied. The rectangular box used to model tidal turbine and the drag force are defined inside the subroutine DRAGFO. To use the DRAGFO subroutine to model a tidal turbine, the user has to define the dimensions of the rectangular box and the value of the drag coefficient. Two models of turbulence are also used for this analysis, and the mesh convergence is analyzed. The methodology for simulating one tidal turbine is defined, including instructions on the choice of the mesh size near the turbine.

-Once it was established that a single tidal turbine in a flume could be modeled, two varying alignments of tidal turbine arrays were simulated in Telemac2D using the same two models of turbulence. There are two methods for modeling the tidal turbines tested in this section. One method where each tidal turbine is associated with one rectangular box containing nodes where a drag force is applied (this case is similar to the case of the part 3), and another where a global box representing all the turbines is defined. In this second case, an equivalent drag coefficient is used for all turbines and a drag force is applied on the nodes inside this global box using this equivalent drag coefficient.

The mesh convergence is again checked at this point in the study. The simulations and experimental results (two experiments carried out in the laboratory at the University of Manchester) are compared to adjust parameters and to obtain a suitable numerical model. At this stage, two methodologies are defined: the first one for the method where a rectangular box is used for each turbine, and the second methodology for the global box containing all turbines method. In this second case, the methodology also explains how to calculate an equivalent drag coefficient to simulate a set of turbines in a large scale basin. In both methodologies, the way of choosing the mesh size (near and far from the

rectangular box(es) and in the transition area ranging from a fine mesh to a larger mesh), the turbulence model, the drag coefficient, and the limitations are given.

With these methodologies, we have the ability to accurately simulate several turbines on a large basin with Telemac2D.

The meticulous approach in 2D is conducted beyond what is required and includes work on one cylinder, one turbine (represented by a rectangular box and defined in DRAGFO), several turbines in two varying alignments (represented by one or more rectangular boxes and defined in DRAGFO), comparisons with several external experiments, and checks on the mesh convergence. This approach was necessary to give confidence in the 2D simulation and to provide the ability to transpose the 2D methodology for the 3D study whose approach is explained below.

The same approach can be done in three dimensions and simulations with Telemac3D proceeded as follows:

-First, it is verified that the subroutine (SOURCE) used to simulate a tidal turbine in Telemac3D produces the same results when launched with one processor as it does with several processors. In particular, an identical energy loss is verified across the two methods. This verification is identical to the one performed in 2D with DRAGFO.

-Second, a tidal turbine in a flume is simulated with Telemac3D. The simulations are compared to the EDF LNHE measurements to adjust the parameters in order to obtain realistic simulations. Two models of turbulence are used, and mesh convergence is analyzed, just like in the 2D cases. Note that, at this step, the tidal turbine is represented by a horizontal cylinder containing nodes where the drag force is applied. The axis of the cylinder is oriented in the same direction as the turbine axis; the diameters are also the same. The volume of the cylinder is roughly equal to the volume bounded by the rotating turbine. The horizontal cylinder and the drag force are defined in the subroutine SOURCE.

-Numerical analysis shows that the Telemac2D approach is transferable to Telemac3D. This lays the groundwork for defining the methodology to be used to simulate multiple turbines in a large maritime area with Telemac3D (particularly, the methodology for calculating a drag coefficient equivalent to a set of turbines for large-scale basin applications).
This methodology defines also the choice of the mesh size (near and far from the horizontal cylinder(s)), the turbulence model, the drag coefficient, and the limitations.

1.3   Specific tasks associated with WG3 WP3

- D1 - 2D shallow water equation model(s) of candidate site(s).
- D2 - Code development in 2D shallow water model Telemac 2D of the Telemac software suite, in order to allow for the implementation of parametric characterization of arrays.
- D3 - Incorporating parametric characterization of an axial flow turbine array (obtained in WG3 WP2) into the 2D basin scale numerical models.
- D4 - Assessment of the effects of energy extraction at various UK sites with the 2D model: Macroscopic, but still reliable, study of the large scale impact of a tidal farm on the hydrodynamic of the area, and accurate assessment of the site tidal resource.
- D5 - Cross-comparison of 2D and 3D results, in terms of energy extraction, for the selected site.

1.4   WG3 WP3 D2 Content

Code development in 2D and 3D shallow water model *Telemac 2D* and *Telemac 3D* of the Telemac software suite, in order to allow for the implementation of parametric characterization of arrays. The deliverable shall be a routine which can account for the hydrodynamic effects of a tidal farm at the basin scale, and can be implemented in *Telemac 2D* and *Telemac 3D*. If possible, that routine shall also focus on farm layout optimisation. The routine should be suitable for assessing any parameterized FDC in 2D and 3D, even if within this work package it will only be implemented with one FDC.

1.5   WG3 WP3 D2 Deliverables

a) Module software code – Telemac 2D and 3D
b) Methodology Report: method used to develop an adequate routine.

1.6   WG3 WP3 D2 Acceptance criteria

a) Module provided in Telemac software – 2D and 3D versions for horizontal axis turbine/device specified in WG0 D2.
•   The software code/routine is capable of enabling the assessment of large scale hydrodynamic effects of tidal energy extraction at basin scale.
•   Software code capable of assessing impact of farm/array layout on large scale hydrodynamic effects, in order to assess and optimise array layouts.

b) Report shall contain the following:
•   Description of the method used to develop the additional routines in sufficient detail to be logically followed by third party.

2   PRESENTATION OF TELEMAC2D AND TELEMAC3D

The TELEMAC-2D and TELEMAC-3D softwares have been developed by the LNHE department (National Hydraulics and Environment Laboratory) of EDF R&D. They allow the modelling and simulation of free surface flows and are based on finite element methods. TELEMAC-2D solves the Saint-Venant equations (or shallow water equations) in a two-dimensional (plane) computational domain. Its principle variables are the water depth and the vertically averaged velocity components, at every point within the domain. The hypotheses used by TELEMAC-2D are: hydrostatic pressure (the vertical acceleration caused by the pressure balances gravity), negligible vertical velocities (this is linked to the hypothesis of hydrostaticity that requires vertical acceleration to be insignificant) and impermeability of the surface and of the bottom (no transfer of water either through the bottom or from the surface, a particle of water located on one of these two interfaces will remain there). TELEMAC-3D software solves the Navier-Stokes equations for free surface flows in three dimensions. It can solve the Navier-Stokes equations with or without the hydrostatic hypothesis. TELEMAC-2D and TELEMAC-3D can take into account the following phenomena:
•   bed friction,
•   impact of the Coriolis effect,
•   effects of meteorological phenomena: atmospheric pressure and wind,
•   turbulence,
•   subcritical and supercritical flows,
•   tidal flats (sections of the shore exposed during ebb tide that are treated as dry areas in the computational field), an option that has been utilised in this study.

These programmes have complete user documentation. TELEMAC-2D has been available in Open Source since 2010 (from version 6.0) whereas TELEMAC-3D became available in Open Source in 2011 (from version 6.1).
The TELEMAC-2D and 3D software uses a number of input and output files, some of which are optional. The input files are the following:

- The geometry file (obligatory). This is a binary file in Selafin format, and can thus be read by FUDAA-PREPRO software and created either directly by MATISSE, JANET or BLUEKENUE or else by the STBTEL module from the file(s) produced by the mesh generator. The structure of the Selafin format is described in [G3],
- The steering file (obligatory). This is a text file created by a text editor or by the FUDAA-PREPRO software. In a way, it represents the control panel of the computation. It contains a number of keywords to which values are assigned,
- The boundary conditions file (obligatory). This is a formatted file generated automatically by MATISSE, JANET, BLUEKENUE or STBTEL. It can be modified with a standard text editor. It describes the contour of the domain trigonometrically, starting from the bottom left-hand corner (X + Y minimum) and then the islands in a clockwise direction,
- The bottom topography file (optional),
- The FORTRAN file (optional, but very often used),
- The open boundary file (optional),
- The previous computation file (optional),
- The binary data file (optional, but sometimes used here),
- The formatted data file (optional, but used here),
- The reference file (optional).

The output files are the results file, the listing printout, the formatted data file (optional) and the binary data file (optional).

3   TELEMAC2D SIMULATIONS

In this section, simulations are launched in Telemac-2D; a numerical code for free-surface hydraulics developed by EDF and based on the Saint-Venant equations [4]. A brief description of the code of Telemac2D is available in appendix 8.1.

The TECs (Tidal Energy Converters) will not be represented in the mesh; they will be modelled through the application of a drag force on the fluid (in a FORTRAN subroutine DRAGFO). This modelling approach is already applied in Telemac-2D to simulate bridge piers; it will be necessary to adapt it to the case of tidal energy converters (TECs).

3.1   Inputs

Comparisons are done in the following chapter between simulation results and several output experimental data of different work packages:

- WG4WP1: experiment done at EDF in a flume.
- WG3 WP2: work of Edinburgh with code Saturne.
- WG4WP2: experiment from University of Manchester (UoM).

These experiment and simulations will be described in greater detail later.

3.2   Verification

The FORTRAN subroutine, where the drag force which can simulate the turbine effect is coded, is called: DRAGFO. To verify this subroutine the following definition will be used:

The process of determining that a model implementation accurately represents the developer's conceptual description of the model and the solution to the model.

In order to do this verification, it has been decided to simulate in one place of the flume a loss of power of 2.6 Watt of the fluid (this value is near the loss of energy of the tidal turbine in the EDF experiment).

Therefore a power deficit of 2.6 Watt was programmed in the FORTRAN subroutine "DRAGFO" on a specific area of the flume in order to verify that after the simulation, the deficit of power is really equal to 2.6 Watt on this specific area (this place is located at 20 m from the beginning of the flume).

The power P(x) of a slice of fluid in the flume at the x coordinate <u>when the Saint-Venant equations are used</u> is given by the following expression:

$$P(x) = \sum \tfrac{1}{2} \cdot \rho \cdot (U(x,y).H(x,y).dy) \cdot U(x,y)^2 + \rho.(U(x,y).H(x,y).dy) \cdot g.H(x,y).$$

- ρ is the water density.
- U(x,y) is the velocity within Ox for the abscise x and the ordinate y.
- H(x,y) is the water depth within Ox for the abscise x and the ordinate y.
- g is the acceleration due to gravity.

The velocity within y is supposed equal to 0. The sum is made within Oy. The step dy is chosen equal to 2cm.

The following figure shows the evolution of the power of in a portion of fluid along the flume (divided by the water density):
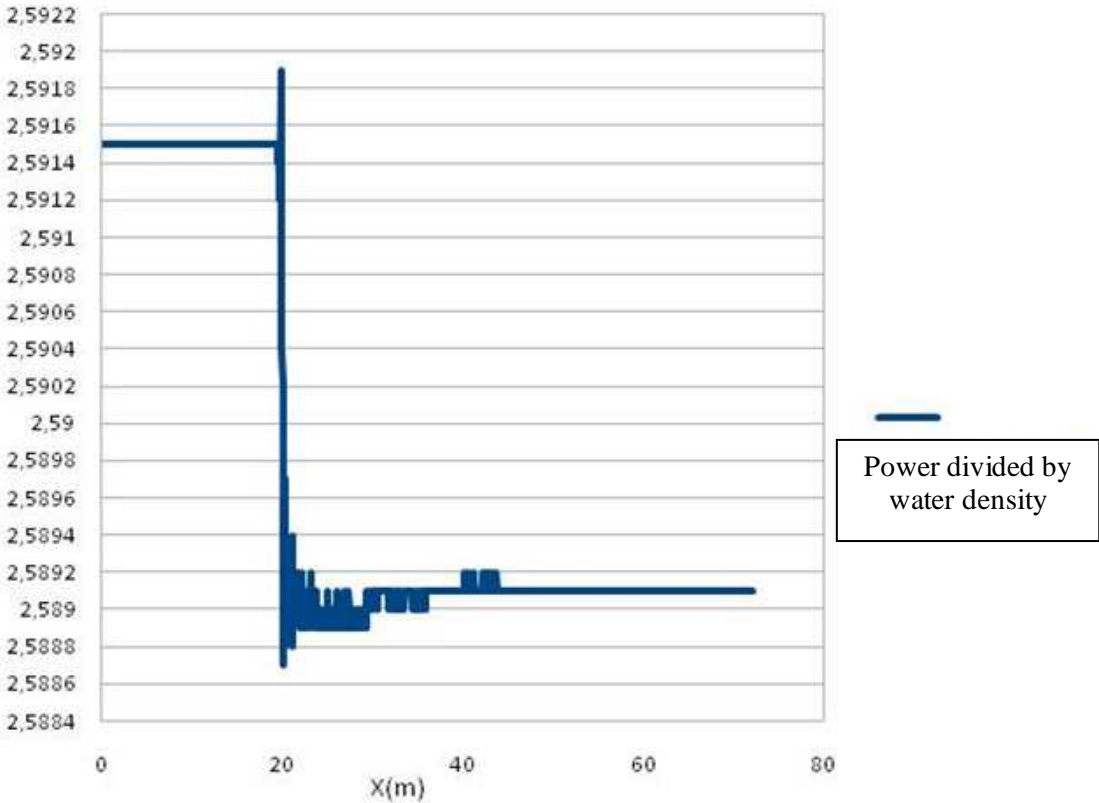
Figure 1: evolution of the power divide by the density of water (J.m³/kg/s) of a slice of fluid along the flume.

This simulation has been done with one processor and in parallel. In both cases, the results were the same: the deficit of power is equal to 2.6 watt and it occurred at the correct location.. Simulations were also done for a power deficit of 1 Watt and the same kind of results was found.

The conclusion of this set of simulation is that the routine DRAGFO has been verified with both one processor and several processors operating in parallel.

3.3   Validation

The validation of a code can be described using the following definition:

The process of determining the degree to which a model is an accurate representation of the real world from the perspective of the intended uses of the model.

Methodology applied for the validation consists of the following steps (we repeat here briefly some points of section 1.2):

a) The initial stage consists of simulating a wake for a simple case: a cylinder in a flume, represented in the mesh as an island disc-shaped. This step is used to test different numerical options. The study on the cylinder just brings us some guidance for the rest of our study.

b) A simulation is then made of the same flow around a vertical cylinder; however the latter is no longer represented in the mesh. The island dimension is defined inside the DRAGFO subroutine. The cylinder is numerically modelled using a drag force which is applied on the nodes contained inside the island; this method is validated for the simple case.

c) This method is then adapted to the tidal energy converter case. This structure is represented by a rectangular box in the DRAGFO subroutine; it is assumed to be valid given that the two problems, cylinder and TEC, are sufficiently similar (same orders of magnitude for the Reynolds numbers and for the dimensions of the obstacle in the two cases). Of course, some adaptation is made here, especially for the rectangle dimension and the drag coefficient. The wake of a tidal energy converter in a flume is then simulated.

d) The wake effect of several rows of TECs is then simulated based on the conclusions resulting from c).

These three cases (a single cylinder, a single tidal energy converter and a TEC array) will be calibrated and validated against experimental data, thereby increasing confidence in Telemac-2D and in the parameters given to reproduce the TEC wake and wake interactions. The limitations of the model will also be analyzed, and it will then be possible to accurately simulate the wake and the extracted energy for a farm of hundreds of TECs.

Simulations are performed for the simple cylinder case and for the case of a tidal energy converter in a flume. The study of the flow around the cylinder is presented in the first part. In the initial stage, the cylinder is meshed and a study was conducted on the code convergence as well as the different numerical options. In the second step, the flow is simulated using the model that is subsequently applied to the tidal energy converter. These simulations and use of the model for the TEC case are presented in the second part. The numerical results are compared with experimental data obtained from a series of tests performed at the LNHE technical facilities. The last part deals with a series of several tidal turbines.

3.3.1   Part A: The simple cylinder case

3.3.1.1 Introduction

This section describes steps a) and b) of the methodology, which consist of the numerical modelling in Telemac-2D of a free-surface flow in a flume around a vertical cylinder. In this case, the velocity field has already been described in scientific literature [16].

Initially (step a)) the cylinder is represented as an island in the mesh.
Successive studies are conducted on:

- Two velocity advection schemes: one of which is based on the method of characteristics (numbered 1 in Telemac-2D) and the other on a conservative PSI scheme, (numbered 5).

- Two turbulence models: a constant viscosity model and the k-ε model.

For each case, the mesh size is varied over the following values:

D, D/2, D/4, D/8 and D/16 where D is the diameter of the given cylinder.

The time-step is also varied. An appropriate value for the latter at the simulation starting point is given by the following formula:

$$\Delta t - \frac{\Delta x}{v}$$

Where Δx denotes the spatial mesh size, Δt the time-step and v the characteristic flow velocity (for example, the velocity at the entry point of the flow into the flume). This formula expresses the Courant-Friedrich-Levy (CFL) condition and provides the maximum usable time-step that satisfies stability constraints.

The aim is to determine whether the advection schemes and the turbulence models provide satisfactory results and in this case from which time-step and for which mesh refinement. The simulation results are validated against experimental data taken from the Yulistiyanto PhD thesis [16].

3.3.1.2 Experimental data

A bibliographical study was conducted in order to obtain experimental measurements of the mean velocity field in a water column for free-surface flow around a vertical cylinder. This type of measurements is presented in the PhD thesis of B. Yulistiyanto's [16] for two different flows having the following characteristics:

	cylinder		channel : uniform flow					$B = 2.0$ [m]			
Test	D	Re_D	Q	S_o	n	U	h	B/h	u_{*r}	Re_h	Fr
	[m]	10^5 [-]	[m³/s]	10^{-4}[-]	[m$^{-1/3}$s]	[m/s]	[m]	[-]	[m/s]	10^5 [-]	[-]
1	0.22	1.48	0.248	6.25	0.012	0.670	0.185	10.8	0.029	1.24	0.5
2	0.22	0.95	0.149	2.80	0.012	0.430	0.173	11.6	0.021	0.74	0.33

Table 1: Characteristics of the two flows studied in [16], where B is the channel width, D the diameter of the cylinder, Q is the discharge, S$_o$ the channel bed slope, n is the friction factor (Manning roughness coefficient), U the flow velocity, h the water height, u* the friction velocity.

The experiments were conducted in a flume 43 m long, 2 m wide and 1 m deep, the cylinder being placed 18 m from the entry. S$_o$ denotes the bed slope, which will be ignored in the simulations as it is so small. Only Test 1 of the above table will be considered for the purposes of this study, with Reynolds numbers of Re$_h$=1.24 10^5 based on the water height and Re$_D$=1.48 10^5 based on diameter of the cylinder.

The velocity was measured using an ADVP (**A**coustic **D**oppler **V**elocity **P**rofiler) in 5 planes around the cylinder and up to 55 cm from the latter, representing about two diameter lengths (see Figure 2). The 0° plane corresponds to the upstream flow, the 45, 90 and 157° planes to the sides of the cylinder and the 180° plane to the downstream flow. The mean velocity field (U, V) over the water column is provided for about 50 different locations
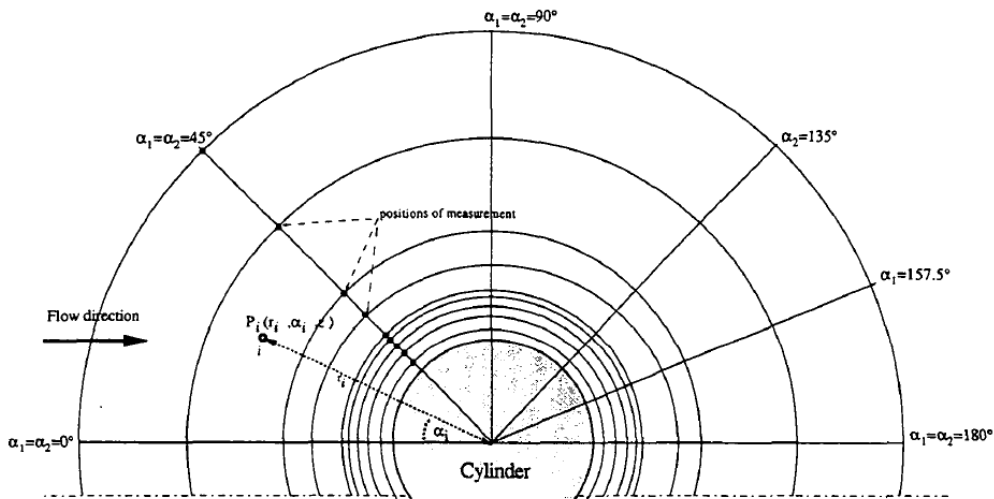
Figure 2: Locations of velocity measurements around the cylinder corresponding to line intersections

According to the description given in [16], the flow observed downstream of the cylinder is a steady symmetric flow without periodic separation. This may seem surprising as a vortex zone is usually present downstream of the cylinder [1] where the cylinder Reynolds number is above 40. There are two explanations for this lack of eddy shedding:

– For the cylinder, Re_L=1.48 10^5, which is near a particular range of Reynolds numbers where no Karman vortices are observed [1], as can be seen in Figure 3. The laminar boundary layer has become turbulent and the wake narrow and disorganised; this regime is called the critical regime.
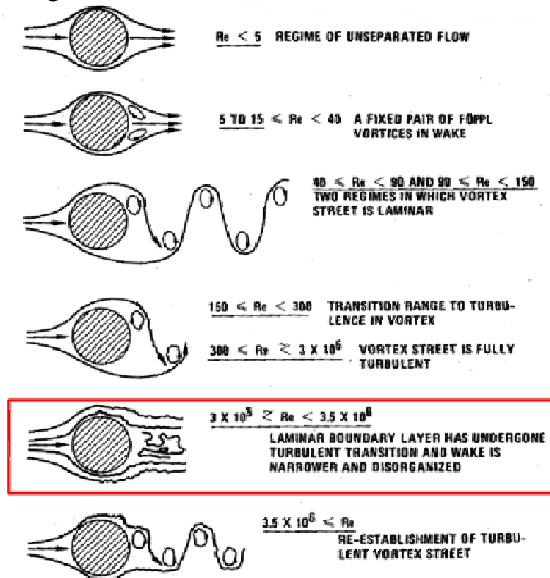
Figure 3: Different flow regimes around a cylinder as a function of Reynolds number [1]

– The preceding data is valid for unbounded domains; in this case the flow is in shallow water and limited by the side walls of the flume. Friction plays a prominent role and this could also explain the absence of vortex shedding [13].

The key point to retain from this is that the flow to simulate is steady, which facilitates the comparison between the experimental data and the simulations. This also means that the use of the k-ε model, which in Telemac-2D does not reproduce this type of oscillation, will not be problematic, as will be seen in more detail at paragraph 3.3.1.5. In addition, as it will be exposed later, the Reynolds number

used for the cylinder is close to the value of the Reynolds number from the EDF experiment, which will facilitate the study of the wake in a flume. At last, others flow regimes will be investigated.

3.3.1.3 Simulation settings and parameters

3.3.1.3.1 Initial and boundary conditions

The bottom friction is modelled using Manning's law (identical to Strickler's law, Manning's coefficient is the inverse of the Strickler coefficient), with a coefficient n of 0.012 given in the thesis [16]. Friction on the sidewalls is ignored.
The inlet flow is fixed at 0.248 m^3/s; the outlet water height at 0.185 m.
The entire length of the flume is considered as having initially a nil velocity and a water height equal to 0.185 m.

3.3.1.3.2 Meshes

The different meshes are generated with Janet[1] pre-processing software. They cover the full extent of the experimental flume with the cylinder represented by an island. The latter is discretized using segments that have the same length as the mesh size.
The different mesh sizes listed in Table 2 will be considered for two types of mesh: structured and unstructured.
A structured mesh is defined as having the most regular pattern of connections; it is composed for the most part of equilateral triangles. An unstructured mesh is the opposite: it is less regular, the triangle elements have different orientations and the size of the grid elements varies (cf. Figure 4). Better results are supposed to be obtained from numerical computations on a structured mesh; however, for the simulations at sea with irregular coastlines an unstructured mesh will need to be used as the latter is flexible in the case of complex geometries. For this reason, it is important to study both cases. If the mesh size is sufficiently decreased, the simulation results should tend towards the same values, regardless of the type of mesh used.

	Mesh size	D 20 cm	D/2 10 cm	D/4 5 cm	D/8 2.5 cm	D/16 1.25 cm
Structured mesh	Number of nodes	2,335	9,161	35,728	66,356	263,207
	Number of elements	4,266	17,514	69,842	130,508	522,008
Unstructured mesh	Number of nodes	Not tested	4,989	17,193	74,438	295,548
	Number of elements	Not tested	9,170	33,284	146,672	586,688

Table 2: Parameterization of the different meshes used

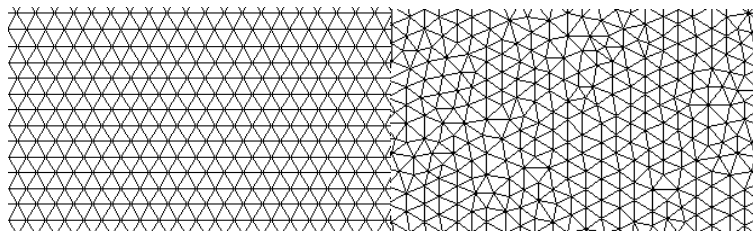**Figure 4: Illustrative example of a structured mesh (left) and an unstructured mesh (right)**

---

[1] Care must be taken to avoid overstressed triangle elements, i.e. whose three nodes are located on the frontier of the computational domain, as these may bring about instabilities in the computations made by TELEMAC-2D.

Two additional remarks can be made:

- Meshes containing right-angled triangles and thus a privileged direction are not considered, as this type of mesh will give a priori poorer results [12].

- Some numerical problems appear in the case of meshing with small mesh sizes: 1.25 cm or even 2.5 cm. It is therefore necessary to adjust several Telemac-2D parameters in order to arrive at steady state without divergence occurring. In particular, the tidal flats option is activated, a Thompson[2] boundary condition used and the SUPG option is set at 0; implicitation for the height and the velocity is set to 1.

3.3.1.3.3 Time-step and convergence in time

As evoked in the introduction, the first simulation is done with a time-step such that:

$$\Delta t = \frac{\Delta x}{v}$$

This is then decreased until there is almost no difference in the results; time-step convergence is thus achieved.

For each simulation, FUDAA-PRE-PRO software, which allows obtaining temporal variations in velocity over every point of the flume, is used to check that the steady-state has been reached. It is therefore possible to verify that a permanent regime is established by checking several points.

3.3.1.3.4 Turbulence models

In Telemac-2D, the Boussinesq model is used to express the strain and Reynolds stress tensors:

$$\frac{1}{\rho}\frac{\partial}{\partial x_i}\left(\tau_{ij} + R_{ij}\right) = \frac{\partial}{\partial x_j}\left(\left(v + v_t\right)\left(\frac{\partial \overline{U}_i}{\partial x_j} + \frac{\partial \overline{U}_j}{\partial x_i}\right) - \frac{2}{3}k\delta_{ij}\right)$$

Where i and j are indices corresponding to the different vector components, x a particular coordinate, U the velocity, τ_{ij} the viscous part of the strain tensor, R_{ij} the Reynolds tensor, v the molecular, v_t the turbulent viscosity and k the turbulent kinetic energy.

The turbulence models differ in the numerical modelling of the turbulent viscosity v_t.

3.3.1.4 Constant-viscosity turbulence model

3.3.1.4.1 The velocity diffusion coefficient

The constant-viscosity turbulence model consists of considering v_t constant. To use this model, it is necessary to first estimate the value of this coefficient in m²/s for the considered flow [4].

In Telemac-2D, a parameter is set; named "VELOCITY DIFFUSION COEFFICIENT"; it groups v and v_t together and also includes the dispersion [4]. No literature was found that would enable determining this coefficient for each individual flow case. However, the following remarks can be made:

- Fixing the coefficient at 10^{-6} m²/s, which corresponds to the molecular viscosity of water, effectively means that the terms due to turbulence are not taken into account.

- The default value in Telemac-2D is 10^{-4} m²/s.

---

[2] This is a Telemac option associated with the method of characteristics. Not all of the boundary conditions are imposed by the user; some are calculated based on the method of characteristics.

- In [4] it is suggested that this parameter takes values between 0.1 and 1500 m²/s,

- whereas the following formula is proposed in [15]:

$$\nu_t \approx \sqrt{k} L_t$$

where k is the turbulent kinetic energy and L_t the characteristic size of vortices. Taking $L_t=D=22$ cm and the values of k given in the thesis [16], it is then found that the turbulent viscosity value should fall between 0.001 and 0.01 m²/s.

3.3.1.4.2 Evolution of the velocity field as a function of ν_t

To select this coefficient it is necessary to understand its influence on the simulation results. In order to fix the ν_t value it is necessary to calculate a velocity field for an equivalent Reynolds number determined as follows:

$$Re_{\text{éq}} = \frac{UL}{\nu_t}$$

An initial series of simulations is performed on a structured mesh with a grid size of 5 cm and a time-step of 0.05 s (selected on the basis of $dt = \frac{\Delta x}{u}$), during which the value of ν_t is varied. A few of the velocity fields thus obtained are presented in Figure 5.

Table 3 illustrates that for a small viscosity value and consequently an equivalent Reynolds number above 50, vortex shedding is present. If the constant viscosity increases sufficiently so that the equivalent Reynolds falls below 50, then the vortex street disappears.
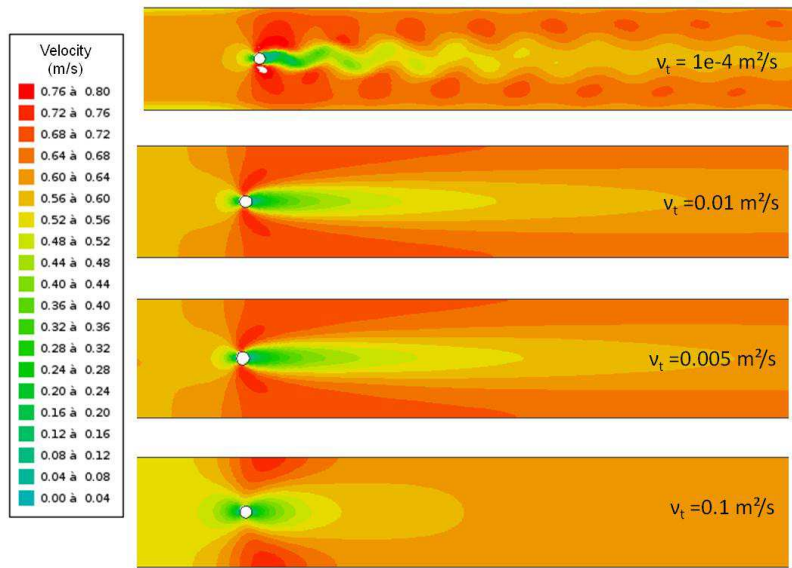
Figure 5: Velocity profiles for different values of turbulent viscosity, for Δt=0.05 s and Δx=5 cm

ν_t	10^{-6}	10^{-5}	10^{-4}	10^{-3}	0.005	10^{-2}	0.1	1
$Re_{\text{éq}}$	147,400	14,740	1,474	147	29.5	14.7	1.47	0.147
Regime corresponding to $Re_{\text{éq}}$ (THEORY)	Turbulent (Re>2000)		Laminar (Re<2000)					
	Vortex shedding (Re>50)				No vortex shedding (Re<50)			
Wake form (SIMULATIONS)	Vortex shedding	Vortex shedding	Vortex shedding	Oscillations	No oscillations	No oscillations	No oscillations	No oscillations

Table 3: Simulation for different values of ν_t and correspondence between $Re_{\text{éq}}$ and the wake form obtained (Δt=0.05s and Δx=5cm, structured mesh)

In summary, the constant value given to the turbulent viscosity allows numerical modelling of a specific velocity field; therefore this value must be chosen so that the model reflects as closely as possible the experimental data.

3.3.1.4.3 Selection of the v_t value for the following part of the study

In the study case, the velocity field is known to be permanent even though it consists of a turbulent regime. For this reason, a viscosity of above 0.005m²/s is chosen. Paradoxically, a turbulent regime is modelled using a laminar flow regime. This is a constraint of Telemac-2D and of RANS models.
A quantitative comparison of the velocity profiles and the results shows that:
$$v_t = 0.005 \text{ m}^2/\text{s}$$
minimises the error between the simulated output and the experimental data. The error calculation is detailed in paragraph 4.1.1.

3.3.1.4.4 Validation of the quality of the simulations based on the Strouhal number

In the case where oscillations are present ($v_t \leq 10^{-4}$), the value of the Strouhal number can be calculated on the basis of the following definition (this is not the same as thesis case [16]):
$$St = \frac{fD}{U}$$
Where D is the diameter of the cylinder, U the uniform flow velocity and f the frequency of the oscillations.
The Strouhal variations as a function of the Reynolds number are well known and described in scientific literature [11]. As demonstrated in Appendix 8.2, the calculated values correspond rather well to those found in the literature on this subject. This constitutes a first validation of the velocity fields obtained with Telemac-2D.

3.3.1.5 k-ε turbulence model

For the k-ε model, the turbulent viscosity is modelled according to the following formula:
$$v_t = f_\mu \frac{k^2}{\varepsilon}$$
Where k and ε are respectively the turbulent kinetic energy and its dissipation, determined using two transport equations.
The Telemac-2D default parameters are not altered for this model. All that is required is to select the sidewall friction for the turbulence regime – smooth or rough. The sidewalls being smooth, the first option is selected. The advantage of this model therefore is that it is not necessary to make setting adjustments, whereas the opposite is the case for the constant viscosity model.
It also allows spatial variation of the turbulent viscosity values, which has more physical sense as the turbulence does not have the same intensity far from the cylinder as it does in the near-wake.
However, the k-ε model does have the following drawbacks:

- Under Telemac-2D, the calculated turbulent viscosity is systematically high; the associated Reynolds number is below 50. It is not possible therefore to reproduce flow regimes displaying Von Karman vortices; these are suppressed by the mean. As this consists of an RANS model, the velocity is therefore averaged, resulting in the suppression in this particular case of the temporal oscillations.

- The model is more complex because it involves two equations to determine the values of k and ε. However, turbulence is a purely three-dimensional phenomenon and the computations are realised in two dimensions – this raises questions regarding the relevance of using a more complex model.

For the simulations performed with this turbulence model, verification is made to ensure that the numerical stability condition $\frac{l}{\varepsilon} > \Delta t$ is well satisfied [14].

3.3.1.6 Advection schemes for flow velocity

Two different advection schemes are used for the velocity calculation:

- The method of characteristics, which has the advantage of being unconditionally stable but which does not conserve mass.
- The PSI scheme, which is conservative but must satisfy the CFL (Courant–Friedrichs–Lewy) condition.

Reference can be made to [4] for more details concerning these two schemes.

3.3.1.7 Model parameterisations of the studied simulations

The graphic below provides a summary of all parameterisations considered in this study.
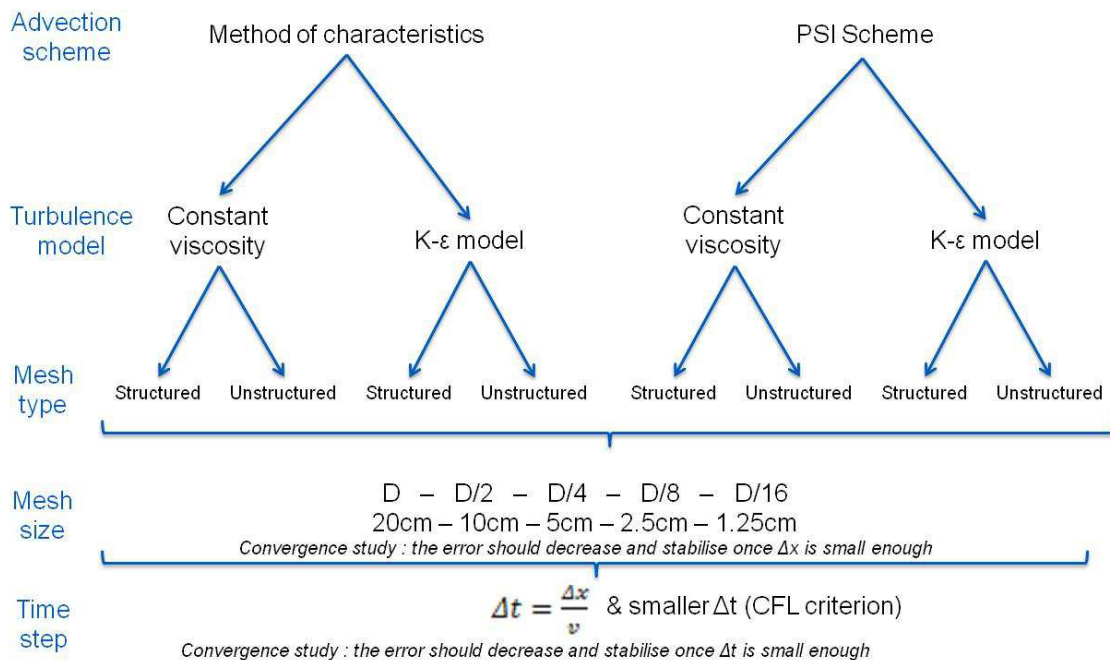
Figure 6: Schematic diagram of all simulations performed for the study

3.3.1.8 Results of the simulations

3.3.1.8.1 Method of characteristics

With this advection scheme, simulations are launched for the two turbulence models, the two mesh types and for 5 different mesh sizes.

3.3.1.8.2 Quantitative comparison with the experiment

The aim of this section is to:

- Verify the mesh size and time-step convergence for each simulation.

- Verify, once convergence has been achieved, that the simulations adequately reproduce the experimental data.

To compare the velocity fields simulated with Telemac-2D to the velocity values obtained at the 50 measurement points described in the thesis [16], the two velocity components at these points are extracted from the file generated by Telemac.

The simulated velocity is then compared to the experimentally observed velocity through the following calculations:

- The sum of the square of the errors:
$$\sum_{i=1}^{N}\left(U_{obs}-U_{simu}\right)^2$$

- The L^1 relative error:
$$\frac{1}{N}\sum_{i=1}^{N}\frac{|U_{obs}-U_{simu}|}{|U_{obs}|}$$

N being the number of measurement points, U_{obs} the experimental velocity and U_{simu} the velocity value resulting from the simulations.

These two errors allow a quantitative evaluation of the quality of the simulations. It is also considered that once these are stabilised with the decrease in time-step and mesh size, the calculation is converged.

The summation over i for the relative error calculation is not performed for all experimental measurement points, because to do so would lead to inconsistent conclusions and results that would not allow a conclusion to be drawn on the mesh and time convergence. For the example presented in Figure 7, simulation results are closer to the experimental data for the 5 cm mesh size (red arrows) than for the 10 cm mesh (blue arrows). This is confirmed by the sum of the square of the errors, which is smaller for the 5 cm mesh, but invalidated with regard to the L^1 relative error (cf. Table 4). The relative error is high as a result of the measurement points located just behind the cylinder, where the experimental data shows velocities up to 6 times higher than those simulated. This isn't reflected in the sum of squared errors because the velocities involved are very small.

2D simulations are known to be unable to reproduce sufficiently well the velocities near the cylinder and downstream of the latter where flow is more turbulent and probably three-dimensional. Furthermore, the far-wake (which is of greater interest) and not just the wake behind the cylinder will be studied. Subsequently, the points circled in blue (Figure 7) will no longer be considered for the relative error calculation. The results are better and more consistent, as can be seen from the last line of Table 4.

Mesh size	10 cm	5 cm
Observations	Further from experimental data	Closer to experimental data
Sum of the squared errors	0.62	0.35
L1 error over all points	46%	76%
L1 error over selected points	19%	11%

Table 4: Errors for the k-ε model and a structured mesh
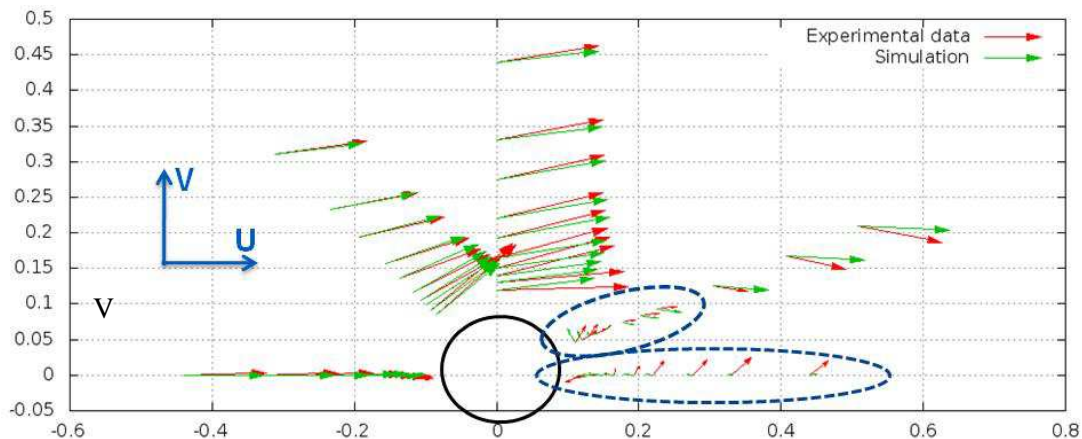
Figure 7: Velocity field around the cylinder (k-ε model, method of characteristics, structured mesh)

It can be seen from Figure 7 that the flow occurs essentially along the U component of the velocity. For simplification, only the U-dependent errors are considered hereafter.

It can be indicated, however, that the sum of the errors in V is in the order of 0.2 m/s (it is of the order of 0.3 m/s for U) and the relative error over V is close to 100%. The V component is not reproduced particularly well, no doubt due to the fact that it is very low.

3.3.1.9   Results and conclusions

An example of the results obtained for a given parameterisation is provided in Table 5. For each mesh size, it can be seen that the two errors stabilise when the time-step is sufficiently diminished. This value is applied to produce the graphics presented in Figure 8 and in Figure 9. With the method of characteristics, convergence in time-step is clearly seen to occur in all cases.

Mesh size (cm)	20	10	5		2.5			1.25			
Time-step (s)	0.1	0.1	0.1	0.05	0.1	0.01	0.005	0.1	0.01	0.005	0.001
Sum of the errors²	0.84	0.52	0.31	0.30	0.25	0.29	0.29	1.18	0.40	0.39	0.39
L1 relative error	0.26	0.22	0.20	0.19	0.19	0.21	0.21	0.32	0.24	0.23	0.23

Table 5: Errors obtained with the constant viscosity model and a structured mesh

Figure 8: Sum of the squared errors, obtained with method of characteristics for the two turbulence models (nut: constant viscosity model, K-eps: k-ε model) and two mesh types

Figure 9: Relative errors (in %) obtained with method of characteristics

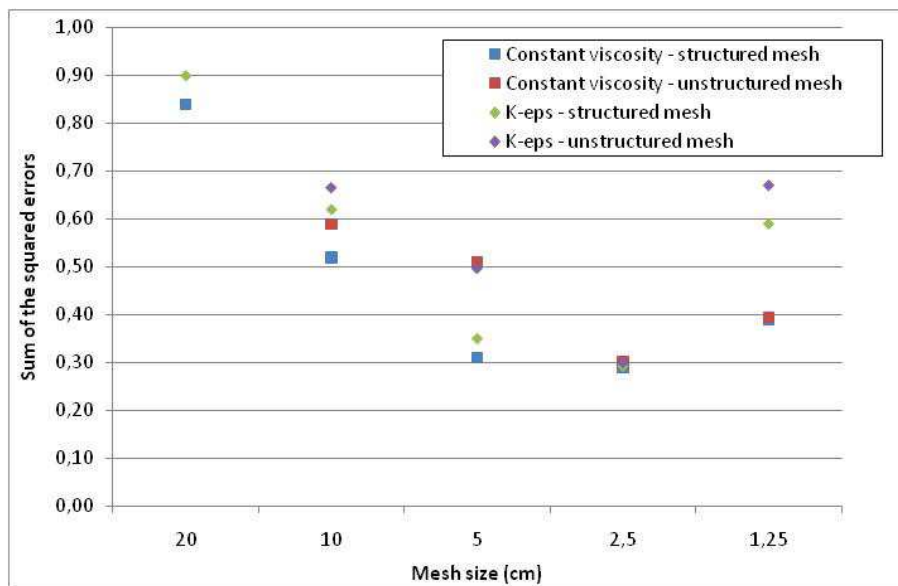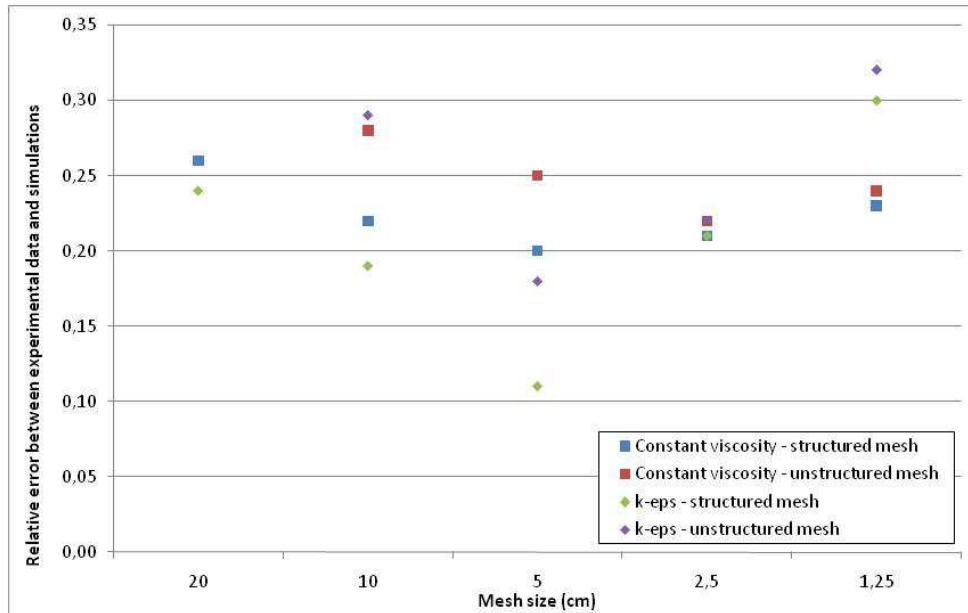The relative error for all configurations is comprised between 10 and 30%, with an error of less than 25% for a mesh size of 5 cm; these results are quite satisfactory (given the probability of errors in the measurements). When the mesh size is decreased, the error diminishes then stabilises and mesh size convergence is achieved.

This is not true, however, for the 1.25 cm mesh, where the error increases again, particularly in the k-ε case. This is probably due to the high number of mesh elements in this case and therefore calculations; increasing the probability of numerical errors being propagated through the solution itself. To check this point, simulations were launched with the CADNA (Control of Accuracy and Debugging for Numerical Applications) library. This FORTRAN library enables to estimate the numerical error on the velocities, due to inevitable round-offs of real numbers. Computational times with CADNA being extremely long, the results are not available at this date.

For the structured mesh, convergence is achieved with a mesh size of 5 cm (D/4, D being the diameter of the island representing the cylinder); this needs to be refined to 2.5 cm (D/8) for the unstructured mesh. For a mesh size of 2.5 cm, the error is the same for the four parameterisations, which appears to confirm the convergence of the simulation. In conclusion, the structured mesh gives better results; but a similar quality of simulation can be obtained with unstructured mesh by decreasing the mesh size.

The turbulence models give different results that do become similar however when the converged solution is obtained. It is not possible, therefore, to conclude that one of the turbulence models is preferable to the other in terms of the calculation of the U component of the velocity. The strong point of the constant viscosity model is that it doesn't require such a small time-step and therefore the calculations are faster. On the other hand, the k-ε model enables attaining an error of 60% for the V component of velocity, against an error over 100% for the constant viscosity model (bearing in mind that this component is very small). It also avoids the necessity of setting an additional parameter.

The mesh sizes and time-steps recommended for each case, as a result of the study, are summarised in the table below.

Case	Mesh size	Time-step
Constant viscosity Structured mesh	D/4 (5.0 cm)	0.1 s
Constant viscosity Unstructured mesh	D/8 (2.5 cm)	0.01 s
k-ε Structured mesh	D/4 (5.0 cm)	0.01 s

k-ε Unstructured mesh	D/8 (2.5 cm)	0.005 s

Table 6: Mesh size and time-step for which convergence is achieved, for method of characteristics

3.3.1.10   Conservative PSI scheme

The same simulations as for the method of characteristics are launched, with the results plotted on the same types of graph (cf. Figure 11 and Figure 12). Before commenting on these graphs, two important remarks need to be made:

- Unlike the previous case, time-step convergence is not always clearly achieved: when the time-step is diminished, there is an initial significant reduction in the error rate, before it stabilizes and then increases slightly. This increase remains negligible in most cases, except for the two unstructured mesh cases with the smaller mesh sizes. This could be explained by the fact that, although the simulation output is supposed to converge as the mesh size and time-step are diminished, an increasing number of calculations are required, thus raising the probability of numerical errors occurring. This hypothesis is currently being verified with the CADNA library. With the unstructured mesh models, care must be taken to limit the degree to which the time-step is reduced. When plotting the graphs, the smallest obtained error was considered, which does not necessarily correspond to the smallest time-step.

- The second remark concerns the k-ε turbulence model, for which asymmetry appears in the flow around the cylinder. On one side of the cylinder, the velocity increases significantly as illustrated by the red and yellow zones in Figure 10. To overcome this problem, which may arise from an implementation issue in Telemac-2D (currently being investigated), the error is only calculated for the side on which the velocity is lower.
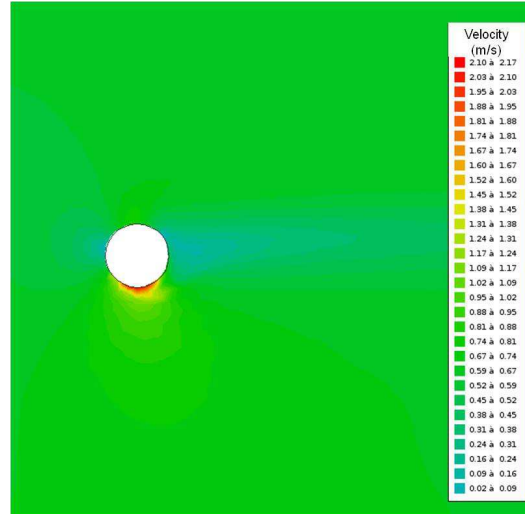
Figure 10: Asymmetric velocity field around the cylinder for the k-ε model (scale: velocity of 0 to 2 m/s, whereas flow velocity is 0.67m/s)
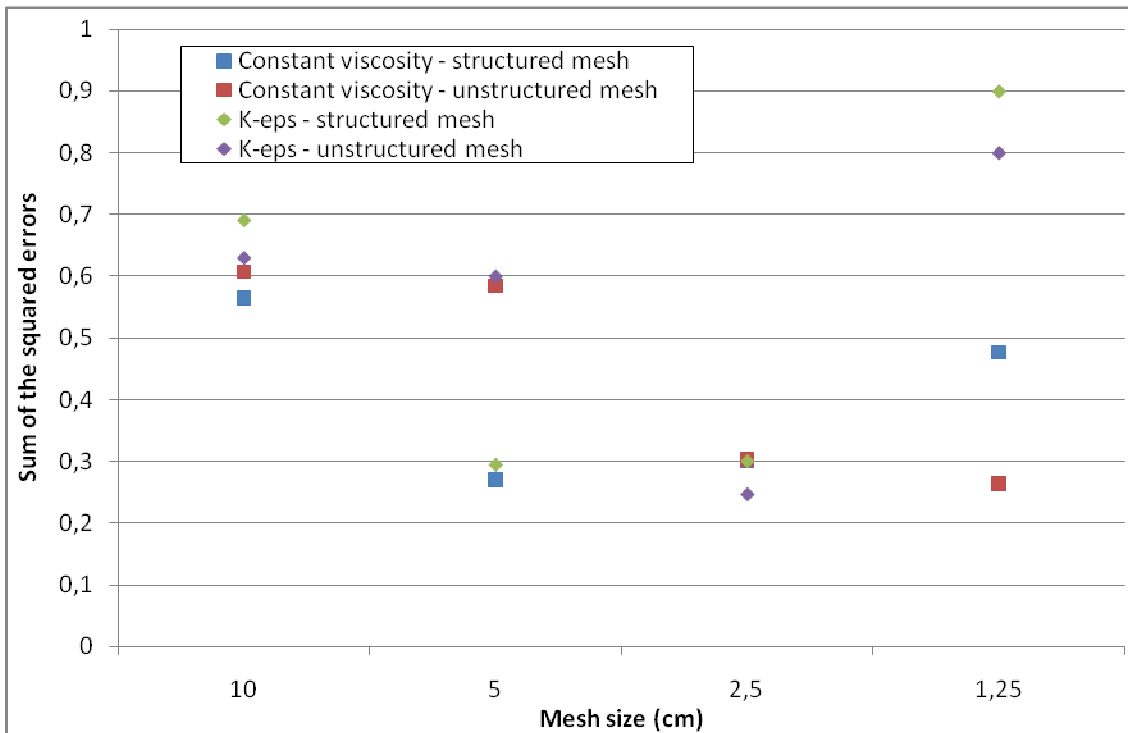
Figure 11: Sum of the squared errors obtained with conservative PSI scheme
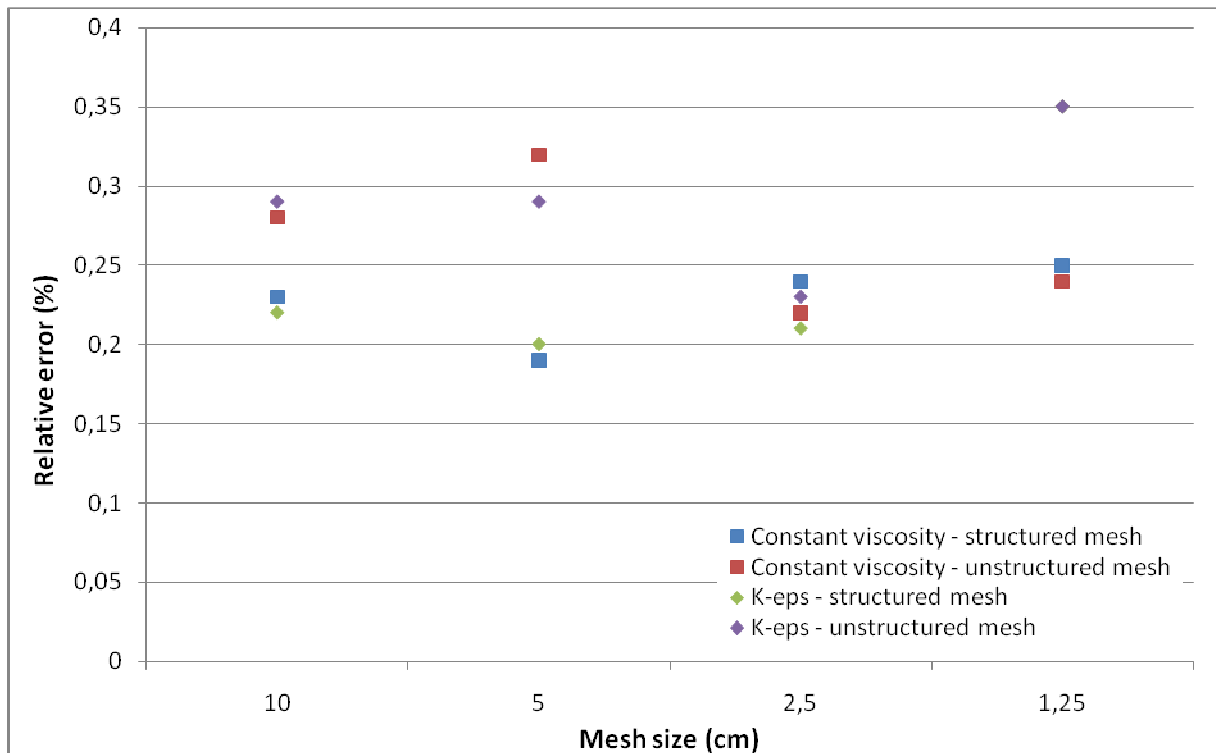
Figure 12: Relative error (in %) obtained with conservative PSI scheme

Looking now at Figure 11 and Figure 12, it can be observed that the error varies between 19% and 35%, with an optimum below 25%, which is satisfactory.

In order to extend these results to other simulations, it is essential to take note of the variations in output as the time-step is decreased. It is also worth noting that, as was the case for the method of characteristics, the error increases significantly with the smallest mesh size. There is therefore an optimum in each configuration where the error is minimal; these optimums are listed in Table 7.

It can be thus concluded that neither one of the turbulence models presents a clear advantage over the other.

Case	Mesh size	Time-step
Constant viscosity **Structured mesh**	D/4 (5.0 cm)	0.05 s (or even 0.1 s)
Constant viscosity **Unstructured mesh**	D/8 (2.5 cm)	0.05 s (even 0.1 s)
k-ε **Structured mesh**	D/4 (5.0 cm)	0.01 s (even 0.05 s)
k-ε **Unstructured mesh**	D/8 (2.5 cm)	0.05 s

Table 7: Mesh size and time-step for which convergence is achieved with the PSI scheme

3.3.1.11 Validation of far wake results using the principle of self-similarity of velocity profiles

The comparison with the experimental data presented in the thesis [16] only allows validation of the wake to a distance of 2D relative to the cylinder. However, it can be demonstrated that there is similarity of the transverse velocity profiles in the wake of a cylinder. This self-similarity can be described with an analytic equation as proposed in [5] and [8] (using a number of assumptions and simplifications). This particularity is used to validate the far-wake form obtained with the simulations. Appendix 8.3 contains details of the analytical equations and the solutions obtained. The key points are summarised hereafter.

Self-similarity is verified only for the two simulation cases used for the tidal energy converter hereinafter (cf. paragraph 5). These cases are based on the PSI scheme and entail using unstructured mesh with a mesh size of 2.5 cm and time-step of 0.05 s for both turbulence models.

The equation proposed by Hinze [5] (see appendix 8.3) does not take account for shallow water and edge effects (the friction on the edges). It works adequately for the k-ε model; as seen in Figure 13, the plot of the normalised velocity deficit obtained from simulations (in colour) corresponds very well to theoretical curves (in black). On the other hand, this equation does not work for the constant viscosity model; the lines are not superimposed (cf. Figure 91 in Appendix 8.3). This is due to strong flow acceleration along the outer edges caused, in the constant viscosity model case, by the flume sidewalls – not accounted for by [5].
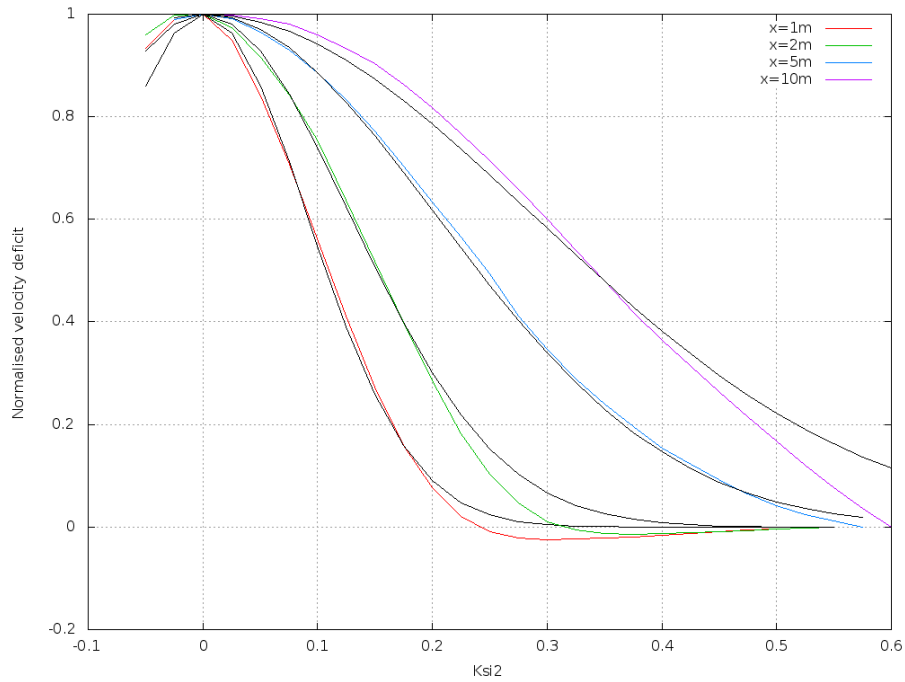
Figure 13: Normalised velocity deficit as a function of Ksi2 at different distances downstream of the cylinder obtained via simulation (coloured lines) or using the analytical equation given in [5] (black lines). k-ε model

The equation suggested by Negretti [8], which is valid for shallow water and channel flows, gives theoretical curves that are close to simulation results for both turbulence models at the following distances: 1m (5D), 2m, 5m et 10m (50D) downstream of the cylinder (figures in appendix 8.3). This confirms that the far-wake is adequately reproduced by Telemac-2d.

3.3.1.12 Conclusions regarding the wake around a cylinder

The two advection schemes for the velocities and the two turbulence models, using a suitable mesh size and time-step, enable the reproduction of the velocity field with a relative error comprised between about 10% and 20% for the best cases. This result is satisfactory, given that there are errors in the measurements and the simulation is performed in two dimensions whereas the flow is three-dimensional in certain areas. The far-wake flow is also well reproduced.

3.3.1.12.1 Time-step and mesh size convergence

For each of the configurations, corresponding to an advection scheme, a turbulence model and a mesh type, a conversion study was conducted, varying the time-step and the mesh size. As these were reduced, the velocity field model converged towards a solution that was in close agreement with the physical data obtained from the experiment. It was also observed in certain cases that, when the time-step and mesh size were further reduced, the solution diverged again from the experimental results, most probably because of propagation of round-off errors.
On the basis of this study, a determination was made of the optimal time-step and mesh size for each of the configurations: either the values for these two magnitudes at which there is convergence or the values for which the error is minimal (cf. Table 6 and Table 7).

3.3.1.12.2 Velocity advection scheme

Both of the velocity advection schemes achieve relative errors of the order of 20%. The method of characteristics is less restrictive and the convergence of the solution can be more clearly judged, however **the PSI scheme is recommended** because it is conservative and it is this scheme that will be retained for the simulations of the tidal energy converter wake.

3.3.1.12.3 Structured and unstructured mesh

Similarly, the use of structured mesh appears less restrictive and leads to lower computation times; however for application in practical cases with more complicated geometries, **the mesh must necessarily be unstructured**. It has been demonstrated that by choosing the appropriate time-step and mesh size, it is just as possible to obtain a good reproduction of the velocity field with this type of mesh.

3.3.1.12.4 Turbulence model

With respect to the turbulence, neither model seems clearly superior. It must be noted however that the use of the constant viscosity model necessitates setting an additional parameter for each flow – the turbulent viscosity. It was demonstrated that $v_t = 0.005$ m²/s is the correct setting for the flume used in this study. However, for application in practical case studies, i.e. at sea, over a large zone and with several tidal energy converters, the selection of the v_t value may not be as simple. For this reason, the k-ε model could be of more interest. On the other hand, it could be questioned as to whether it is really necessary to complicate the two-dimensional turbulence models given that this phenomenon is essentially three-dimensional.

3.3.1.13 From cylinder to tidal energy converter: numerical modelling with the FORTRAN DRAGFO routine

3.3.1.13.1 Principle of tidal energy converter wake simulation

The eventual aim of the study is to simulate the wake of tidal energy converter (TEC) arrays at sea and to study the interaction between several arrays. A TEC farm might cover an area of up to 100 km² and there could be several hundreds of kilometres distance between farms; for this reason simulations would need to be performed on very large scales. The use of a 2D model is an intelligent choice as it will ultimately reduce the computation cost.

At the same time, a tidal energy converter is about 10 metres high (therefore is much smaller than the basin scale), and it has a complicated structure with rotating parts. Given that the difference in scale is of such a high order and that meshing of such a complex structure is not possible in Telemac-2D, it is therefore necessary to model the TEC in a simplified manner. This is done with the aid of the DRAGFO routine, already implemented in Telemac-2D to simulate, for example, bridge piers in a river flow.

The tidal energy converter will not be meshed, the DRAGFO routine allowing the application on a defined surface of a drag force modelling the TEC.

3.3.1.13.2 Validation of the methodology applied to the tidal energy converters on the simple cylinder case

In order to validate this modelling method, results for the simple cylinder case are verified for consistence. The same simulations as previously are performed only with the exception this time that the cylinder is no longer represented in the mesh. In this case, the wake is generated by the drag force that is applied by the DRAGFO routine. This force is applied on a surface 'A' corresponding to the position of the cylinder. At each node of this surface, the following term is added to the equations:

$$F = -\frac{1}{A}\frac{1}{2}C_d u^2 \frac{S}{h}$$

This is a volumetric force applied on the fluid; by multiplying this term by the volumetric mass and integrating over a volume, a force is obtained. This force corresponds to the reciprocal of the drag force that the fluid exercises on the turbine:

$$F = \frac{1}{2}\rho C_d u^2 S$$

Where Cd is the drag coefficient of the cylinder, S the surface of the cylinder orthogonal to the flow equal to $h.D$. The values of Cd for a cylinder as a function of the Reynolds number are well known (Figure 14). $Re = 1.18 \times 10^5$ corresponds to Cd = 1.15.

The velocity u implicated in the equation is usually the flow velocity were the tidal energy converter not to be present. In practice, u is considered to be the value of the velocity upstream of the TEC, before the flow is disturbed. For reasons of numerical stability and through simplification, it was decided in this case to consider u at the point of application of the force, which is possible as the TEC is not meshed. **This entails a new definition for the drag coefficient Cd, which becomes an adjustment parameter of the model. Then Figure 14 is not applicable.**
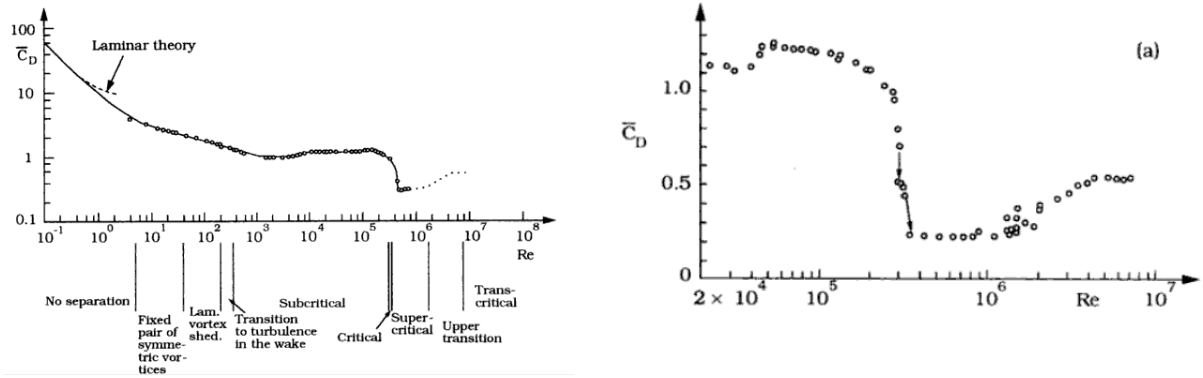
Figure 14: Drag coefficient as a function of Reynolds number for a smooth cylinder [13]

Simulations are then performed for the two cases selected for the subsequent part of the study, as described in paragraphs 3.3.1.11 and 3.3.1.12.

3.3.1.13.3 Constant viscosity model

As previously verified, the simulations with the meshed cylinder (red line) reproduce well the experimental results data from the thesis (black points). The constant viscosity model and a drag coefficient fixed at 6 enable to obtain good results with the DRAGFO routine (blue line, cf. Figure 15): the velocity is reproduced well both downstream and upstream, only the points in the very near vicinity of the cylinder are not well reproduced.

The drag coefficient is fixed at 6 in order to obtain the same energy loss at cylinder level as that obtained previously with the meshed cylinder[3]. This is essential for validation of the DRAGFO routine. This coefficient is higher than the tabulated value (1.15) , which corresponded to a drag force calculated with a reference velocity whereas this new drag coefficient is valid when the local velocity is used.

Figure 15: Velocity (m/s) and mechanical power (kW) – constant viscosity model; experimental data (black points), simulations with meshed cylinder (red line) and with DRAGFO at different Cd values (1.15 in green and 6 in blue). The centre of the 22 cm cylinder is plotted at position 0 along the flume length.

---

[3] For the mechanical power, a significant decrease in the power values is observed at the level of the cylinder., The power also decreases regularly along the flume because of the bottom and sidewall friction.
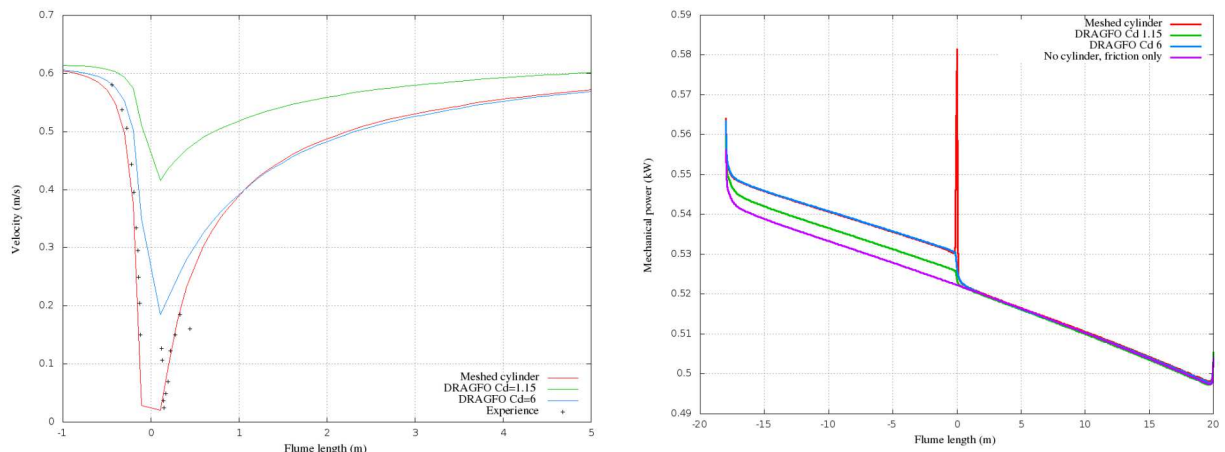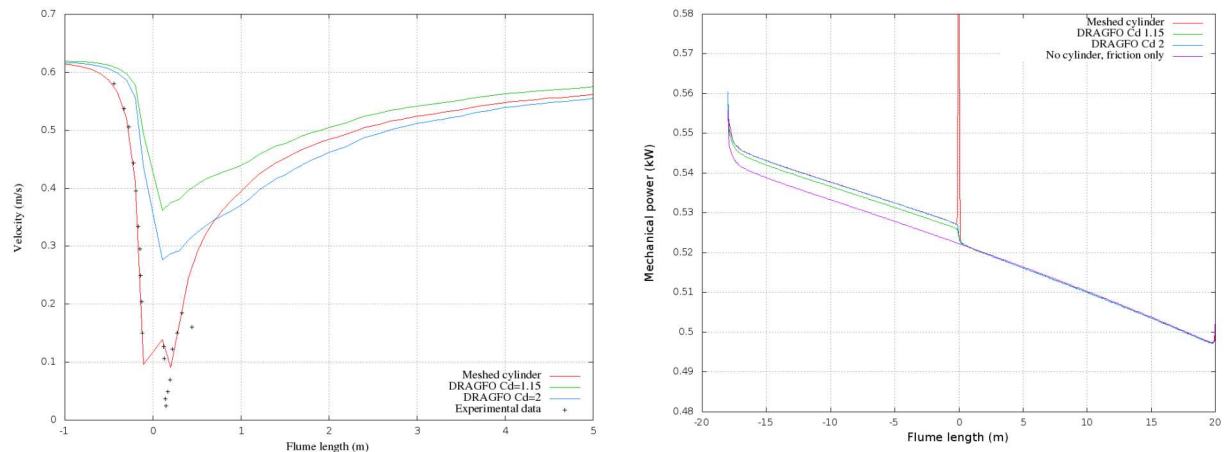
3.3.1.13.4 The k-ε model

Figure 16: Velocity (m/s) and mechanical power (kW) for the k-ε model; experimental data (black points), simulations with meshed cylinder (red line) and with DRAGFO at different Cd values (1.15 in green and 2 in blue). The centre of the 22 cm cylinder is plotted at position 0 along the flume length.

Figure 16 shows the same type of results for the k-ε model. For this case, a drag coefficient equal to 2 allows obtaining the same energy loss with the DRAGFO routine as with the meshed cylinder. The velocity is then well reproduced from a distance of 2 or 3 diameter equivalent lengths downstream of the cylinder.

The adjusted drag coefficients Cd used to represent the cylinder in the flow modelled using different turbulence models (constant turbulent viscosity or k-epsilon) are different because the energy deficits calculated when the cylinder was meshed were not the same either. It was two times higher in the constant viscosity case; the Cd used is therefore also higher. The difference in energy losses is due to the fact that the transverse profiles are not the same for the two turbulence models. The same inlet flow gives rise to different velocities in the middle of the flume and, consequently, different energy losses in the wake of the cylinder.

3.3.1.14 Conclusions for part A

The DRAGFO routine appears to give consistent results for simulations of the wake behind a cylinder to the simulations where the cylinder was meshed physically, starting at a distance 2D or 3D downstream. Whilst it is less reliable to obtain good reproduction of the wake immediately downstream of the obstacle with this routine, within a few diameter lengths the results become much more consistent with physical data. This does not present a notable drawback as the ultimate aim of the study mainly requires a good reproduction of the far-wake. Therefore it can be concluded that the subroutine DRAGFO can model the far-wake of the cylinder.

In addition, the DRAGFO routine can be used to model tidal energy converters, as different parameters, such as the drag coefficient Cd or the area over which the force is applied, can be adjusted to align the simulated wake closely to the experimental data. It is worth highlighting at this point a fundamental assumption of this approach: the far wake engendered by a tidal energy converter and a bridge pier are considered to be similar (if the Reynolds numbers are similar) and it is therefore possible to simulate the wake around a tidal energy converter using the subroutine DRAGFO. Part B of the study will test this assumption.

3.3.2 Part B: Simulations for the wake of a tidal energy converter

3.3.2.1 Introduction

This section presents step c) of the methodology (cf. Introduction), which is the numerical modelling in Telemac-2D of the flow around a tidal energy converter (TEC) in a flume, validated via an experiment conducted at the EDF LNHE facility [2, 3].

Based on measurements taken during the experiments, as well as the results of the simulations for the simple cylinder case, the flow around a TEC is numerically modelled in Telemac-2D with the aid of the DRAGFO routine.

The effect of changing different parameters, such as the drag coefficient or the surface over which the drag force is applied, is studied in order to obtain the most accurate reproduction of the wake. Parameter adjustments are made for different TEC operating regimes (i.e. different rotation speeds that, in turn, lead to different drag coefficients and wake forms) as well as for different experiments:

- A test at low velocity and turbulent intensity (test n°1)

- A test at high velocity (test n°3)

- A test at high turbulent intensity (test n°2)

The aim of this study is for conclusions to be drawn that will later enable accurate numerical modelling of the flow around and downstream of any TEC with knowledge of the drag coefficient of the TEC and of a few of the upstream flow characteristics only and without having to once more perform a full parametric study.

3.3.2.2 Experimental data

The simulations that follow are based on a series of experiments performed at the LNHE testing facility at Chatou [2, 3].

A 1/30 scale model of the TEC was placed in a flume. A schematic illustration of the lay-out of the experiment is provided Figure 17.
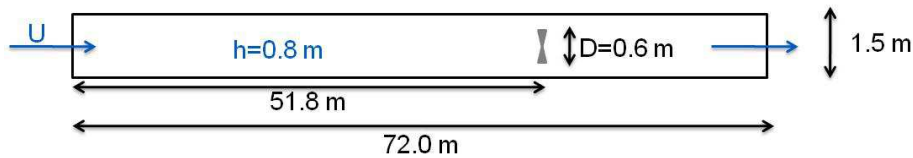
Figure 17: Schematic of flume and TEC

Table 8 provides the specifications of the three tests conducted in the flume. For each test, measurements were made for different TEC operating regimes, i.e. different rotations speeds, ω and different Tip Speed Ratios, λ:

$$\lambda = \frac{\omega R}{U}$$

	Test n°1	Test n°2 High turbulent intensity	Test n°3 High velocity
Flow velocity (m/s)	0.27	0.55	0.27
Turbulent intensity	5%	5%	15%
Number of operating regimes	5	5	2
Reynolds (TEC diameter)	1.62×10^5	3.3×10^5	1.62×10^5

Table 8: Specifications of the different tests conducted

For each test, the velocity and the water height as well as the loads induced on the turbine by the flow are measured. The loads enable calculation of the drag and power coefficients of the TEC. Velocity is

measured with an Acoustic Doppler Velocimeter (ADV), with an uncertainty equal to 1% of the velocity and, at minimum, +/- 0.25 m/s. This data also enables determining the instantaneous velocity variations u' and consequently, the turbulent intensity TI and the turbulent kinetic energy k:

$$ TI = \frac{\overline{|u'|}}{\overline{|u|}} \quad \text{and} \quad k = \frac{1}{2}\overline{u'u'} $$

Measurements are performed upstream and downstream of the TEC, at different points as illustrated in Figure 18. The X axis starts at the downstream end of the flume (X=0) and goes back up towards the flume inlet, the TEC rotor being located at X=20.3 m.

The upstream cross (X=23.2 m) enables finding the reference velocity (where there is no flow disturbance), the downstream grid pattern (X=19 m) enables to determine precisely the velocity field directly behind the turbine. It is important to note that to compare the test results to the simulations performed with Telemac-2D, generating a vertically-averaged velocity field, reference can be made just to these points for which a vertical average can be calculated. This means that the longitudinal profile is known at six points, including the upstream point. All of the crosses being relatively close to the turbine (the furthest distance is 8 diameter equivalents), the two points at X=5 and X=10 are taken into account to have an idea of the far-wake (even though the vertically-averaged velocity is not known for these points). The transverse profile is also known at the cross-grid level, 2.2 diameters downstream of the turbine.
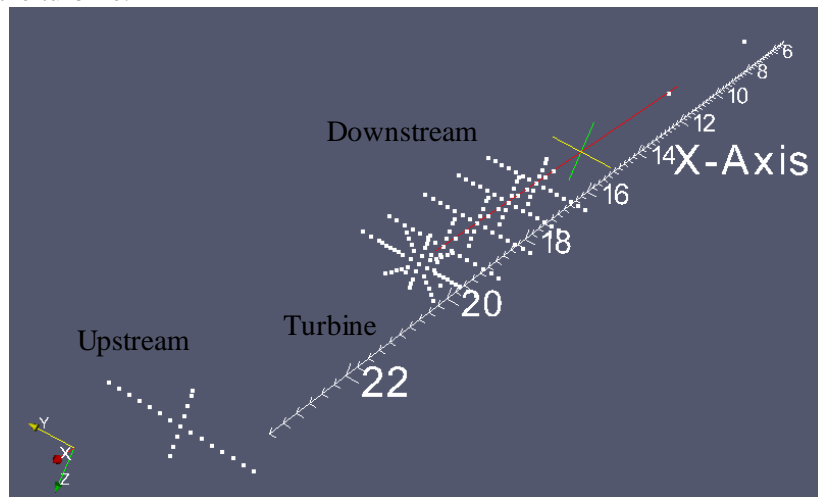

Figure 18: Graphical representation of measurement points along the flume (TEC is located at x=20.3 m and the downstream end of the flume at x=0 m)

3.3.2.3 Telemac-2D and the DRAGFO routine

3.3.2.3.1 Models and options of Telemac-2D

Consequent to the study on the simple cylinder case, involving a Reynolds number of the same order of magnitude as the present study, use of the following Telemac-2D options is advocated (cf. paragraph 3.3.1.12 of Part A):

- The PSI scheme for velocity convection

- An unstructured mesh

- The constant viscosity and k-ε turbulence models

- The DRAGFO routine for building the model of the TEC

The orders of magnitude of the mesh size and time-step that should be used are inferred from their values in the simple cylinder case and from a proportionality calculation based on the velocity inverse

(example given in Table 9 for low velocity, 0.27 m/s). These values give a first indication for the Δx and Δt. However, as the flow is different, a quick convergence study is still required.

	Cylinder	TEC
Reynolds number	1.48×10^5	1.62×10^5
Velocity	0.67 m/s	0.27 m/s
Mesh size (constant viscosity or k-ε)	2.5 cm	6.2 cm
Time-step (constant viscosity or k-ε)	0.05 s	0.12 s

Table 9: Specifications of the two flows (cylinder and TEC) with calculation of order of magnitude for the mesh size Δx and time-step Δt, in the case of the TEC

3.3.2.3.2 The DRAGFO routine applied to the TEC

The DRAGFO routine, already tested in the cylinder case, was modified to adapt it to the TEC case. In the modified version, it enables applying, over an area A, a term equivalent to a drag force in the quantity of motion (St Venant) equation, of the form:

$$F = -\frac{1}{A}\frac{1}{2}C_d S \frac{u^2}{h}$$

Where u and h are the local velocity and water height, Cd the drag coefficient of the TEC, S its surface orthogonal to the flow, equal to πR^2.

As for the cylinder, the TEC is thus no longer represented in the mesh; it is simply modelled by this load loss. The user can define the value of Cd, choose the area 'A' over which the force is applied, as well as the area S of the TEC that obstructs the flow.

As was noted previously, the velocity u is, in theory, the velocity of the flow in the case of no obstacle being present. In general, the far velocity is considered as being the reference velocity. In this case, for numerical stability reasons and since the TEC is not meshed, the velocity u is simply taken at the computational node.

3.3.2.3.3 Study parameters

To best adapt the simulations to the experimental tests, the following parameters are taken into account:

– Bottom and sidewall friction, determined by the law of friction (Strickler's law is selected) and the coefficient of friction, Cf (Strickler coefficient)

– For the constant viscosity model, the value of ν_t must be set

– The DRAGFO routine allows the manual resetting of the TEC and the area A. The latter was set as a rectangle of dimensions 2L x 2D, as shown in the Figure 19 diagram. The location of the TEC is defined as the centre of this rectangle.
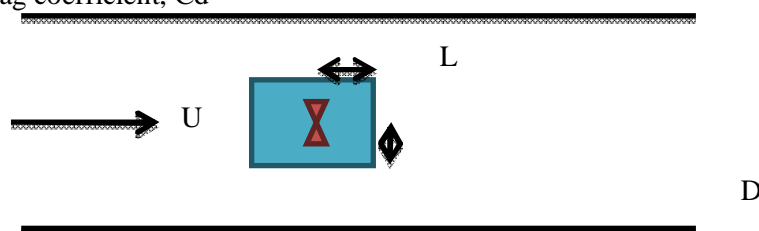
– The drag coefficient, Cd

Figure 19: Schematic of surface A (in blue) over which drag force is applied

With regard to the latter, a first indication of its value can be obtained from the experimental measurements of the loads induced on the rotor. Nevertheless, modelling the TEC on the unique basis of load loss, fails to take full account of the energy losses. In practice, three sources of energy loss can be identified:

– Extraction of energy from the fluid by the turbine, due to the drag force (pressure (or form) drag and friction drag) as well as the thrust force

– Energy losses caused by wake shear (due to wake rotation as well as the velocity gradient induced by the latter)

– Energy loss due to turbulence generated by the turbine

Because the TEC is not meshed, DRAGFO only takes account of the first source of energy loss; the two other are not modelled (moreover, Telemac2D uses averages over the vertical). Consequently, a change in the Cd value is therefore expected to take the latter into account.

3.3.2.4 Simulations for the test at low velocity and low turbulent intensity (test n°1)

The first simulations of test n°1 is made, for which $U \approx 0.27 m/s$ and turbulent intensity is low (5%). Consideration is given initially to a single turbine operating regime for which the tip speed ratio (TSR) is 3.5. The drag coefficient for this regime is calculated equal to 0.91. **Note that, this TSR is very close to the optimal Cd for the operating regime of the tidal turbine (as observed in Figure 26).** A quick convergence study is carried out; it is clearly observed that convergence is achieved for the time-step. On the other hand, results are not completely converged even with a mesh size of 2.5 cm, which already corresponds to D/24. It was decided that this mesh size (D/24) would suffice however as further decreasing the mesh size would not only require much longer computation time but would lead to the appearance of other numerical problems.

	Mesh size	Time-step
Constant viscosity model	5 cm	0.1 s
k-ε model	2.5 cm	0.1 s

Table 10: Time-step and mesh size selected for modeling of test n°1

3.3.2.4.1 Influence of different parameters on the wake field

As expected, a higher drag coefficient (Cd) leads to increased velocity deficit (Figure 20).
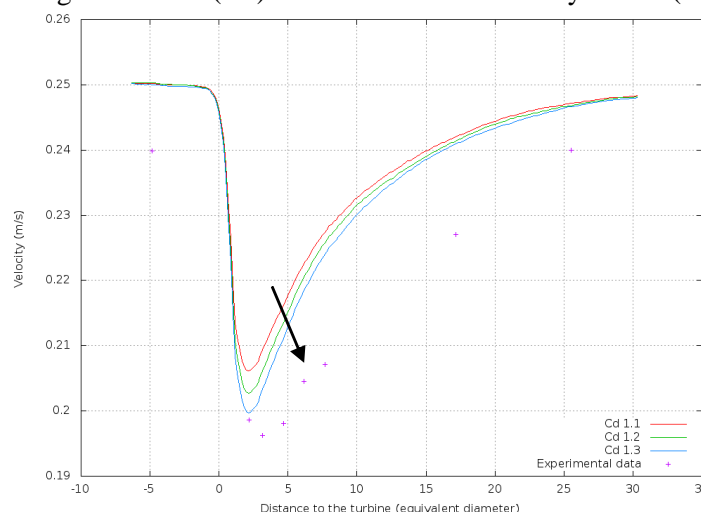

Figure 20: Wake for k-ε model and different values of Cd. Arrow indicates an increase in Cd.

As observed in Figure 21, if the value of D (the cross-sectional dimension of rectangle A) is increased, a lesser degree of minimum velocity is attained. However, to maintain the same energy loss conditions, there is increased spreading of the wake in both directions (longitudinal and transversal).
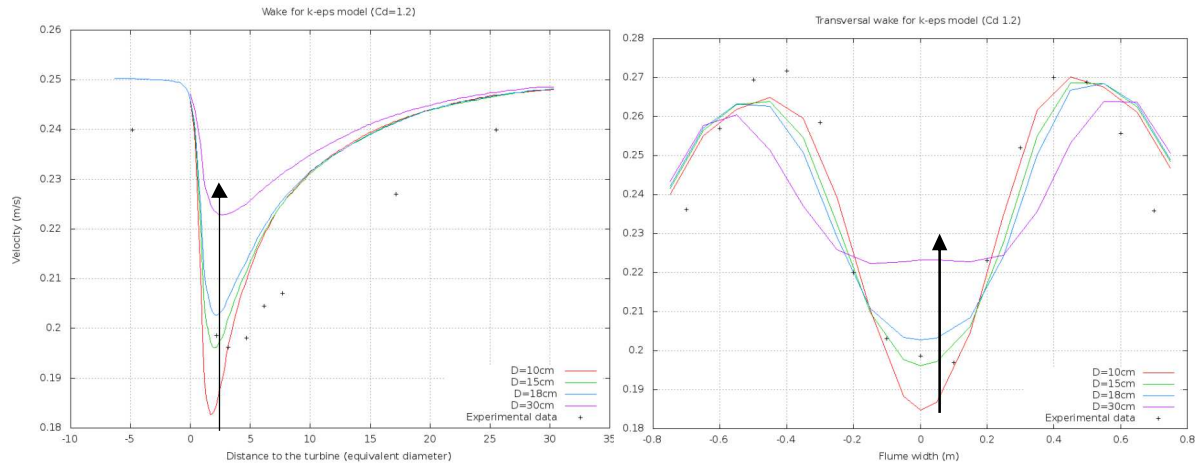
Figure 21: Longitudinal and transverse wakes for k-ε model, for different values of D. The arrow indicates an increase in D (from 10 to 30 cm)

The same applies if the value of L is increased: minimum velocity attained by the flow is less pronounced but there is more wake spreading in the stream-wise direction. The minimum is also located further downstream (Figure 22).

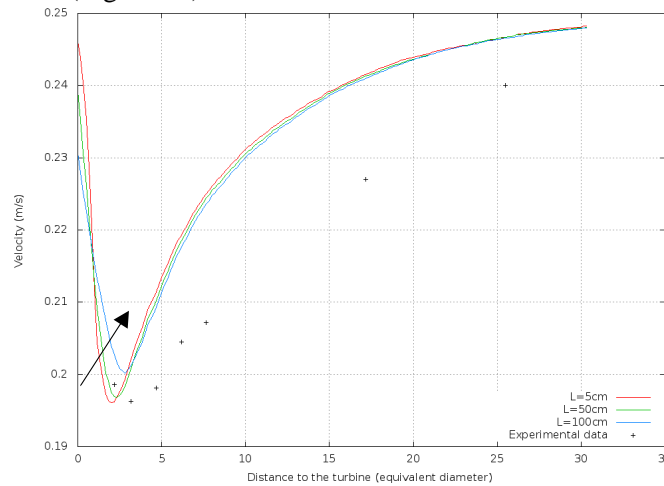**Figure 22: Wake for k-ε model, for different values of L. The arrow indicates an increase in L (5 to 100 cm)**

Moving the position of the TEC has the effect of displacing the minimum velocity location.
In the case of the constant viscosity model, adjusting the v_t plays a role in wake recovery to the free-stream flow velocity: the lower the viscosity, the more gradual is the slope of the wake recovery (curve) (Figure 23).
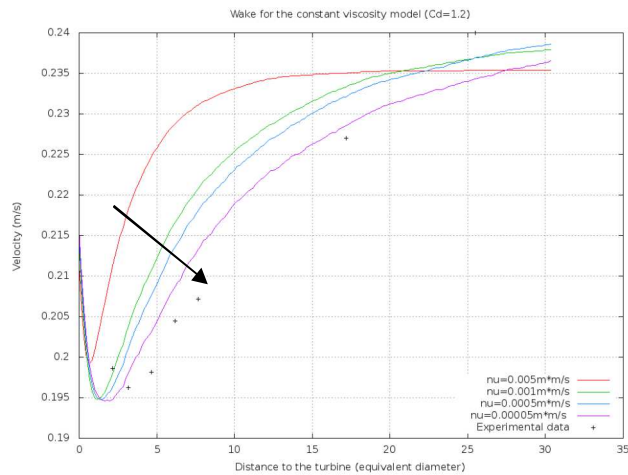
Figure 23: Wake for constant viscosity model, for different viscosity values, from 0.005 to 0.00005 m²/s

In light of these observations, the following methodology is adopted to calibrate parameters to match the experiment as best possible:

- Firstly, the coefficient of friction is adjusted, with the aid of values published in the literature, the flume sidewalls being of glass and concrete. The coefficient is calibrated using the transverse profile of the vertically-averaged velocity.

- The inlet flow is then adjusted to calibrate the upstream flow velocity of the simulations to match the experimental upstream velocity.

- The minimum velocity value is subsequently adjusted by varying the values of D, then Cd, with the help of the transverse velocity profiles.

- The final step consists of adjusting the position of the minimum velocity relative to the TEC by varying the position of the latter and the value of L, whilst attempting to use values having a physical sense.

Before continuing, the following remark is necessary. The velocity scale on the preceding graphs is comprised between 19 cm/s and 24 cm/s; altering the parameters plays an influence, ranging from 1 to 2 cm/s, while the measurement precision, under optimum pitch conditions, is 0.25 cm/s. Compared to the velocities involved, in seeking to achieve errors of less than 5% of the total velocity, a high demand is being placed on the model. However, compared to a velocity deficit that is in the area of 5 cm/s, it is being sought to achieve errors below less than 20% lower.

3.3.2.4.2 Optimal parameter set

The set of parameters giving the best results as well as the corresponding velocity curves are provided in Figure 24. A good representation of the wake is reached with the two turbulence models; the transverse profile is not reproduced as well (by 1cm/s, which is still small).
Parameterisation is the same for the two turbulence models, with the exception of the imposed value for the inlet flow. The latter is adjusted so that the correct value is obtained for the velocity upstream of the TEC[4].
Cd is increased from the experimental 0.91 to 1.05, or a rise of 15%, which is lower than might have been expected. The area, A, over which the drag force is applied is centred at the downstream end of

---

[4] The transverse profiles being different for the two models of turbulence (notably due to the law of turbulence at the sidewalls that is specific to the k-ε model), to obtain the same upstream velocity at the turbine centerline, the inlet flows must be different.

the nacelle and is 2m long, which is 4 times the length of the turbine. The width of this rectangle is 30 cm, or half the diameter of the TEC; this is justified given that the TEC is not a solid disc. Finally, the constant viscosity is set to 5.10^{-5}, which is relatively low.

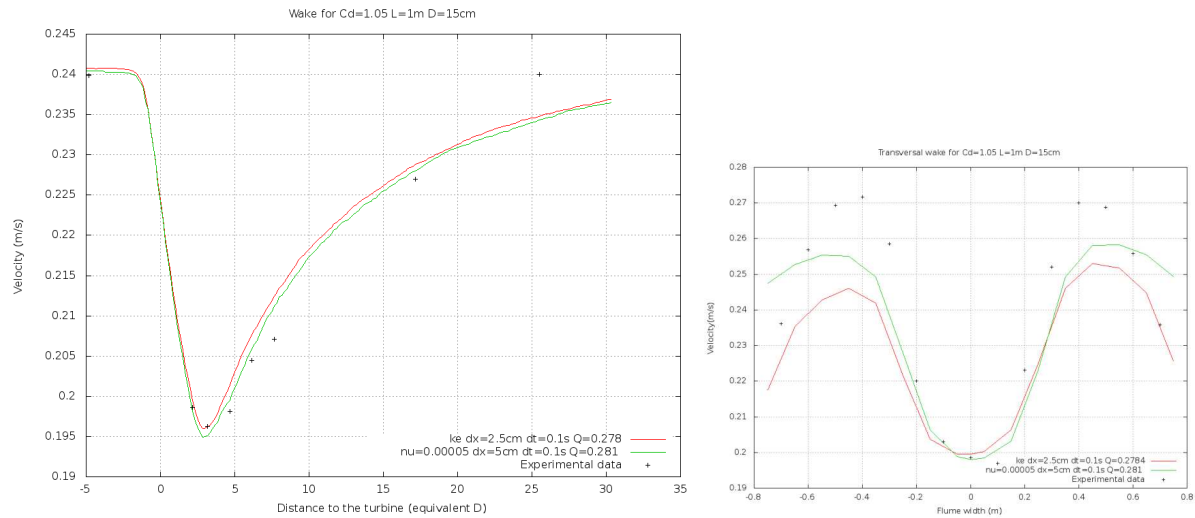**Figure 24: Longitudinal and transverse wakes for k-ε (red) and constant viscosity (green) models, for Cd=1.05, L=1m, D=0.15m**

3.3.2.4.3 Validation of mechanical energy variations

The simulations can be validated by looking at variations in mechanical energy, presented in Figure 25.

It is verified that energy decreases along the flume as a result of friction and that energy loss is greater at the level of the TEC, corresponding to:

$$\frac{\Delta E}{\Delta t} = -\frac{1}{2}\rho S C_d U^3$$

This is effectively the case for both turbulence models[5]. **Note that, this is here, a second verification of the subroutine DRAGFO.**

---

[5] In order to observe accurate variations, simulations must be launched using a small time step and a long run time. Although this has practically no influence on the velocity variations, the energy can vary considerably, notably as a result of the 1000 factor introduced by the volumetric mass of the water.
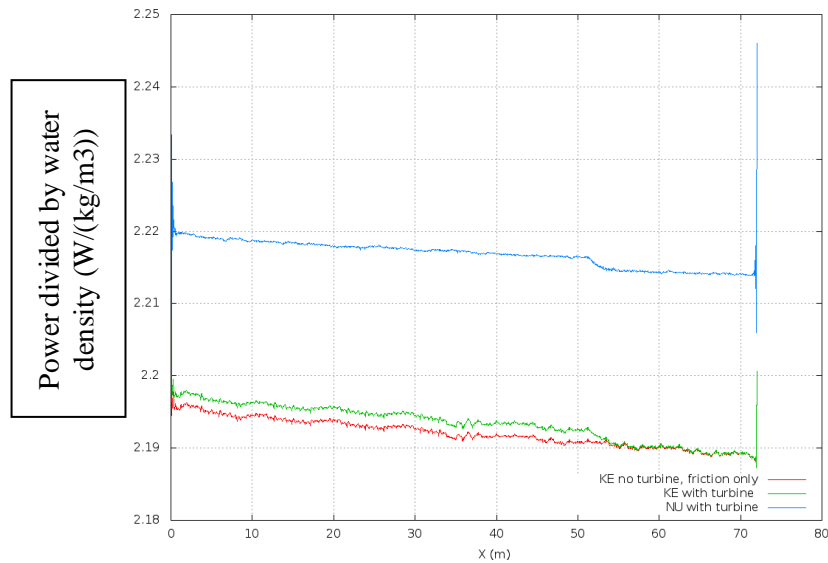
Figure 25: Power evolution divided by water density (W/(kg/m3)) for a fluid layer along the flume for constant viscosity model (blue) and k-ε model (in green or in red for the case without TEC)

3.3.2.4.4 Simulations for other operating regimes

Measurements of the velocity field were performed for four other TEC operating regimes as well as for turbine stoppage. As demonstrated by the Figure 26 curve, a different operating scheme (or different Tip Speed Ratio) corresponds to a different value for both the drag and power coefficients, resulting in a modified wake structure.

It may be supposed that a relationship exists between the measured Cd value and the Cd used in the simulation. As it was determined that, for the W3 regime simulations, an increase of 15% be applied to the measured Cd, it could be assumed that imposing a similar increase to the measured Cd values would allow adequate simulation of the corresponding wakes.

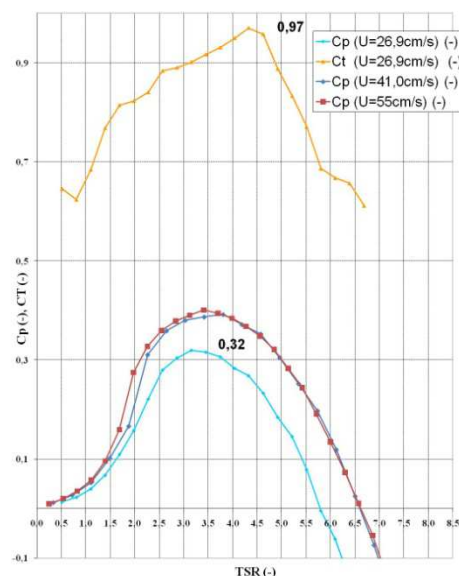| Operating regime	W1	W2	W3	W4	W5
TSR	1.5	2.5	3.5	4.5	5.5
Ct	0.78	0.88	0.91	0.97	0.77

Figure 26: Drag coefficient and power values as a function of TSR for Test n°1

The experiment results, however, contradict this hypothesis, as demonstrated by Figure 27. For example, the observed maximum velocity deficit is lower for Cd=0.77 and Cd=0.97 than for Cd=0.91. It is not possible therefore to find a simple relationship.
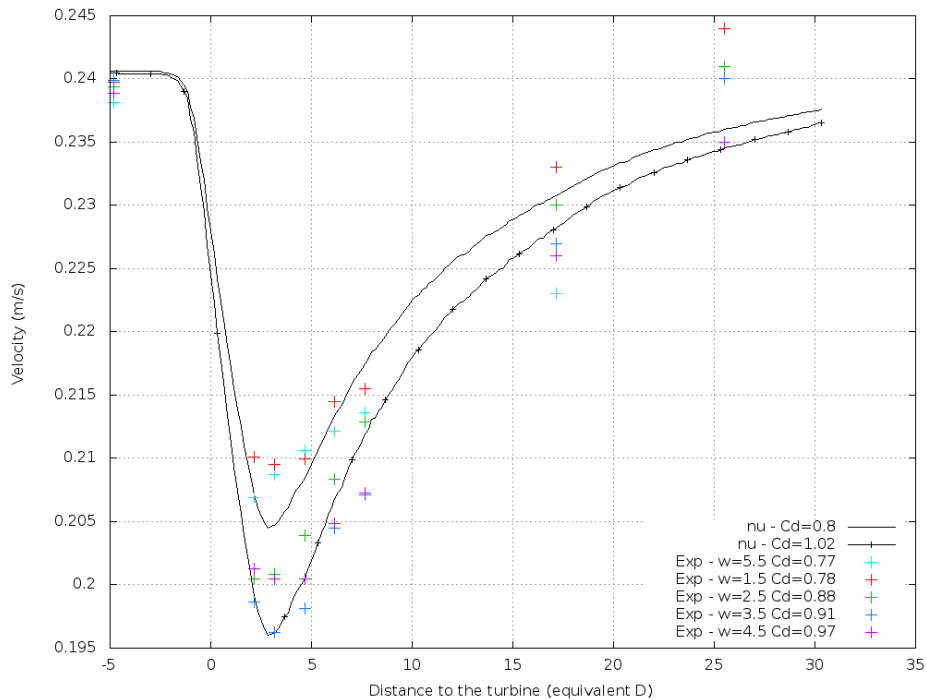
Figure 27: Simulated wake velocities for different operating regimes (colours) and Cd values (black)

There could be several explanations for these unexpected variations. They might be due, for example, to measurement imprecision or a problem occurring whilst measurements were performed, the orders of magnitude of the differences in velocity being only a few centimetres per second.

Nevertheless, the following is the more probable explanation. A priori, the drag coefficient varies in the opposite sense to the velocity deficit, which can effectively be seen in the simulations. In reality, though, the two curves are offset from each other, as illustrated by Figure 28. This figure provides an explanation of what is observed in Figure 27 for the w3 and w4 operating regimes: the velocity deficit is greatest for the smallest value of Cd.

Thus a complex relationship exists between the drag coefficient value and the wake velocity. The rotation of the latter, induced by TEC-rotation, together with complex recirculating fluid flow phenomena in the flume can intervene and modify the wake region.

This demonstrates a limitation of the model used, as illustrated in Figure 29. Actually, a Cd corresponds to a single wake in the simulations. In reality, as shown by Figure 29, a Cd corresponds to two TSR values and thus to two rotational velocities (U and D, these being moreover constant). Nevertheless, this is not true when Cd is close to the optimal value of the operating regime. Elsewhere, for two identical Cd values and although the same drag is applied, the turbine rotates much faster in the case of the higher. It seems logical, in this case, that the wake is different.

However, this is not a big issue for two reasons:

-The first reason is that near the optimal Cd, we observe that only one TSR corresponds to one Cd, so only one wake can be generated. However, the turbines are supposed to work around a Cd value close to the optimum case, and parameterization in this part of the study was based around this optimum case.

-The second reason is that when we look closely at the coordinate scale, it can be observed that the velocity deficit are very close to each other (about 5% of difference) for different values of the Cd coefficients (the range of variation of the Cd coefficients is about 20%).
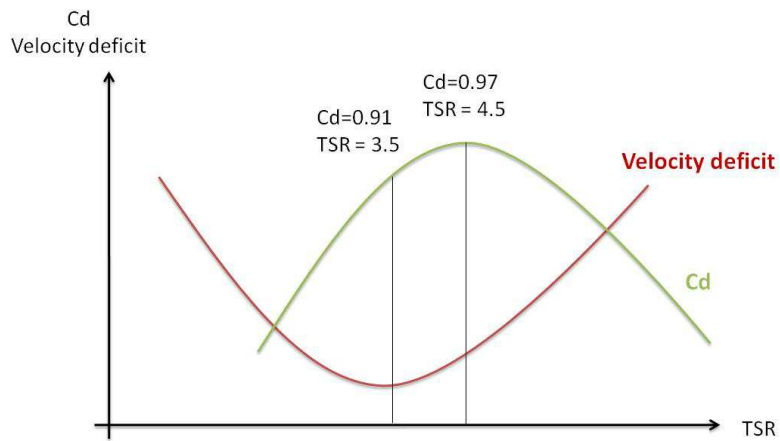
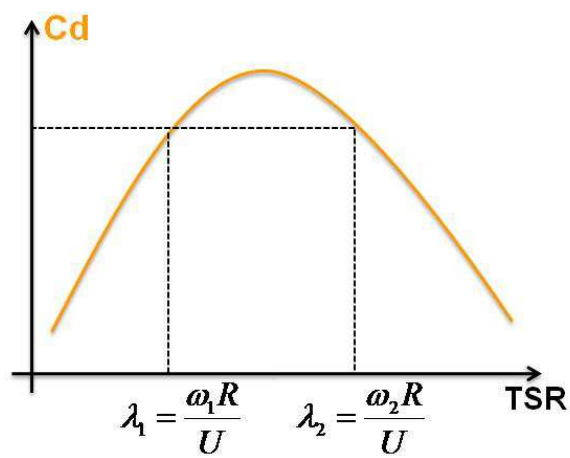**Figure 28: Schematic of the variations in Cd and velocity deficit**

Figure 29: Schematic of Cd as a function of TSR and demonstration of one of the model limits

3.3.2.5 DRAGFO enhancement: Turbulent kinetic energy production model

3.3.2.5.1 Identification of a shortcoming in the routine as it stands

As explained in paragraph 3.3.2.3.2, the DRAGFO routine doesn't generate turbulence since the obstacle is not meshed. However, looking at the variations in turbulent kinetic energy 'k', illustrated by the red line in Figure 30, a decrease in k (which follows the variations in velocity) is noted, whereas in reality there is a strong increase in k.

Where the k-ε model is being used, this problem can be resolved by adding a production term to the equations for k and for ε.

3.3.2.5.2 Addition of a turbulent production term in the k and ε equations

This production term is added to the equations for k and ε, by modifying the Fortran KEPSIL routine. The turbulent production only takes place at the turbine level; it is decided therefore to add the term over the area 'A' already used in DRAGFO.

The new production term for the turbulent kinetic energy, at a node, is the following:

$$ \eta \times \frac{1}{2} C_a S U^3 \times \frac{1}{Ah} $$

In the equation for the dissipation ε, the term must be multiplied by $C_{1\varepsilon} \frac{\varepsilon}{k}$.

The right side of the above formula corresponds to the energy extracted from the flow using the DRAGFO routine. The inclusion of a coefficient η is naturally consistent because only part of the energy extracted from the flow by the turbine is dissipated through turbulence; the rest is converted into thermal energy by friction, into mechanical energy for the turbine or else dispersed by wake shear.

3.3.2.5.3 Results of the simulations

Figure 30 and Figure 31 present a comparison between experimental measurements of k and the simulations, as well as illustrating the effect of the production term on the velocity. A value η equal to 0.05 enables accurate reproduction of the variations in k[6]. A simulation without using the KEPSIL routine was run with bathymetry added at the TEC level in order to represent the obstacle, which also generated turbulence (blue line).

On first observation, it is clear that the use of the KEPSIL routine or the addition of the bathymetry allows retrieving correct values for the variation of k: at the TEC level, the turbulent kinetic energy increases rather than decreasing as was previously the case.

---

[6] The higher the value of η, the higher will be the production of k occurring at the level of the TEC. Taking η equal to 0.05 allows a better following of the experimental results.
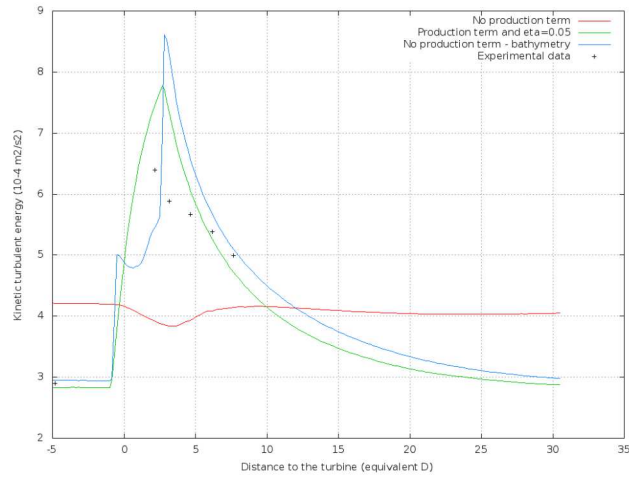
Figure 30: Turbulent kinetic energy along the flume with (blue and green lines) and without (red line) production term for k and ε
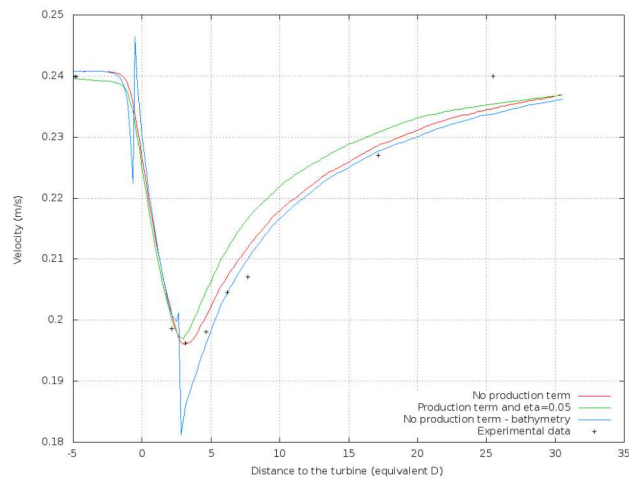
Figure 31: Velocity along the flume with (blue and green lines) and without (red line) production term for k and ε

As shown above, the variations in k have only a slight influence on the velocity variations. This slight variation reflects the experimental results: when there is an increase in turbulent intensity (or turbulent kinetic energy), the upstream flow velocity is recovered more quickly due to increased velocity mixing [3].

In summary, knowing the upstream value of k enables us to more precisely adjust the coefficient of friction used in the simulations. In a simple flume, turbulence is only generated by the bottom and sidewall friction. Consequently, the coefficient is set so that the upstream value of k is calibrated to the experimental value, giving: Cf=140 (Strickler coefficient).

3.3.2.6 Conclusions for part B

Owing to the simulations and the parameter adjustments carried out for the different tests (low and high velocities, weak and strong turbulent intensities, see also appendix 8.5) and different operating regimes, appropriate parameters are now known for a large range of flows. These are summarised in the table provided in Appendix 8.4.

Some of the conclusions facilitate the use of the model, whereas others complicate its use: it became apparent, amongst other factors, that it is difficult to adjust the simulated Cd on the basis of the experimental Cd because complex phenomena come into play. Nevertheless, this is not a big issue around the optimal Cd, since only one TSR correspond to one Cd, so only one wake can be generated and therefore the parameterization is easier. Furthermore, the turbines are supposed to work around a Cd value close to the optimum, and parameterization in this part of the study was mainly made around the optimum.

In the case of the experiment, turbulent intensity has the effect of shortening the wake, but this is not necessarily reproduced with the correct order of magnitude in the current TEC model. It is however difficult to investigate this aspect in further depth in Telemac-2D.

3.3.3 Conclusion for parts A and B

The aim of this part was to build and validate a model of the TEC in Telemac-2D in order to eventually simulate a large-scale farm. Due to the large scales involved, 2D modelling is preferred in order to reduce the computation cost. As it is impossible to represent in a Telemac-2D mesh a rotating TEC, this led to modelling the latter using a drag force and a production term for turbulent kinetic energy[7], all of which are brought together in two Fortran routines, namely DRAGFO and KEPSIL.

Initially, the Telemac-2D numerical options were tested using the study of flow around a cylinder (represented by an island in the mesh) as a basis and those that were the most appropriate for this study were selected. A convergence study was also conducted, which led to caution being taken with respect to the mesh sizes and time-steps used for the study. To better understand the behaviour of the code when Δx and Δt decrease, a study of numerical error generated during computations is currently underway.

The flow around a cylinder is then simulated using the model evoked previously and based on the application of a drag force and a turbulent production term (at this stage, the cylinder is no longer meshed). The velocity along the wake centerline is reproduced well, which validates the pertinence of the representing an obstacle in Telemac2D as a drop in energy.

The assumption is then made that the model is also valid for a TEC-type obstacle. It is used to simulate an experiment carried out at the LNHE installation: flume flow around a TEC. By using previous conclusions and adjusting various model parameters, it is possible to achieve adequate reproduction of the experimental wake, especially near the optimal Cp value.

The experiment was carried out for different operating regimes and flow configurations, which should enable us to generalise the model application and avoid the need to calibrate all parameters for each new case. At present, it is possible to simulate these different wake structures choosing the appropriate set of parameters, but it is not possible to generalise this parameter setting, especially far from the optimal operating regime. Near the optimal regime, where roughly one Cp corresponds to only one TSR, the 2D modelling is necessarily easier since only one wake can be generated and this part of this study can be helpful for the parameterization in this case.

---

[7] Addition of the production term for turbulent kinetic energy is only possible in the case of the k-ε turbulence model.

3.3.4   Part C: Validation with several tidal turbines

This part of this report describes the procedures and results of a 2-dimensional model of two varying alignments of tidal turbine arrays and how this work builds off previous work done under the ETI's tidal energy directive.

The goal of this section and modeling exercise is to create a robust 2-dimensional model of a tidal turbine array in a laboratory setting that can be scaled up and applied to an actual oceanic landscape in the Pentland Firth and other potential installation points in Northern France and Scotland. In the first step of the modeling process, the turbine array is modeled by individual units for each turbine. This 2-d model strives to represent two experiments carried out in the laboratory at University of Manchester by mimicking the experimental set-up and matching the velocities measured at varying distances downstream of the turbine arrays. The first iteration of the model represents each turbine in the array individually, and the second mimics the energy loss associated with the first case to represent the array as a single body in the flow. In this way, the far-field wake of each version of the model will be near identical.

The 2-d models created for this report is also compared to the 3-d models created by the University of Edinburgh (UoE) to achieve a second method of validation and provide an additional platform for error analysis. This comparison was made by matching the downstream wakes of the Telemac 2-d models with the Code Saturne 3-d models, and comparing the energy losses found in each model due to the tidal array.
Analysis at each step of the process was made to maximize model accuracy and input parameter variations with a constant goal of making realistic conclusions.

Summary of Methodology:

The University of Manchester conducted a series of experiments in a laboratory flume measuring the energy extraction and down-stream wake characteristics of tidal energy turbines in different array alignments. The data recorded during these experiments provides the basis from which the numerical model in Telemac 2-d was created and compared to. The UoM experimental data can be found in the shared PerAWaT folder.

Manchester Experiments 19 and 20 were selected by EDF, UoE, and UoM to model numerically in 2 dimensions. Each of these experiments feature two rows of tidal energy turbines, but the number of turbines and inter-row spacing is different in each case.
Experiment 19 features 2 rows of 5 turbines with 8-Diameter inter-row spacing and 1.5-Diameter spacing between the centers of adjacent turbines (see **Figure 32**). It was chosen because of the symmetric alignment of each of the rows so that a numerical model of this alignment can be extrapolated to feature the desired number of turbines. The large number of turbines (relative to the other experiments) also limited the impact that edge effects would have on the results and provide a clearer look at what occurs downstream of a symmetric array of turbines.
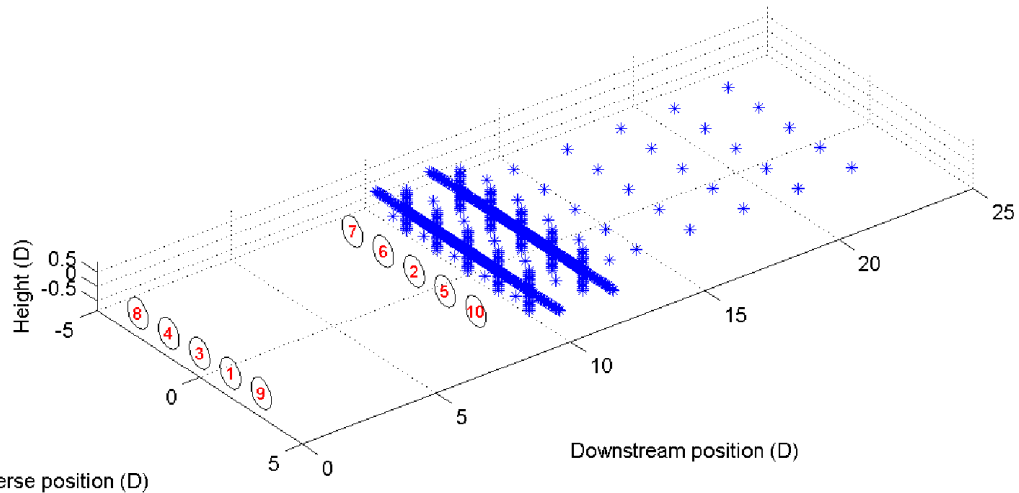
Figure 32: Test 19 configuration (tidal turbines are represented by the numbers inside the circle) and UoM measurement points (in blue). See Appendix A of PerAWaT WG4 WP2 D5, page 8.

Experiment 20 features a front row of 3 turbines and a second row of 4 turbines 4-Diameters downstream (see **Figure 32**). The results from this non-symmetrical, staggered alignment of turbines are compared to the symmetric alignment in respect to downstream wake effects and energy extraction. This was the largest number of staggered turbines in a two-row configuration observed by UoM which will make it easier to expand to model a larger number of turbines in a similar alignment.
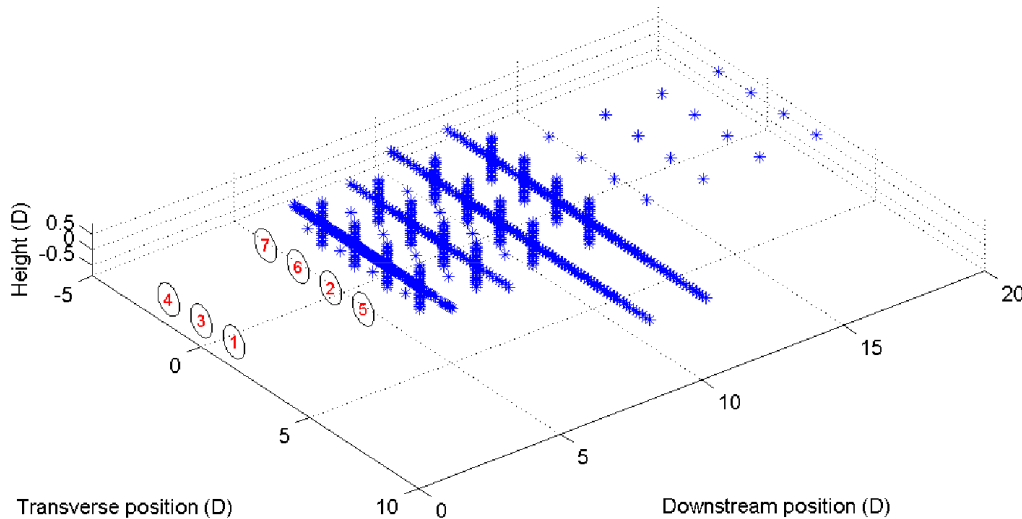

Figure 33: Test 20 configuration (tidal turbines are represented by the numbers inside the circle) and UoM measurement points in blue (see Appendix A of PerAWaT WG4 WP2 D5, page 8).

3.3.4.1 The Model Flume

The numerical flume was constructed in order to most accurately model the 12mx5m flume employed in the UoM experiments. As performed in the UoM flume, the inflow velocity was held constant in the numerical flume, and the outflow was controlled by maintaining a constant height along the back boundary of the flume. The numerical flume was lengthened upstream of the turbines to allow the inflow velocity to become uniform across the width of the flume. This was accomplished with a weir in the UoM experimental flume. The numerical flume was also lengthened downstream of the turbines to allow the array wake to return to normal flow patterns and reach the flume exit at a uniform velocity across the width. This limits the potential effects of numerical errors occurring due to varying speeds across a boundary layer in the Telemac 2-d software. The extended length of the flume will improve analysis and comparisons of the long-field wake energy assessments as a part of the model analysis.

The numerical flume is therefore 67 m x 5 m, but the inter-row and inter-device spacing within the array of turbines and velocity measurement locations remain unchanged relative to one another (and identical to the University of Manchester alignment). A mesh size of 5cm was chosen to most accurately capture the variance of the cross-width velocity profiles for comparison against the UoM measurements. This mesh size is close to the optimal mesh size found in part B of the validation study. Mesh sizes of 1 cm, 2 cm, 7.5 cm, and 10 cm were also attempted (this test for small mesh size is only in a reduce scale model and around the turbines).

The inflow volume flow rate was established in an empty numerical flume so that at a distance 6.12 meters upstream of the first row of turbines (the distance from the start of the UoM flume to the turbine location), the velocity was a near uniform 0.46 m/s across the width of the flume. At this point, the model turbines were added to the flume.
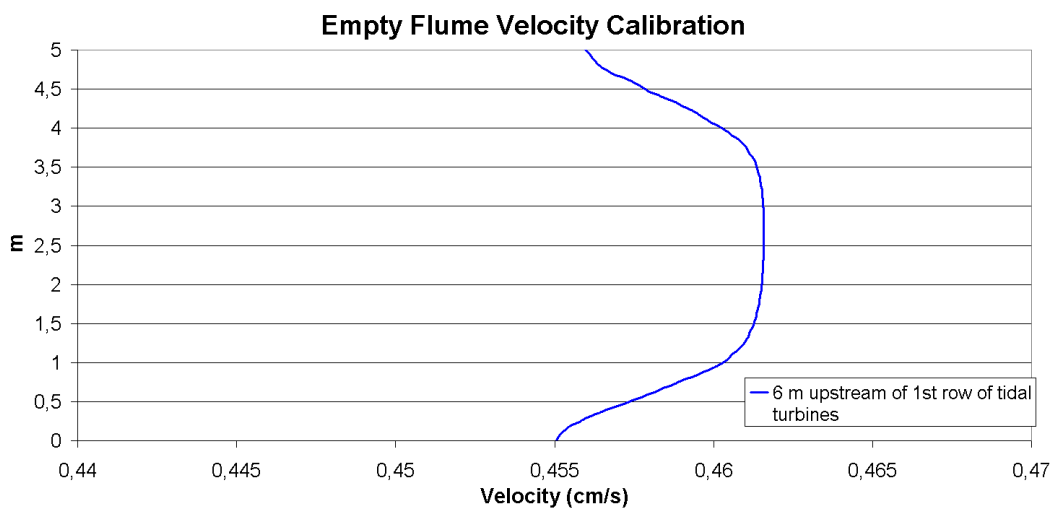

Figure 34: Empty flume Velocity Calibration: Calibration measurements taken 6 m upstream of front row of turbines in the Telemac model to imitate the inflow speed to the UoM flume, also 6.12 m upstream.

The Model Trials:

In this section Ct and the drag coefficient Cd are the same values because the same UoM notations are used.
The turbines were modeled in this 2-dimensional simulation by several rectangular boxes that mimics the energy loss from the flow caused by each turbine. The Coefficient of Thrust (C_t) for each turbine was measured at each turbine-location in the UoM experiments and applied to the rectangular box in the corresponding location in the numerical model (Ct and the drag coefficient are the same values. The same UoM notations are used). However, as it has already been said, modeling the TEC on the unique basis of load loss, fails to take full account of the energy losses. In practice, three sources of energy loss can be identified:

– Extraction of energy from the fluid by the turbine, due to the drag force (pressure (or form) drag and friction drag) as well as the thrust force.

– Energy losses caused by wake shear (due to wake rotation as well as the velocity gradient induced by the latter).

– Energy loss due to turbulence generated by the turbine.

Because the TEC is not meshed, DRAGFO only takes account of the first source of energy loss; the two other are not modeled (moreover, Telemac2D makes average on the vertical). Consequently, a change in the Cd value is therefore expected to take the latter into account.

For these reasons, it was known that the Cd measured in the UoM experiments would be an underestimation, and necessary to increase Cd slightly in order to duplicate the UoM experimental results with the numerical model.

The objective of the model was to match the velocities produced by the Telemac representation to the velocities measured by ADVs in the UoM flume by changing the Cd values of the turbines. Each turbine in the experiments had a different Cd, however, because the experiments held the Tip Speed Ratio for each turbine constant. It was therefore necessary to change the Cd value for each turbine by the same ratio in order to maintain an accurate model of the relative drag coefficients across the array.

Telemac2d models were executed using two different turbulence models. The two different turbulence models used were the 'constant turbulence model' (also referred to as the constant viscosity model, or the CV model) and the 'k-epsilon model of turbulence' (the KE model). These two models (also studied in part A and B) were selected for their accuracy and robustness as well as past success when utilized during similar, past research efforts (in part A and B). The coefficient of diffusion of the velocity was varied in the constant turbulence model from 0.01 – 0.00001 in an attempt to find the closest match to the experimental data from University of Manchester. A velocity diffusion coefficient of 0.0001 was decided to be the final values used for the constant viscosity model. This model's shortcomings are that it cannot accurately represent the decay in turbulent intensity as the water flows down-stream of the hydro-turbines. The k-epsilon model calculates the turbulence at many places as the water continues downstream. Its shortcomings are numerical errors that can be propagated through the canal as the water travels, but its results have generally been more accurate than the CV results in similar past applications.

The Reynolds number of the flume compared to the turbine diameter is $Re_D = 1.242 \ 10^5$, which is very close to the RE_D of $1.62 \ 10^5$ used in the Dragfo experiments modeling the EDF single turbine case. As explained with Figure 3 earlier in this report, it can therefore be assumed that the Dragfo program will not experience a lot of error due to a change in flow regime as both Reynolds Numbers fall in the feature a fully turbulent vortex sheets.

3.3.4.2   Results/ Procedural Summary

Results Step 1, calibrating the Turbine Scale Model:

- The initial Cd values used in this modeling process were found in the UoM Processed data folder in the PerAWaT project shared folder. As stated above, the initial input C_d was known to be an underestimation of the drag exerted by the turbine and its casing system. Initial models with these preliminary values did indeed reveal an underestimation, and the wake downstream was not adequately equivalent to the University of Manchester experimental findings. As expected, the wake intensifies as the amount of energy extracted from the flow increases due to raising the C_d. In the end, a C_d ratio of 3:1 was found between the numerical model C_d and the measured values for the isolated turbines in the UoM experiments. The cause of this factor 3 is mainly due to the fact that we used the local velocity instead of the far velocity to compute the drag force (this was done to reduce computational time). When the local velocity is used for the simulation, the equivalent Cd is theoretically multiply by a factor equal to (Vref/Vlocal)², where Vref is the far velocity. For those simulations, we have found that, the multiplication factor is theoretically around 2.7. Here, a multiplication factor of 3 is used, which increase the theoretical value of Cd by about 10% (and then we have the same kind of increase that the one found in part B).

Summary of Results Format:

Included in the results section for each experiment are graphs of each measurement location downstream displaying the mid-depth velocity profile measured by 3 ADVs in the UoM laboratory in pink, red boxes showing the depth averaged velocity measured by UoM, the Telemac2D results for the

constant viscosity model in blue, and the Telemac2D results for the K-epsilon viscosity model in green. A flume-length view and a zoomed view on the turbine locations displaying the water velocity also accompanies the results of each experiment.

The depth averaged UoM results are larger in magnitude than the mid-depth velocity profile. This is expected as the turbines are situated at mid-depth and the velocity downstream at mid-depth will be lower than the depth-averaged value. The distance between these two measurements decreases as the flow progresses downstream of the turbines. The Telemac2D model outputs depth-averaged velocity, and therefore the measurements represented by the red boxes in the graphs were the points of focus while trying to calibrate the Telemac model.

It is difficult to utilize any error term calculated between the Telemac2D model and the UoM experiments. First, some of the UoM experimental measurements from two different ADVs at the same location recorded sometimes drastically different values. In addition, only 6 points of depth averaged data exist that can be directly compared to the depth-averaged Telemac2D model results. Additionally, the near-wake limitations of modeling turbine wakes has been well documented, and validating results with just 2 measurement series downstream of 4D between the two experiments is difficult and risky given the lack of data.

3.3.4.3 Experiment 19

The 10-turbine experiment only contained velocity measurements until 4D downstream of the turbines. The 2-d model has shown limited accuracy inside of 5D or 6D downstream of the device in previous experiments performed in a flume at EDF, as it has been shown before. Additionally, increased variability of the experimentally observed velocity measurements inside of 6D further compound the inherent error present in any comparisons made at these distances downstream. Therefore, the results of the model 4D downstream will hold more weight than those 2D downstream in experiment 19.
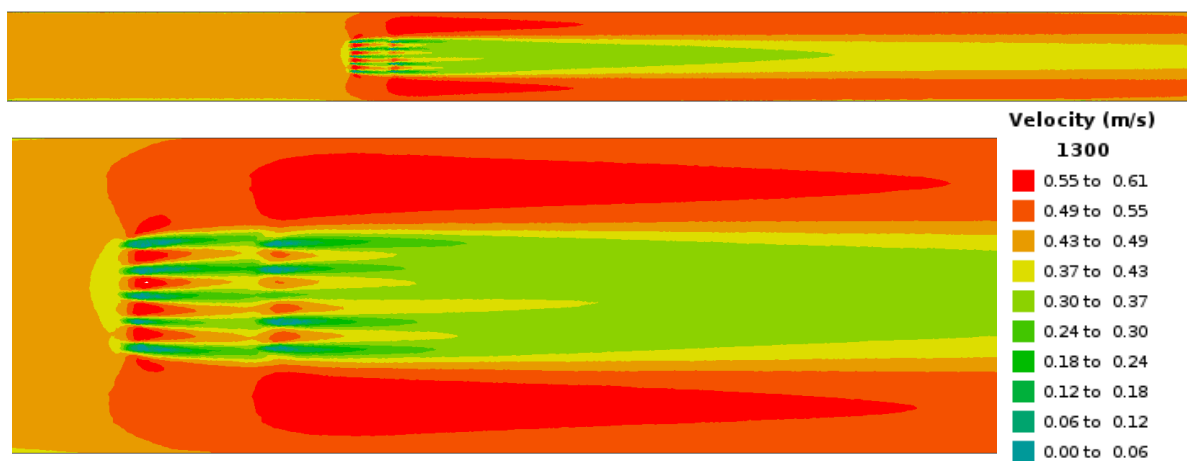

Figure 35: Experiment 19 Velocity Schematic. Full length of flume and zoomed view.

Due to the fact that the Cd values of the turbines are not exactly the same and slight variations in the propagation of the calculations downstream in the non-uniform mesh, the results are not exactly symmetrical.
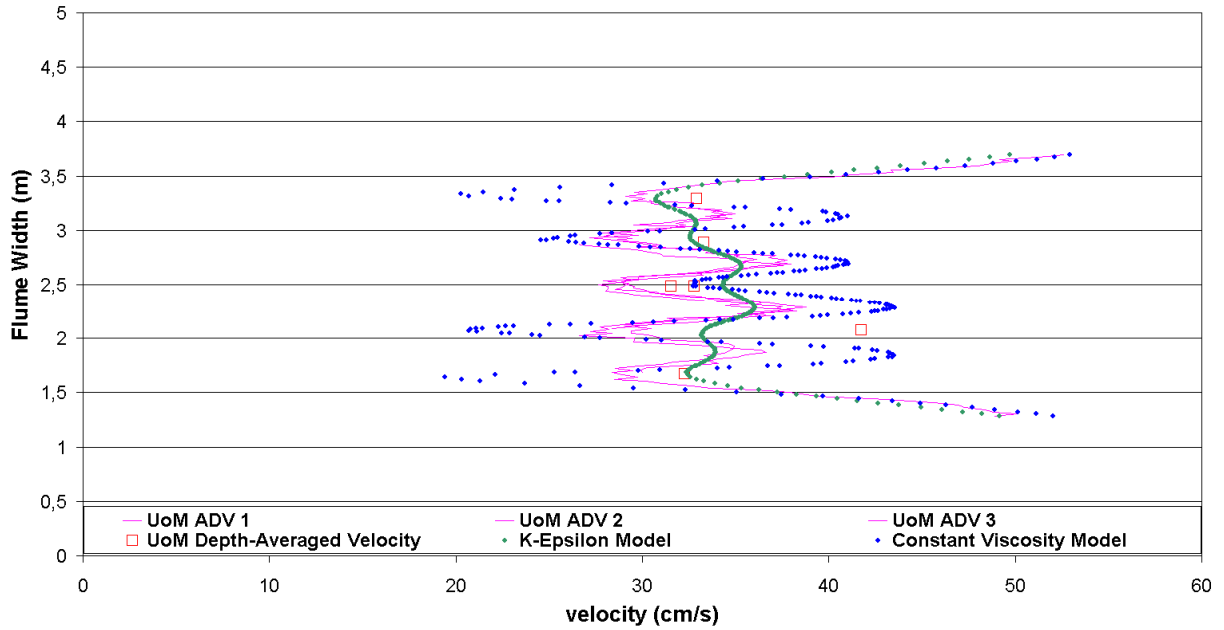
Figure 36: Experiment 19 Velocity Profile, EDF Telemac2D model compared to UoM data at 4D downstream of final row of turbines. ADV's 1-3 represent the time-averaged, mid-depth velocities in the UoM flume. The six locations of UoM depth-averaged velocity measurements are represented by the red squares. The final two curves are the Telemac2-d k-epsilon and constant viscosity models.
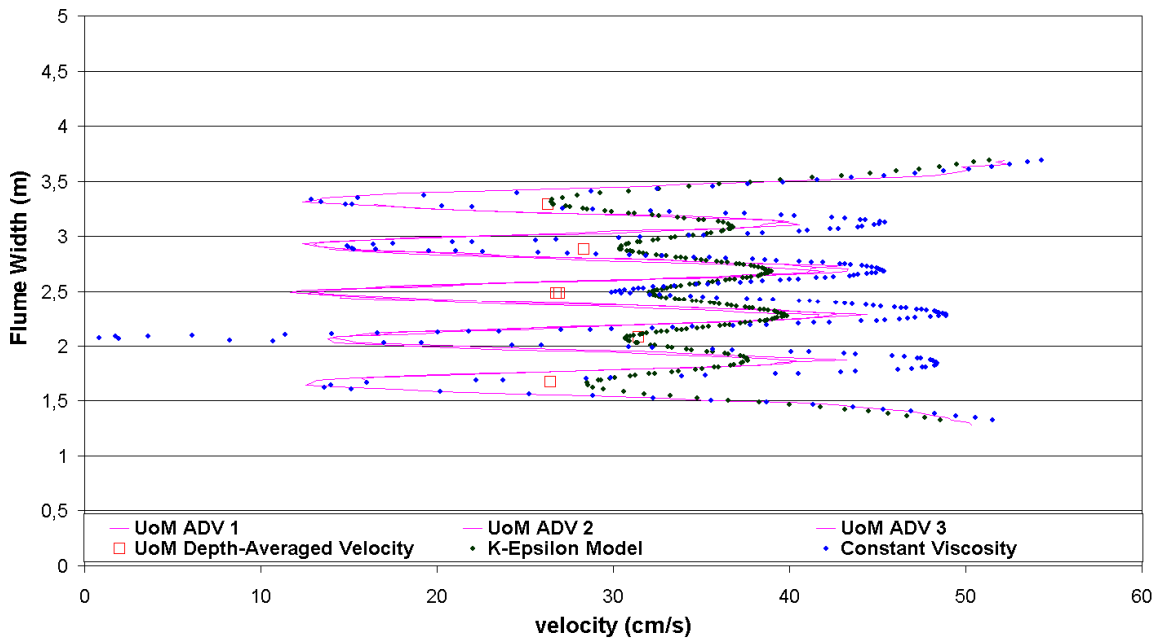

Figure 37: Experiment 19 Velocity Profile, EDF Telemac2D model compared to UoM data at 2D downstream of final row of turbines. ADV's 1-3 represent the time-averaged, mid-depth velocities in the UoM flume. The six locations of UoM depth-averaged velocity measurements are represented by the red squares. The final two curves are the Telemac2-d k-epsilon and constant viscosity models.

The K-Epsilon and the constant viscosity models lead to different results: the mean of the velocity are similar but the variance of the velocity for the constant viscosity is greater and then closer to the experiment. However, it is easy to see the error present at distances 4D downstream of the turbines. Therefore, we suggest to focus our attention on the comparison made with experiment 20.

3.3.4.4 Experiment 20

The 7-turbine experiment contains velocity measurements at 2D, 4D, 6D, & 8D downstream of the second row of devices. This allows for the velocities of the model and the experiment to be compared in the regions where the model's accuracy is sufficient to mirror the experimental results. Just as in Experiment 19, more weight will be placed on the depth-averaged measurements further downstream of the turbines as the flow in both the model and the Manchester experiments exhibit higher consistency and reliability of measurements.
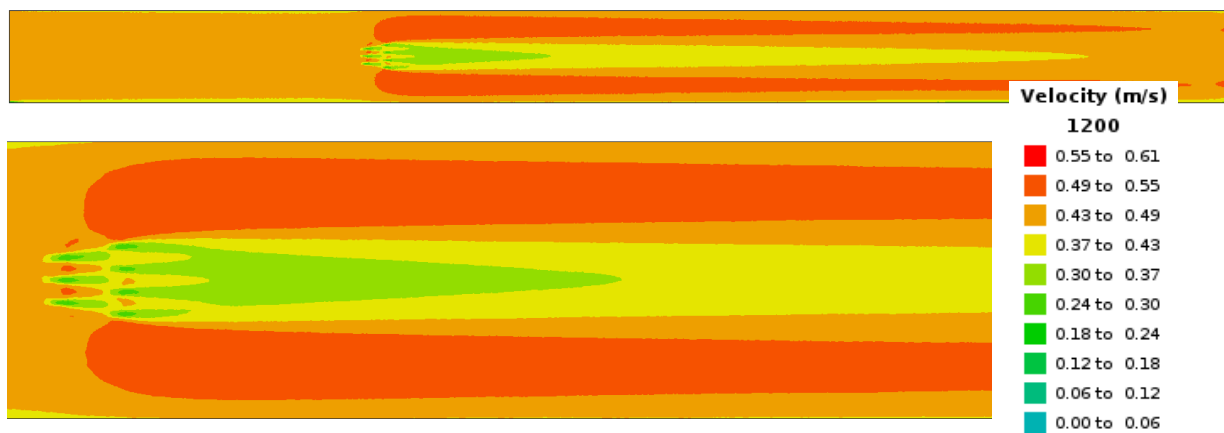

Figure 38: Experiment 20 Velocity Schematic. Full length of flume and zoomed view.

Just as was found in Experiment 19, the model results are not exactly symmetrical due to the fact that the Cd values of the turbines are not exactly the same and slight variations in the propagation of the calculations downstream in the non-uniform mesh.

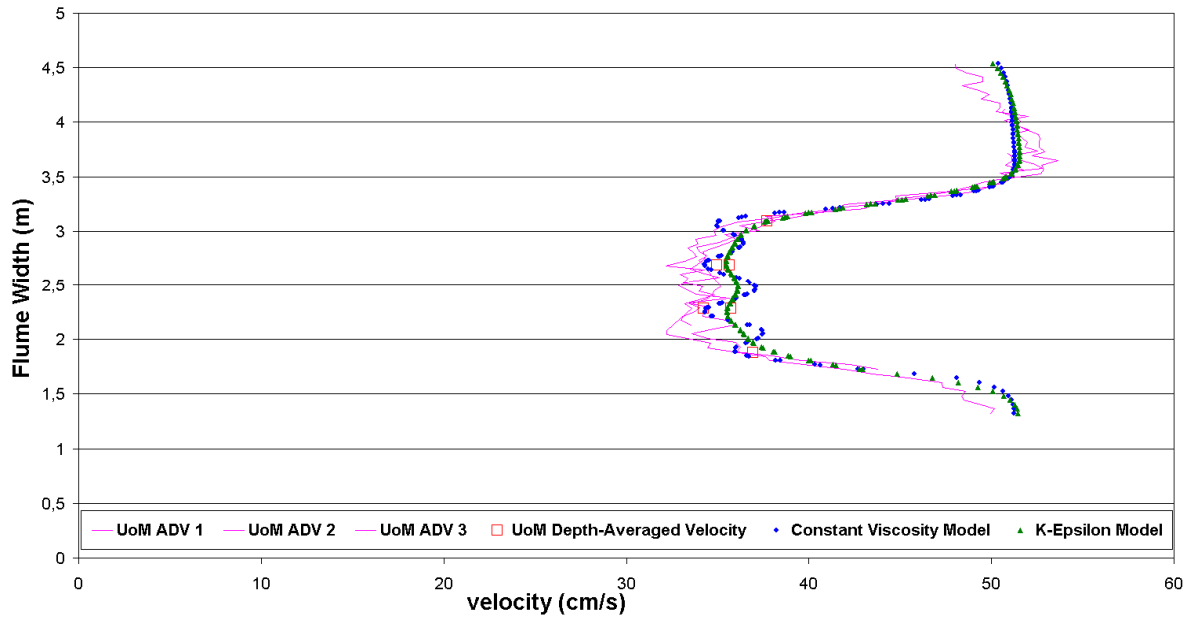**EXP. 20 8D Downstream Depth Averaged Velocity Profile**

Figure 39: Experiment 20 Velocity Profile at 8D downstream. ADV's 1-3 represent the time-averaged, mid-depth velocities in the UoM flume. The six locations of UoM depth-averaged velocity measurements are represented by the red squares. The final three curves are the Telemac2-d k-epsilon and constant viscosity models.

EXP. 20 6D Downstream Depth Averaged Velocity Profile

Figure 40: Experiment 20 Velocity Profile at 6D downstream. ADV's 1-3 represent the time-averaged, mid-depth velocities in the UoM flume. The six locations of UoM depth-averaged velocity measurements are represented by the red squares. The final three curves are the Telemac2-d k-epsilon and constant viscosity models.

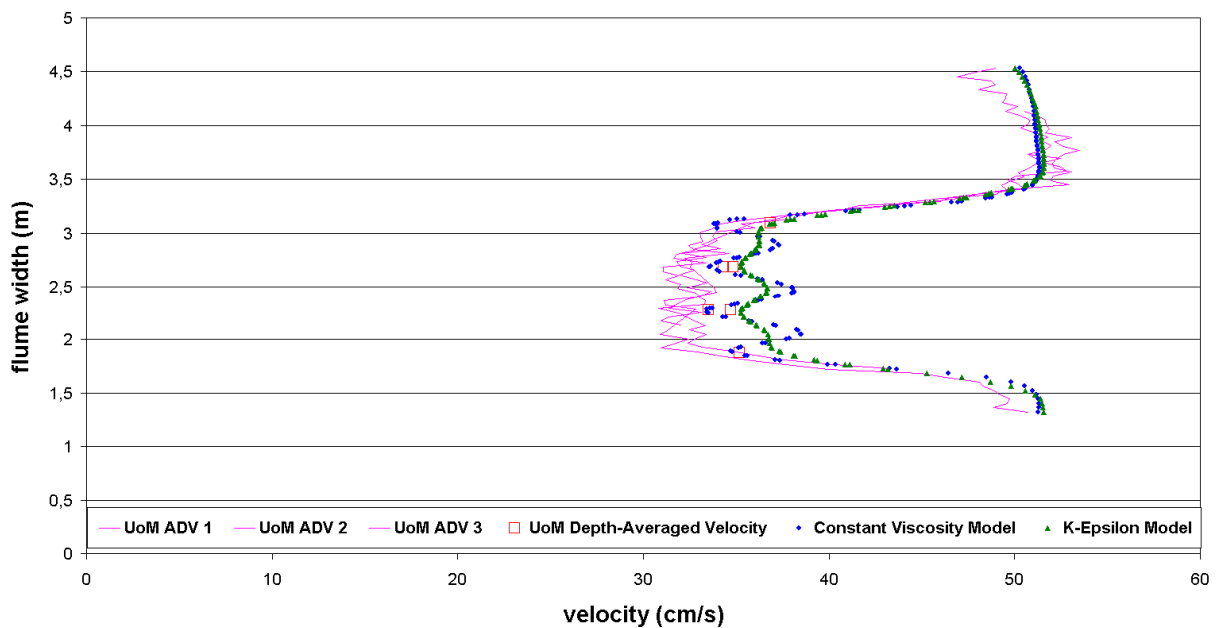## EXP. 20 4D Downstream Depth Averaged Velocity Profile

Figure 41 : Experiment 20 Velocity Profile at 4D downstream. ADV's 1-3 represent the time-averaged, mid-depth velocities in the UoM flume. The six locations of UoM depth-averaged velocity measurements are represented by the red squares. The final three curves are the Telemac2-d k-epsilon and constant viscosity models.

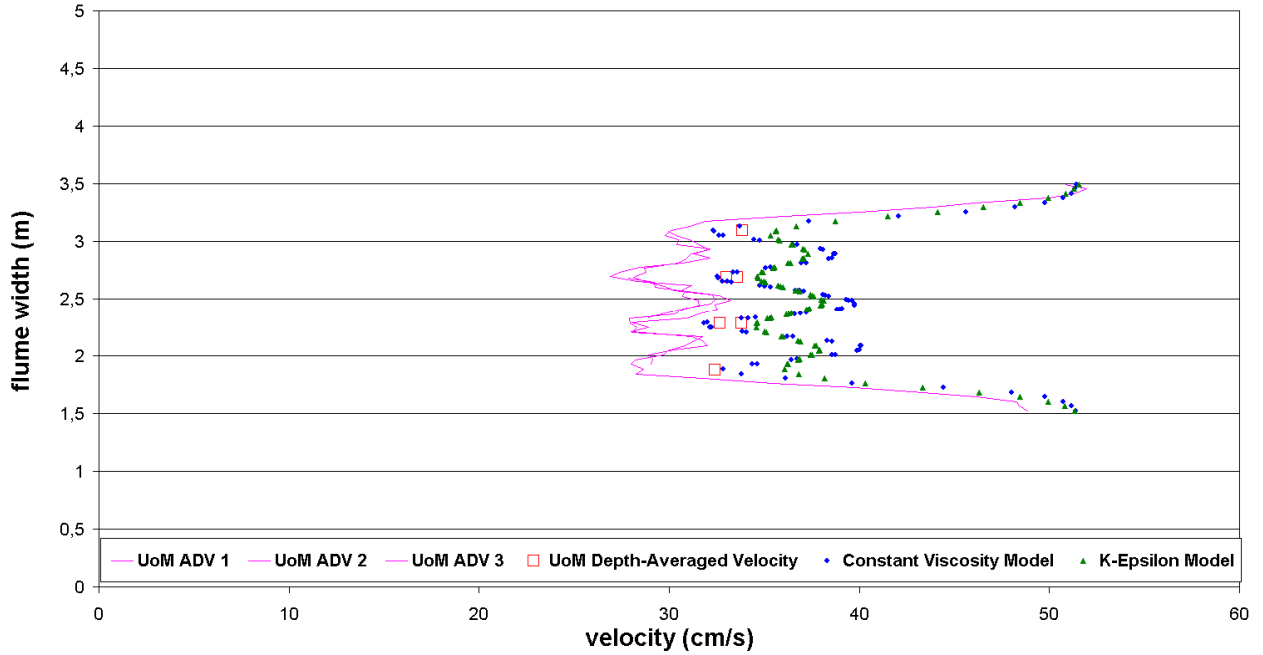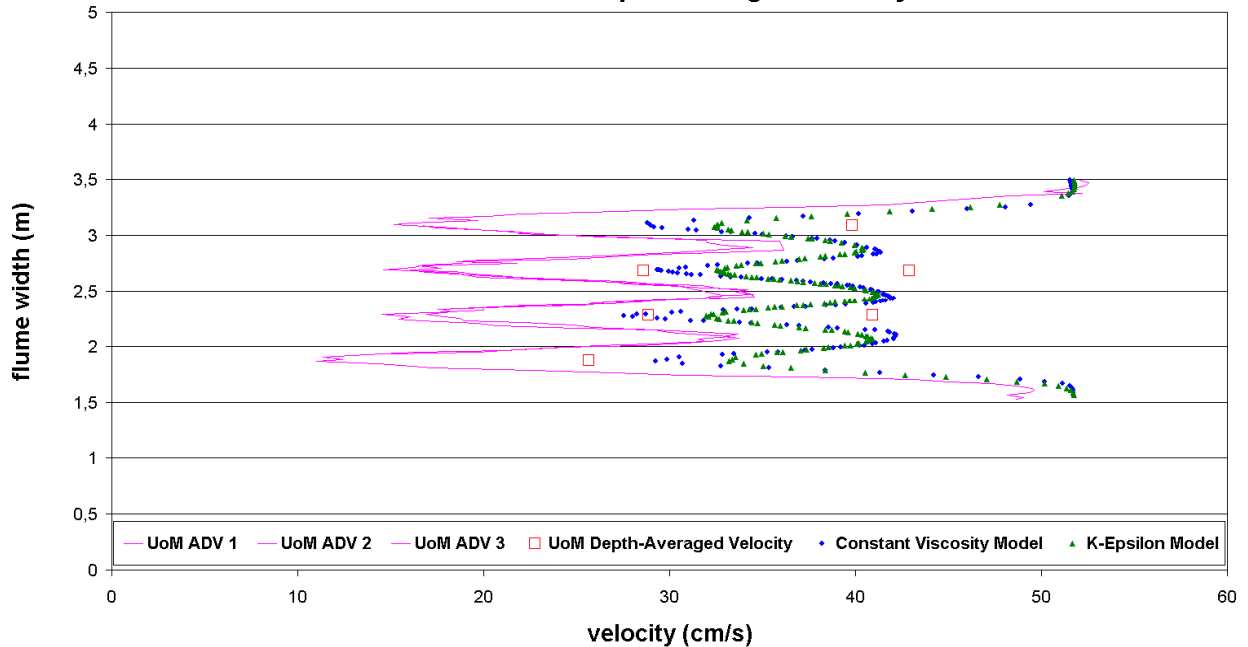## EXP. 20 2D Downstream Depth Averaged Velocity Profile

Figure 42: Experiment 20 Velocity Profile at 2D downstream. ADV's 1-3 represent the time-averaged, mid-depth velocities in the UoM flume. The six locations of UoM depth-averaged velocity measurements are represented by the red squares. The final three curves are the Telemac2-d k-epsilon and constant viscosity models.

For those simulations, the calculation of the drag force has been made using the local velocity (near the turbines) and not the far velocity. As it is already explained, when this local velocity is used for the simulation, the equivalent Cd is theoretically multiply by a factor equal to (Vref/Vlocal)², where Vref is the far velocity. For those simulations, we have found that, the multiplication factor is theoretically around 2.7. Here, a multiplication factor of 3 is used, which increase the theoretical value of Cd by about 10% (so this is the same kind of increase that the one found in part B).

Turbine numbering scheme can be viewed in Table 11.

Turbine #	C_d UoM	C_t Telemac
1	0.76	2.28
2	0.61	1.83
3	0.76	2.28
4	0.76	2.28
5	0.73	2.19
6	0.675	2.025
7	0.675	2.025

Table 11: Experiment 20 Cd values, multiplication factor of 3.

By using the far velocity instead of the local velocity, and then with a multiplication factor equal to 1, we have found for example the following profile 8D downstream.
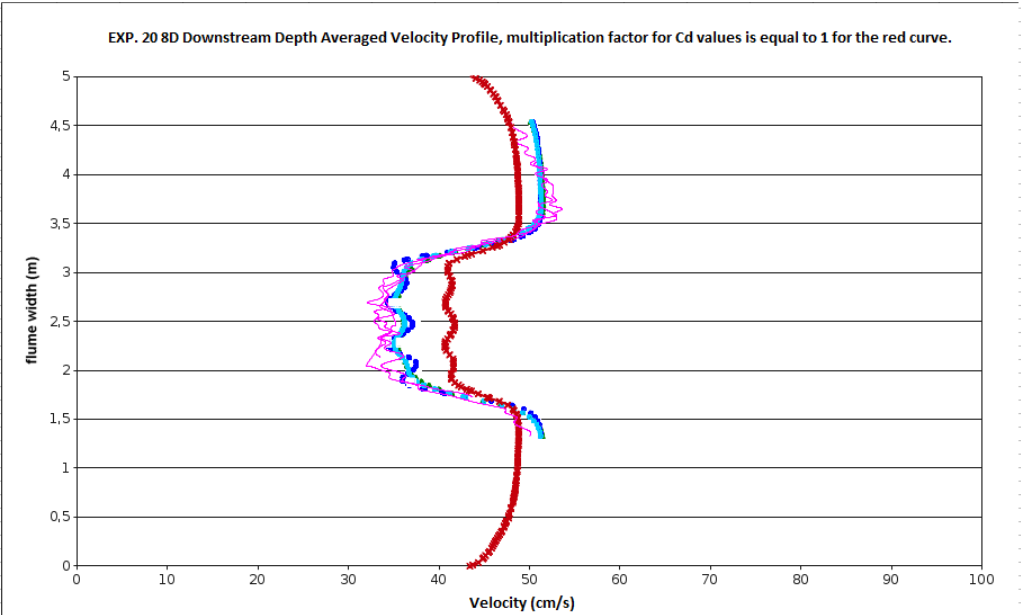

Figure 43 : Experiment 20 Velocity Profile at 8D downstream. ADV's 1-3 represent the time-averaged, mid-depth velocities in the UoM flume, in pink. The red curve is obtained by using the far velocity (the multiplication factor is 1), and the blue one with the local velocity (the multiplication factor is 3). Both simulations are made with the constant viscosity model.

As it can be seen in **Figure 43**, the red curve is closed to the blue curves, there is about 15% of difference, and this difference is localised at 8D. Therefore, at a greater distance downstream (and that is what is important), typically 20D, the difference will be even smaller. For this reason, we recommend to use the far velocity, with a multiplication factor of 1 on the drag coefficient, to compute the drag force for large scale simulations. The local velocity has been used here only to reduce the computational time.

Results Step 2: Calibrating the Array Scale Model

Once the velocity profile of the numerical model was matched with the experiment, the net power loss due to the turbines was calculated by a post-processing FORTRAN program to find a global coefficient of thrust of the entire array. This global C_d is then applied to the large scale representation of the array and calculated using the following equation:

$$(½)\rho C_d U_{ref}^2 A U_{local} = (\Delta E/\Delta t)$$

where ρ is the density of water (1000 kg/m^3); C_t is the coefficient of thrust (the unknown); U is the flume-length-wise velocity (0.46 m/s, the far upstream velocity); Ul is the mean velocity on each node which defined the turbines; A is the combined areas of the turbines in the cross-section of the flume (0.572 m^2 for Experiment 19, and 0.401 m^2 for Experiment 20); and ΔE is the change in energy (then, $\Delta E/\Delta t$ is the loss of power). The ΔE was estimated based on the drop in energy across the model turbines shown in Figure 44 and Figure 45 for Experiments 19 and 20, respectively. The ΔE used for Experiment 19 was a loss of 4.6 kJ at this scale, and 2.0 kJ was used for Experiment 20. This led to the calculation of the global C_t values for the array-scale model using the above equation. For Experiment 19, a C_t of 1.65 was used, and for Experiment 20, a C_t of 1.078 was used based on the calculations described above. Apart from the C_t values and the method of representing the tidal turbines in the model, no other numerical inputs to the model were changed. Figure 44 and Figure 45 shows the global-scale energy plots for each experiment imposed on the energy plot of the individual-turbine-scale model.

The large scale representation features one rectangular box that simulated the energy loss in the flume due to all of the turbines combined. After the global C_t found in the energy loss calculations is applied to this large box, the dimensions of the box are adjusted to align with the long-field wake of the model with the long-field wake of the UoM experiments (when possible) and the long-scale wake of the individual turbine models.

Figure 44 and Figure 45 show the global-scale power plots for each experiment imposed on the power plot of the individual-turbine-scale model.
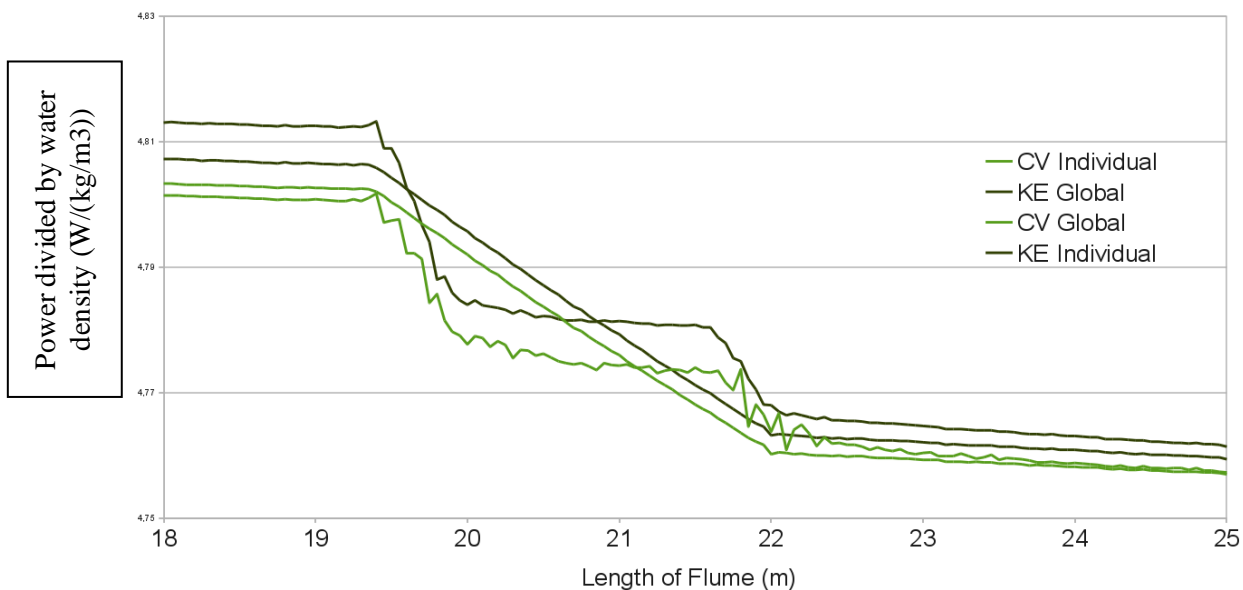

Calibration of Power Curves
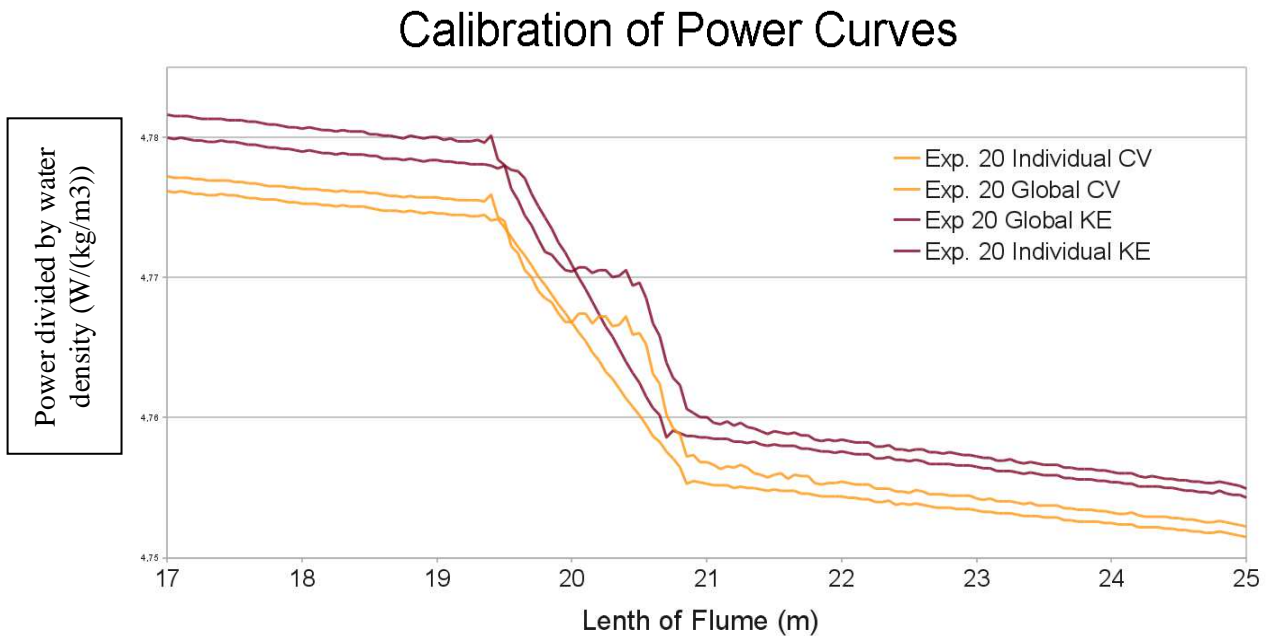
Calibration of Power Curves

Figure 45: Calibration of Power Curves: Experiment 20. The global plots have one, gradual drop in power, whereas the individual plots have two sharp drops. *Note: Length of Flume refers to the length of the modeled, numerical flume, which is 67 m long, not the 12 m long UoM Flume.*

The difference in total energy in the flume between the CV and KE models is not readily explained at this point. It could be a result of a slight difference in how each turbulence model handles surface friction, but the difference between the two turbulence models is consistent in both Experiments 19 and 20.

Another issue worth noting and trying to solve is the numerical explanation within Telemac2D as to why the energy profile plots for an empty flume, experiment 19, and experiment 20 all converge at the same energy level downstream of the tidal turbines and begin the simulation at different energy levels as seen in Figure 46. Though this is irrelevant as the important aspect is matching the energy loss in the section of the flume containing the hydro turbines and achieving a nice wake structure downstream as a result of an accurate energy loss.
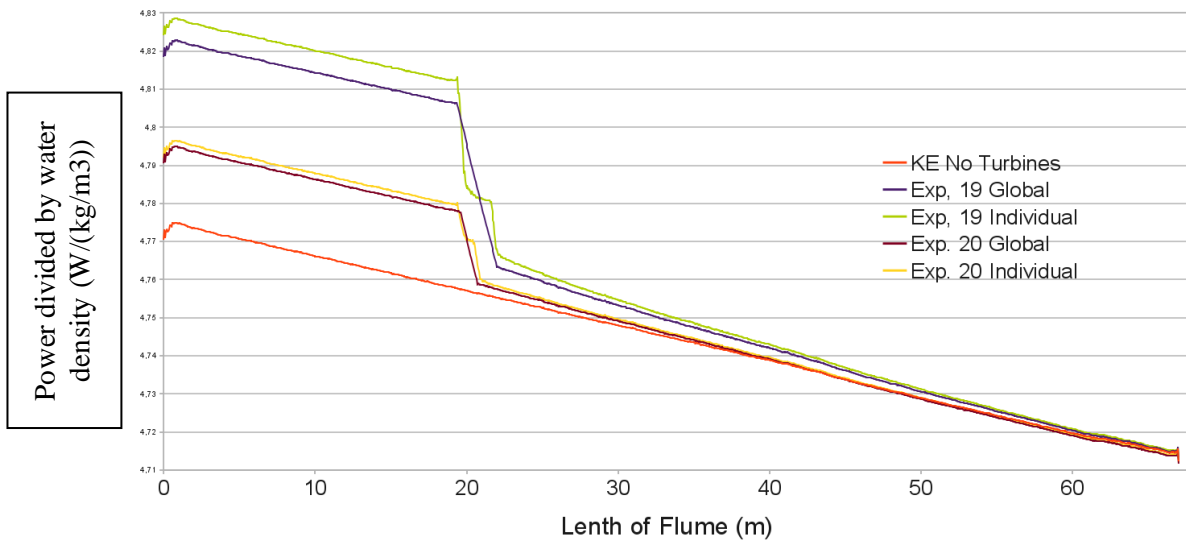
Calibration of Power Curves

Figure 46: Calibration of Power Curves. All curves represent k-epsilon models of the experiment indicated. 'No Turbines' represents an empty flume for a baseline reference. 'global results 20 #2' is the global 'array scale' model of experiment 20. *Note: Length of Flume refers to the length of the modeled, numerical flume, which is 67 m long, not the 12 m long UoM Flume.*

To further compare the accuracy of the global array model with the individual array model, the downstream velocity profiles at 6D, 8D, 10D, 15D, & 20D past the last row of turbines in each experiment. Figure 47 to Figure 51 illustrate the wake velocity profile comparisons for both the KE and CV Telemac 2-d models from each experiment. Tableau 12 and Table 13 display the maximum % error between the two models, average % error, and the % error found in the center of the width of the canal (focusing on the portion directly downstream of the turbines) for each distance downstream of the turbines. In Experiment 19, with 5 turbines across the width, the middle 3 m of the flume is analyzed, and for Experiment 20, with 4 turbines across the width, the middle 2 m is analyzed. The increased error seen in the CV models is due to the slower diffusion of the wakes behind the individual turbines. The KE model recovers to a uniform speed across the width of the wake (as evident in below figures), and therefore matches the global array model closer.

Experiment 19: 6 D

Figure 47 : Experiment 19: Velocity Profile Comparisons of Array-Scale and Individual-Scale Models. 6D downstream for both Constant Viscosity (CV) and k-epsilon (KE) models of the tidal array modeled by a single box as well as the model where each turbine is modeled individually.

Experiment 19: 8 D

Figure 48 : Velocity Profile Comparisons of Array-Scale and Individual-Scale Models. 8D downstream for both Constant Viscosity (CV) and k-epsilon (KE) models of the tidal array modeled by a single box as well as the model where each turbine is modeled individually.

Experiment 19: 10 D
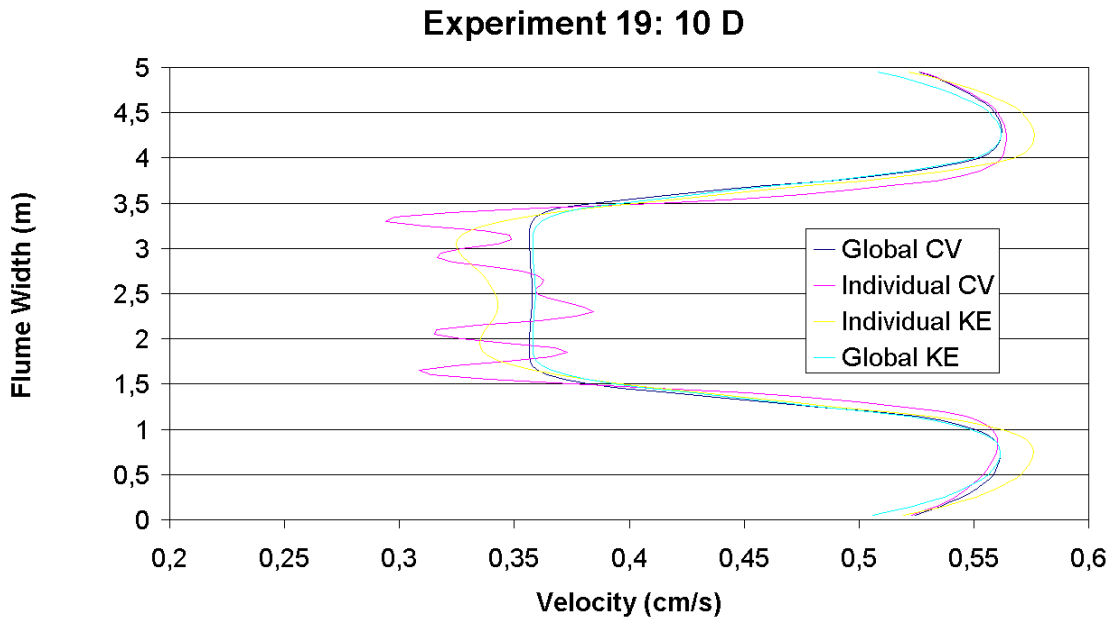
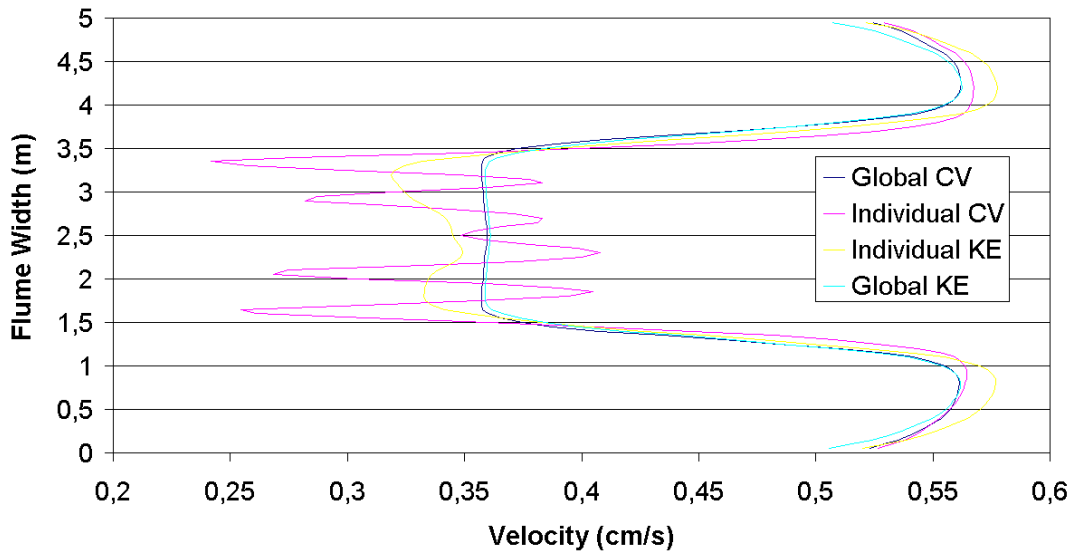**Figure 49 : Velocity Profile Comparisons of Array-Scale and Individual-Scale Models. 10D downstream for both Constant Viscosity (CV) and k-epsilon (KE) models of the tidal array modeled by a single box as well as the model where each turbine is modeled individually.**

Experiment 19: 15D

Figure 50 : Velocity Profile Comparisons of Array-Scale and Individual-Scale Models. 15D downstream for both Constant Viscosity (CV) and k-epsilon (KE) models of the tidal array modeled by a single box as well as the model where each turbine is modeled individually.
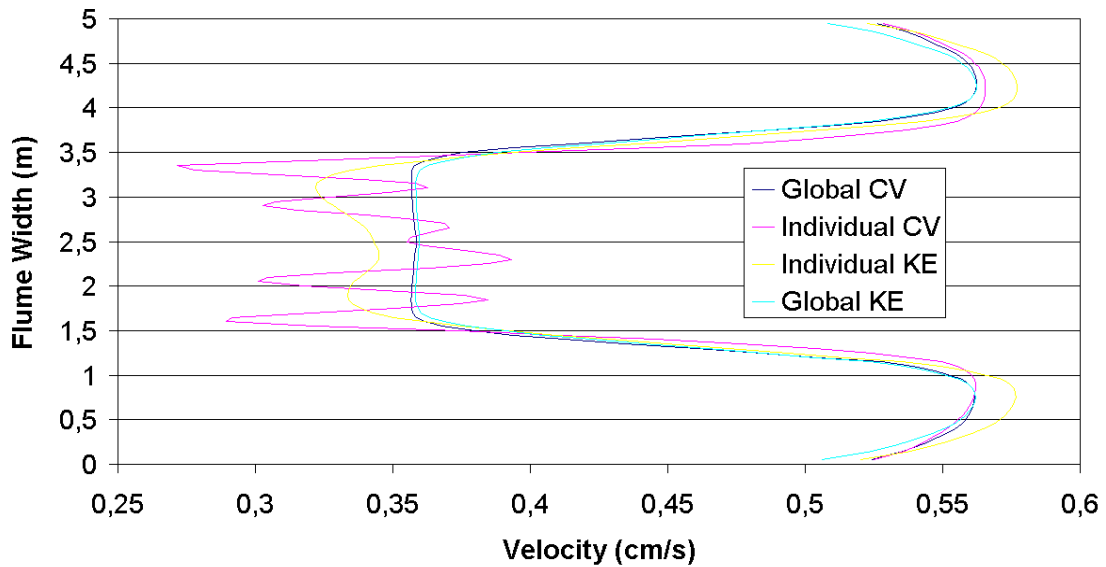
Experiment 19: 20 D

Figure 51 : Velocity Profile Comparisons of Array-Scale and Individual-Scale Models. 20D downstream for both Constant Viscosity (CV) and k-epsilon (KE) models of the tidal array modeled by a single box as well as the model where each turbine is modeled individually.

Experiment 19 CV   Experiment 19 KE

Distance Downstream	MAX % ERR	AVG. % ERR	AVG. % ERR (CENTER)	MAX % ERR	AVG. % ERR	AVG. % ERR (CENTER)
6 D	32.4	6.5	10.2	11.2	4.3	5.2
8 D	24.1	4.9	7.8	10.1	3.9	4.7
10 D	17.8	4.2	6.6	9.4	3.6	4.3
15 D	10.8	3.2	4.9	7.9	3.1	3.6
20 D	8.2	2.8	4.1	7.2	2.7	3.1

Tableau 12: Error summary between Global and Individual Array Models. For Experiment 19. For Experiment 19, the center of the flume that was focused on is the middle 2 meters.

Figure 52 : Experiment 20: Velocity Profile Comparisons of Array-Scale and Individual-Scale Models. Results given at 6D downstream for both Constant Viscosity (CV) and k-epsilon (KE) models of the tidal array modeled by a single box as well as the model where each turbine is modeled individually.
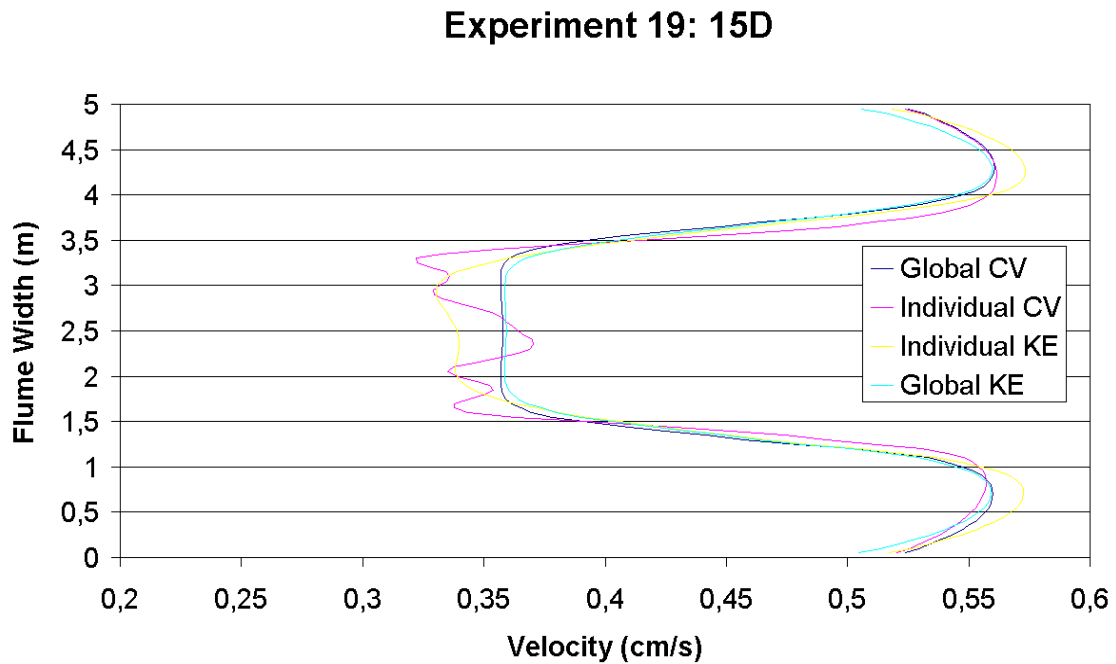

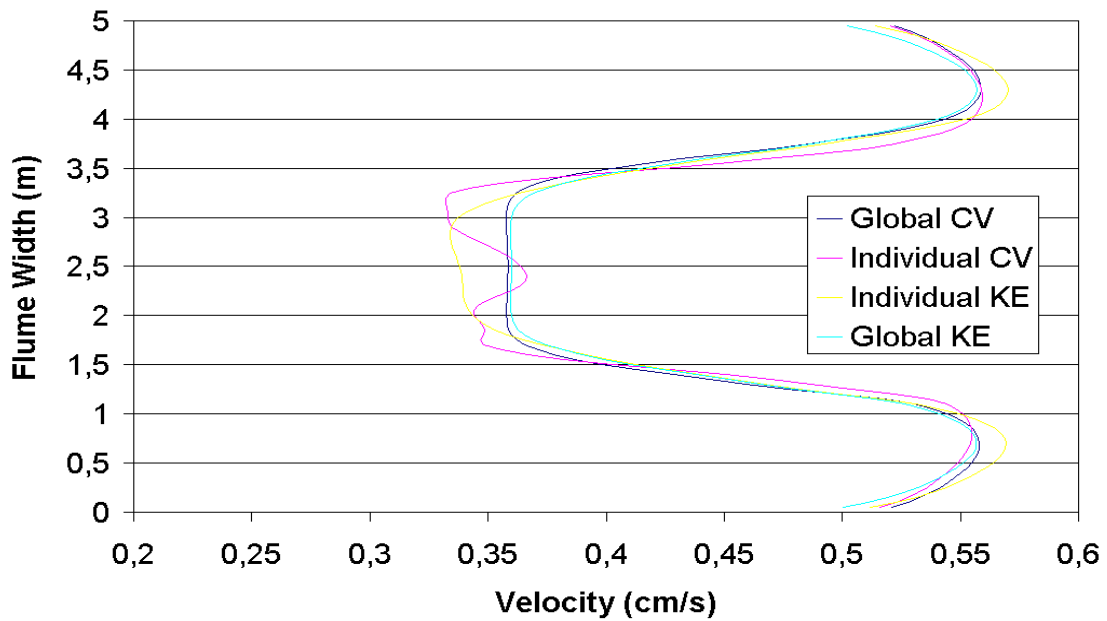**Figure 53 : Experiment 20: Velocity Profile Comparisons of Array-Scale and Individual-Scale Models. Results given at 8D downstream for both Constant Viscosity (CV) and k-epsilon (KE) models of the tidal array modeled by a single box as well as the model where each turbine is modeled individually.**

Figure 54 : Experiment 20: Velocity Profile Comparisons of Array-Scale and Individual-Scale Models. Results given at 10D downstream for both Constant Viscosity (CV) and k-epsilon (KE) models of the tidal array modeled by a single box as well as the model where each turbine is modeled individually.

Figure 55 : Experiment 20: Velocity Profile Comparisons of Array-Scale and Individual-Scale Models. Results given at 15D downstream for both Constant Viscosity (CV) and k-epsilon (KE) models of the tidal array modeled by a single box as well as the model where each turbine is modeled individually.
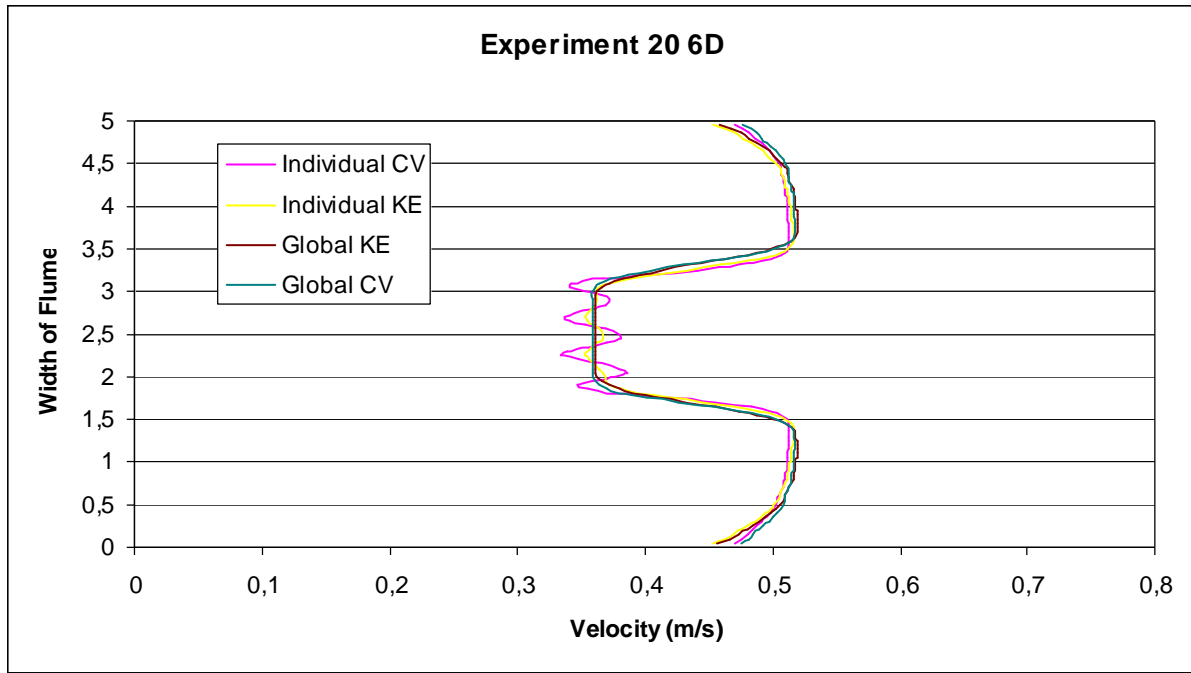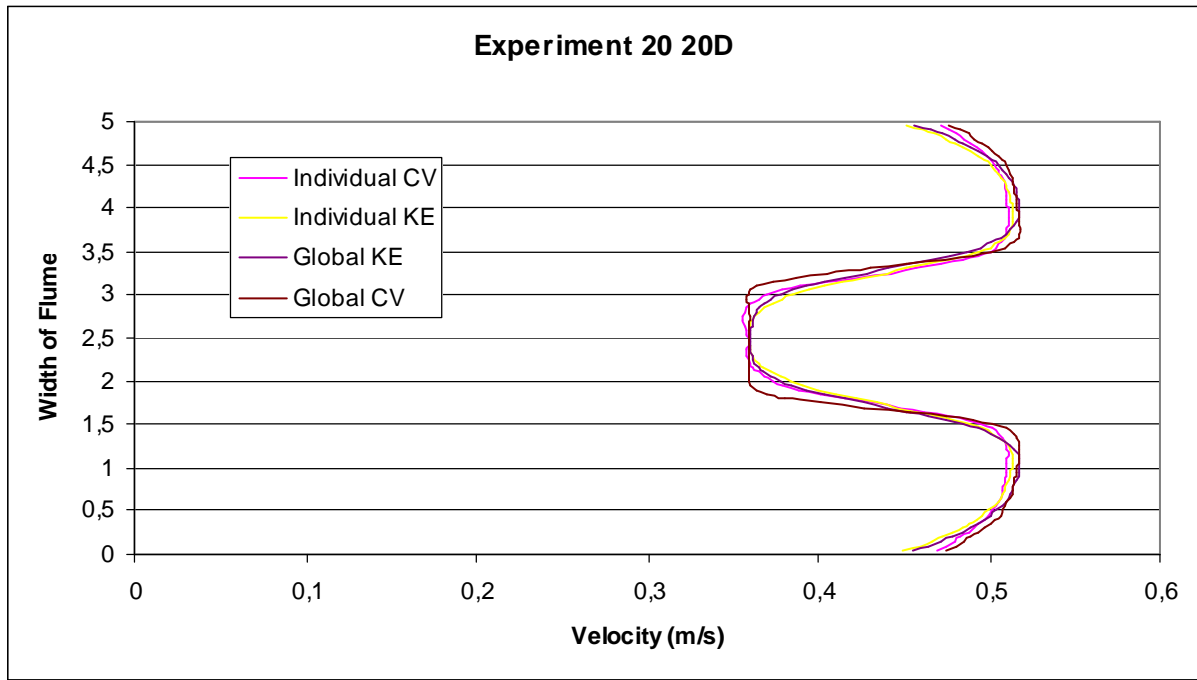
Figure 56 : Experiment 20: Velocity Profile Comparisons of Array-Scale and Individual-Scale Models. Results given at 6D downstream for both Constant Viscosity (CV) and k-epsilon (KE) models of the tidal array modeled by a single box as well as the model where each turbine is modeled individually.
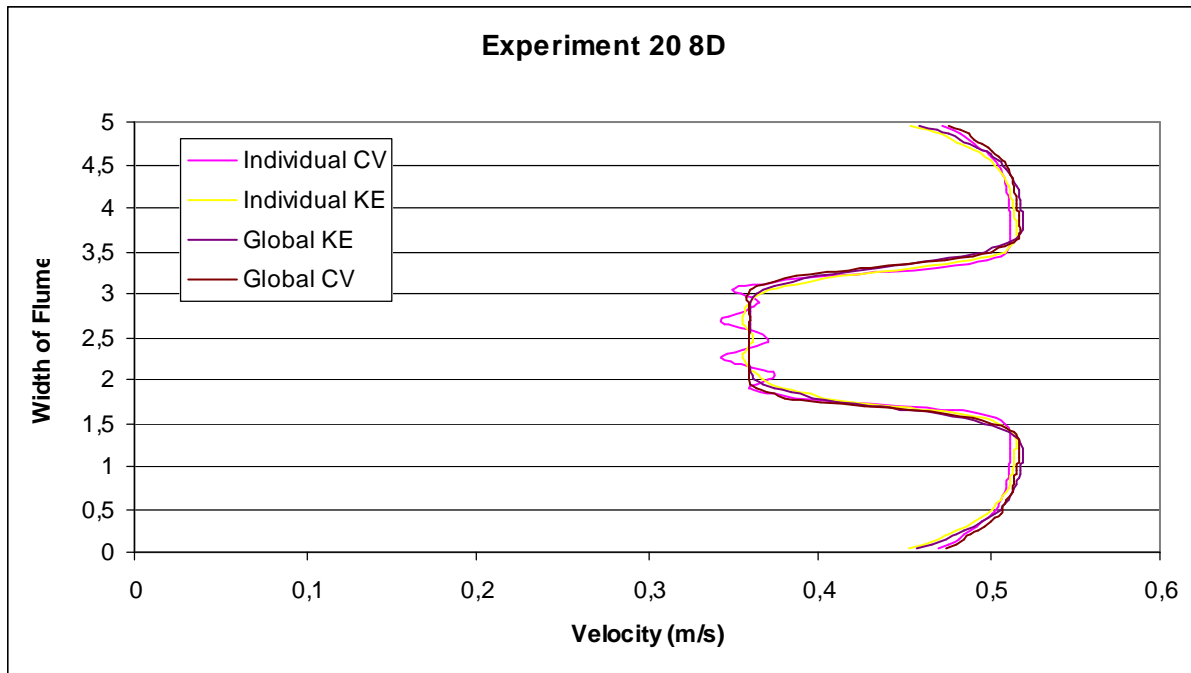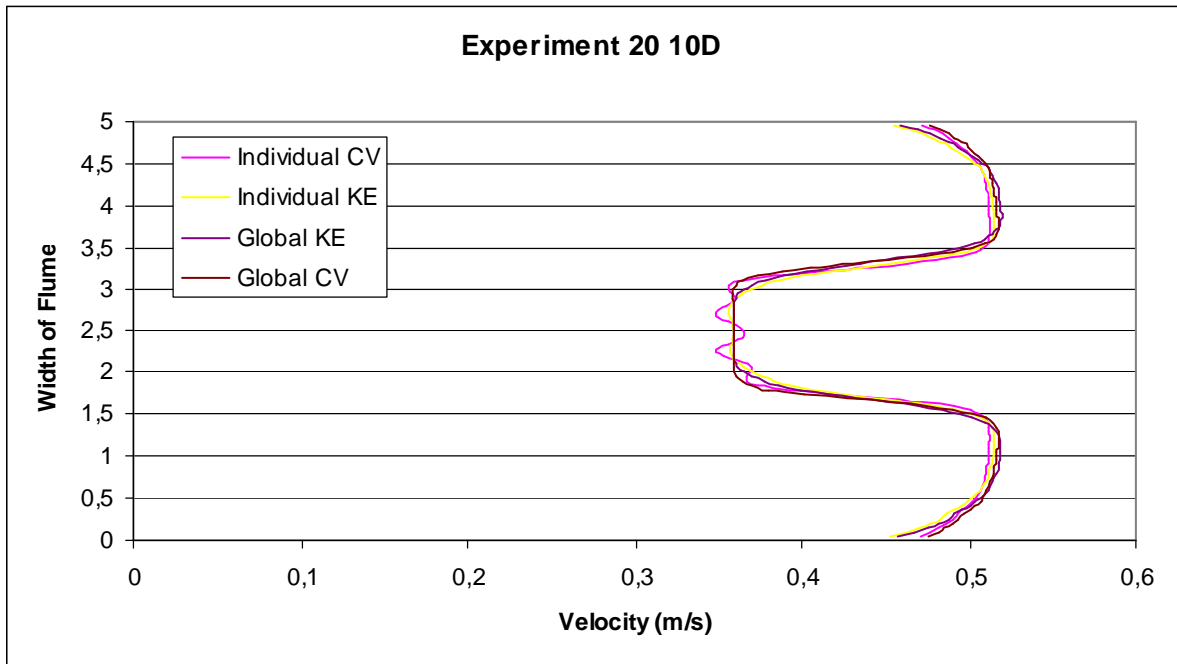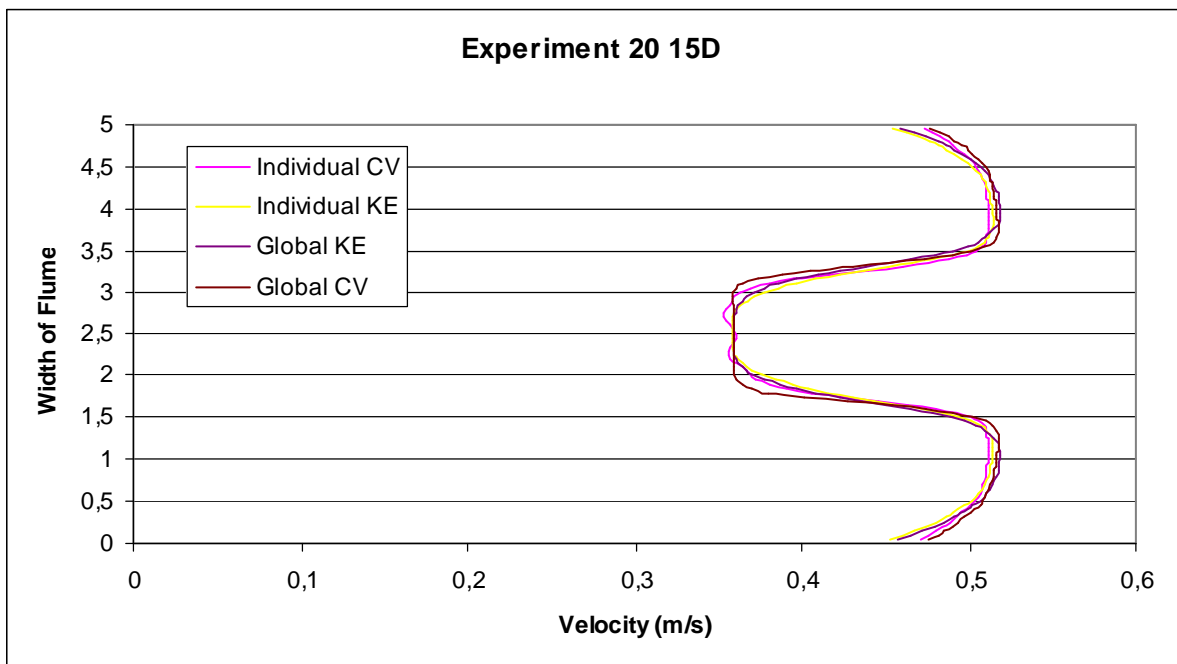
Experiment 20 CV   Experiment 20 KE

Distance Downstream	MAX % ERR	AVG % ERR	AVG. % ERR (CENTER)	MAX % ERR	AVG % ERR	AVG. % ERR (CENTER)
6 D	10.7	2.5	4.7	6.4	0.3	1.8
8 D	8.4	2.3	4.1	5.6	0.2	1.8
10 D	6.9	2.1	3.8	5.2	0.2	1.8
15 D	5.5	1.9	3.4	4.9	0.2	1.7
20 D	5.1	1.8	3.1	4.7	0.2	1.6

Table 13: Error summary between Global and Individual Array Models. For Experiment 20. For Experiment 20, the center of the flume that was focused on is the middle 2.25 meters.

After reviewing the results, it was decided to use the k-epsilon model for both experiments, as the average error, maximum error, and center-flume-focused error were all found to be lower.

3.3.4.5 Results Step 3

Comparing 2-D Telemac Results to University of Edinburgh 3-D Code-Saturne Model Results:

The University of Edinburgh created a three-dimensional model of a simplified representation of the University of Manchester Experiments, and it is beneficial to compare the results of the 2-d model with the 3-d Model to identify and attempt to explain differences between the two methods. The detailed University of Edinburgh report can be found in the shared PerAWaT folder, but only a comparison of their findings will be made in this report.

The EDF 2-d model and the UoE 3-d model are compared in this report by analyzing the velocities of the wake downstream of the turbines. Using the depth-averaged Edinburgh results as a baseline for the purpose of comparison; the Cd in the EDF 2-d model was changed, to match the results found by Edinburgh's actuator disk model. The comparisons are made starting at the farthest extend downstream of the turbines as the data in WG3 WP2 D5a allowed, at a distance of 13-Diameters for both Experiments 19 and 20. Comparisons are also made at distances of 12D, 10D, 8D, and 6D.

It is important to note that UoE used a different baseline Cd than published in the raw data of the UoM report. The UoE value is higher because the Cd accounts for the thrust on the entire turbine casing system as well as the blades. It should also be noted that the UoE was also comparing their model to the mid-depth velocity and not the 6 depth averaged points. This may make their model an over estimation of the wake intensity, and further increase the Telemac model's Cd.

Once matching the velocities, the energy loss across the tidal turbines was analyzed. Matching the Telemac energy results with the Edinburgh results proved challenging because the Edinburgh results showed an increased in total energy after the flow passed by the numerical turbines. The counter-intuitive nature of this result lends doubt to the ability of the Edinburgh model results to serve as a verified baseline of comparison.

3.3.4.6 Experiment 19

The Results for Experiment 19 comparisons yielded significantly different velocities and Energy content of the water.
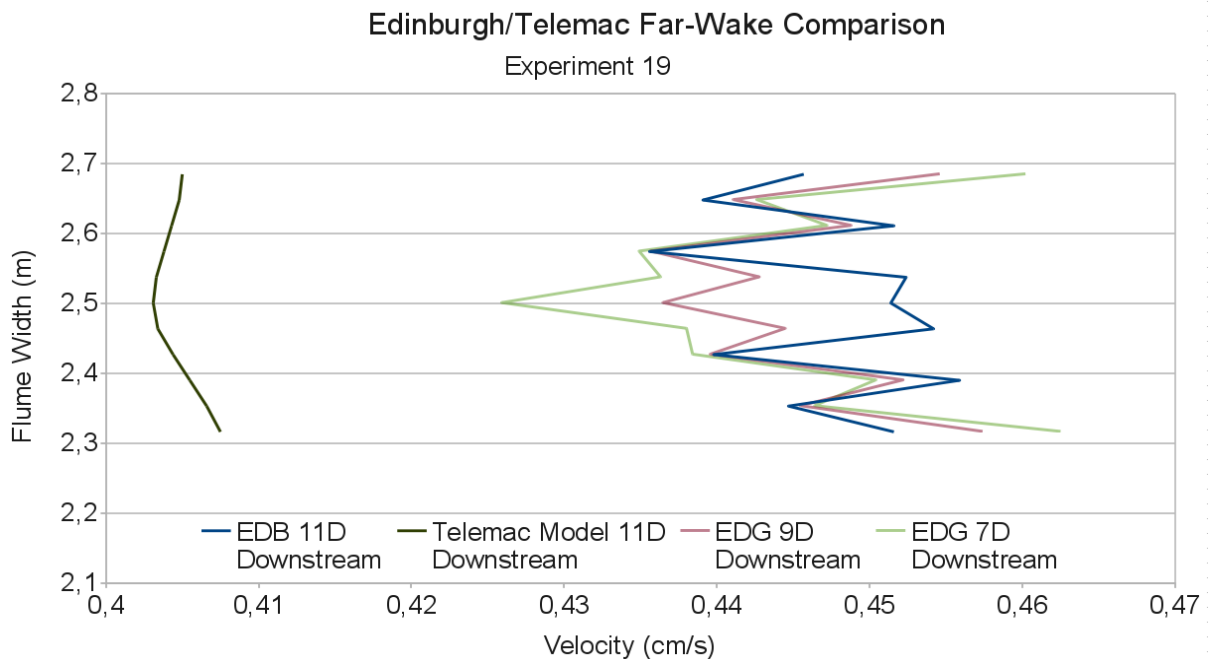
Figure 57: Edinburgh/Telemac Far-Wake Comparison, Exp. 19.

Comparison takes place at 9D Downstream in the Telemac model. Additional Edinburgh measurements from 7.5D and 6D have been added to show the sporadic nature of the data and increased speed, thus higher energy, from Telemac data.

Edinburgh Power Profile
Experiment 19
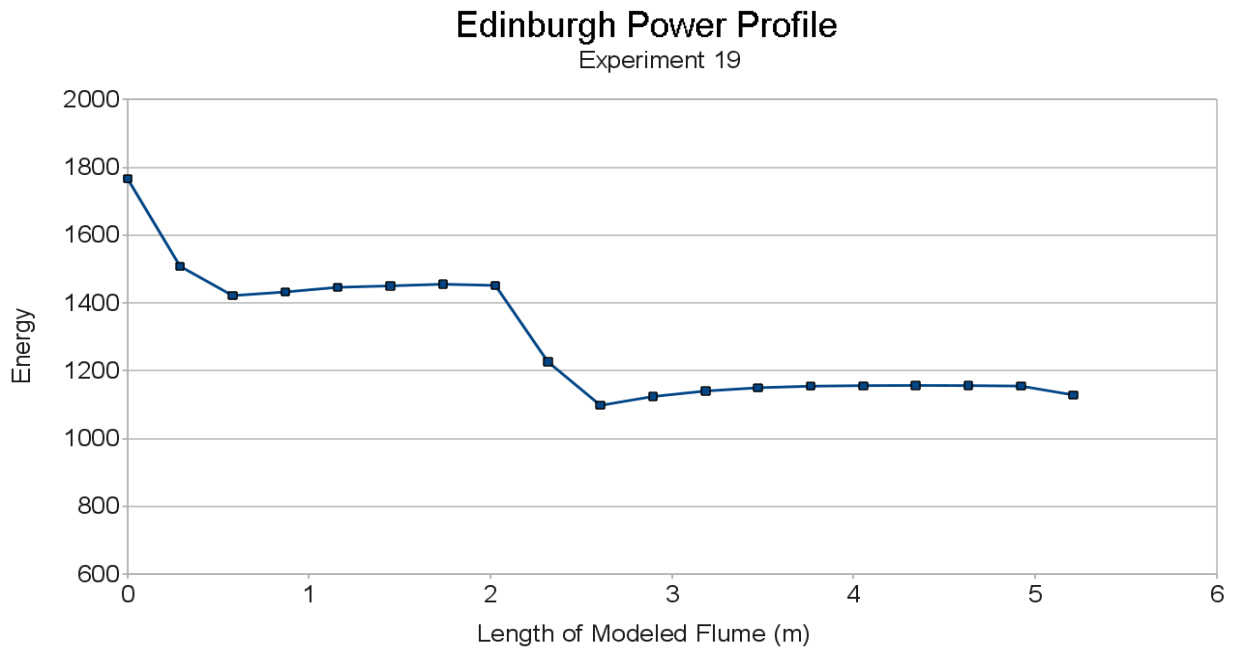
Figure 58: Edinburgh Power Profile. Experiment 19. Note that this is the energy profile for just 2 turbines in series, and not for an array of 5 turbines in series as modeled in Telemac.

It is evident from the velocity measurements that there is a significant level of error, or inaccuracy, in the measurements. We therefore decided that Edinburgh's representation of Experiment 20 could not be used as a baseline for comparison for the Telemac model.

3.3.4.7 Experiment 20

The velocity comparisons from Experiment 20 were more promising than Experiment 19, but significant differences still existed between the power measured in the flume.

Edinburgh/Telemac Far-Wake Comparison
Experiment 20

Figure 59: Edinburgh/Telemac Far-Wake Comparison, Exp. 20.

Comparisons take place at 8D downstream of the downstream turbines. KE indicates a k-epsilon turbulence model and CV indicates a constant viscosity turbulence model used in the Telemac model. The number following Cd (the drag coefficient), indicates the factor that the Cd's in the Edinburgh equations were multiplied by to achieve the results displayed.

Edinburgh Power Profile
Experiment 20

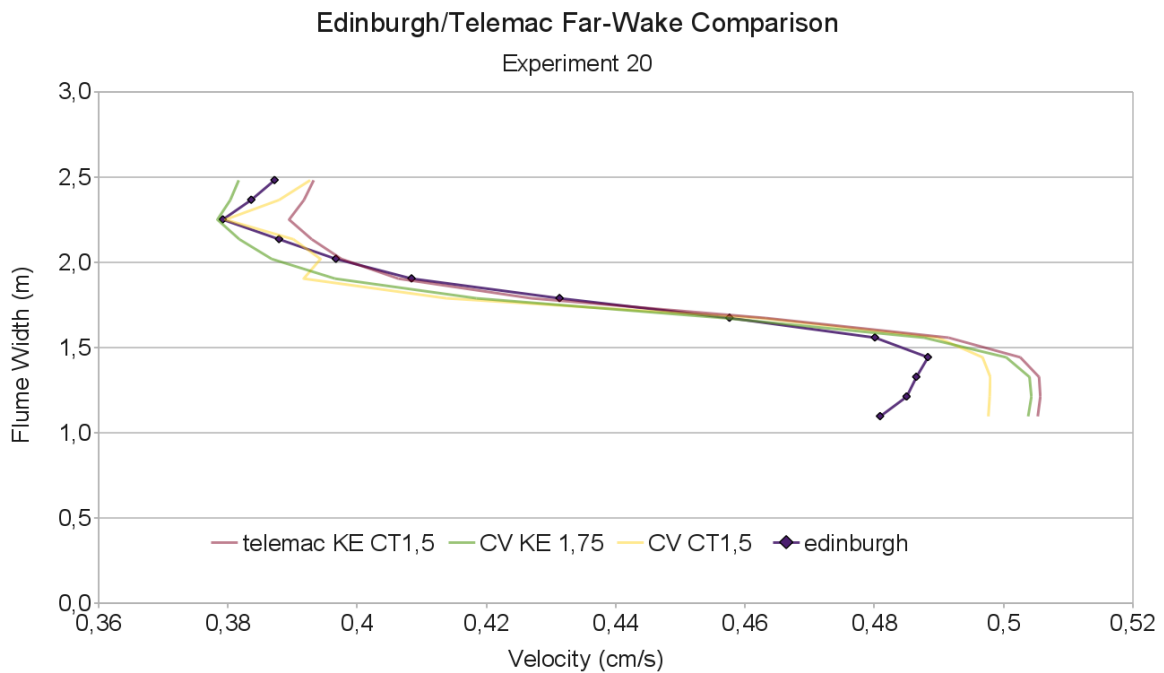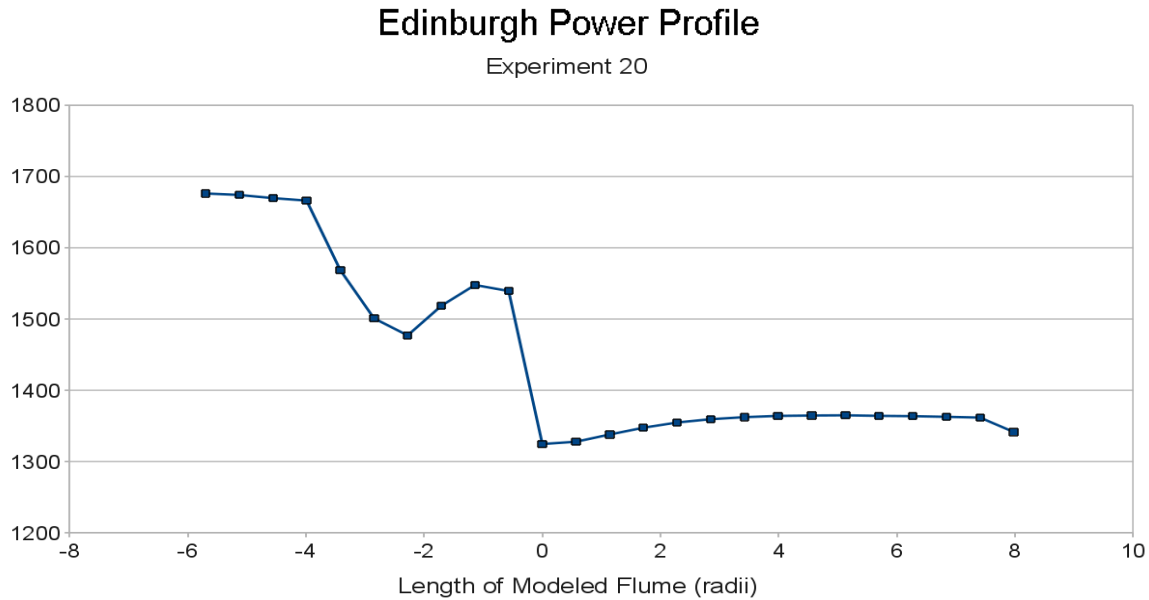**Figure 60: Edinburgh Power Profile. Experiment 20. Note that this is the energy profile for just 3.5 staggered turbines, ½ the array of 7 turbines modeled in Telemac.**

It is evident from the energy calculations that there is a significant level of error, or inaccuracy, in the measurements. We therefore decided that Edinburgh's representation of Experiment 20 could not be used as a baseline for comparison for the Telemac model.

3.3.5 Conclusion of parts A, B, C

At this point, several validations have been done:

- The first one with a cylinder in a flume. Telemac2D reproduces quite well the downstream wake. Comparisons have been made with experimental data, and the auto-similarity technique has been used for the far wake.
- The second one with one tidal turbine in a flume represented by nodes inside a rectangular box where the drag force is applied. This works especially well when the turbines are operating near the optimal operating regime, as only one TSR is associated to one Cd, it has been shown a good agreement between the 2D simulating results and experimental data.
- The last one with several turbines placed in two rows represented either by imposing a drag force in several rectangular boxes corresponding to each turbine or by using only one global box corresponding to all turbines, where a constant equivalent drag force is applied over the whole area. Again, far from the turbines, where the validation is important, the 2D simulating results correspond to experimental data. For the global model (where the individual turbines are not represented anymore), a global Cd has been defined.

In addition, the verification of the DRAGFO subroutine has also been done in section 3.2.

From these test it can be concluded that representing a turbine by a drop in energy is a valid approach to model the far wake. They also show that the DRAGFO subroutine allows users to simulate in an accurate manner the wake downstream of several tidal turbines with Telemac2D.

The following chapter describes the methodology recommended in order to simulate several turbines in a large scale basin. The conclusion from the tuning of the modeling parameters are given to ensure that a user can model accurately a farm of Tidal Energy Converters at a large scale.

3.4 Methodology for large scale simulation with Telemac2D

3.4.1 Introduction

As a result of the above sections, we can proceed forward with the following assumptions:

- The far wake of a tidal turbine array can be represented accurately with a global box model representation featuring an equivalent Cd in addition to a model where each turbine is represented individually.
- Both k-epsilon turbulence model and the constant viscosity scheme can be used for simulation.

With these assumptions, we are ready to confidently apply the Telemac2d model to a large-scale simulation using the k-epsilon turbulence scheme. We start by scaling up the global box model method used to represent the UoM experiments in above section. That global box will represent the tidal array. The first site in WG3 WP3 D3 will be used to illustrate the methodology. Two parallel approaches will be followed towards achieving the same end goal of modeling a tidal array in the Pentland Firth region off the coast of Scotland. The problem will be modeled by representing individual turbines and by adopting the global box method. This is done to ensure that both modeling approach yield consistent, accurate results. Both models build off the Pentland Firth regional tidal current model featured in an earlier deliverable under the PerAWaT project (WG3 WP3 D1).
For the two other sites, the less computationally expensive method will be applied.

3.4.2 Similar Aspects of Approaches

3.4.2.1 Converting Longitude and Latitude Coordinates to Telemac Coordinate System

The calculations in Telemac2d and Telemac3d use a planar coordinate system, as opposed to the longitudinal/latitudinal degrees. This requires the user to carefully convert between these two coordinate systems in order to place turbines in the correct arrangements.
In this study, the tidal currents have already been modeled in a previous PerAWaT deliverable, and a program that converts the long/lat coordinates to the mercator/Telemac coordinate system (this program is called conv_longlat2mercatortelemac.f). This program provides an accurate conversion for tidal basin scale regions, provided the user accurately defines the origin of the Telemac coordinates with the appropriate lat/long degrees.

3.4.2.2 Scaling-up the Global Box Model

The global box method is scaled by expressing the size of the global box used in the DRAGFO models of the UoM flume as a function of the diameter of the turbines being simulated. The DRAGFO code will be used in this basin scale model. The Reynolds Number based on the turbine diameter of these environmental conditions is a high value ($2.0 \ 10^7$), which features a similar turbulent flow regime as the Manchester experimental flume as well as the Dragfo validation with the EDF single turbine experiments.
The box dimensions yielding the best results for the experiment 19, the non-staggered case, was 2.2m x 2.6m (flume-width direction x flume-length direction) (Shown in Figure below). With the center

point of the box at mid-flume width and half way in between the two rows of turbines, the box extends 51% of a turbine diameter (0.27m = diameter) on each side of the outside turbines (the outer extents sweeping blades, not the center point of the turbine) and 81% of a turbine diameter up- and down-stream of the center line of each row of turbines. These distances in terms of turbine diameter should be translational into a large-scale, realistic model in an ocean setting.

The box dimensions yielding the best results for the experiment 20, the staggered case, was 1.5m x 1.4m (flume-width direction x flume-length direction) (shown in the figure below). With the center point of the box at mid-flume width and half way in between the two rows of turbines, the box extends 6% of a turbine diameter on each side of the outer edge of the wider, back row of turbines and 59% of a turbine diameter up- and down-stream of the center line of each row of turbines.

These values describing the box size have been determined through the fine-tuning of the model through changing the box sizes and comparing the velocities measured downstream in the global box model with the downstream velocities calculated by the individual turbine-array modeling in Telemac2d and minimizing the average % error. The reason that the boxes extend beyond the area directly covered by the turbines is due to the turbulent properties found as the water approaches the individual turbines. These turbulent properties contribute to the dissipation of energy and it is important to attempt to capture this area in the global box so as to best represent the wake downstream.

To apply this global box method to an array that would be modeled in a large-scale setting that features, for example, 3 staggered rows of turbines with 100m inter-row spacing and a 10m diameter, we take the following steps:
- Using the relationships found in Experiment 20 from UoM, which featured 2 staggered rows of turbines, we see that the box extends 0.06D on each side of the outer edge of the outside turbines in the widest row, and 0.59D upstream of the front row and downstream of the back row.
- Therefore, if the longest row is 3 km wide (at 1.5 interturbine spacing), the global box surrounding the turbines that yields the best wake configuration downstream will have the following dimensions:
  Width = 3000 m wide + 2*(0.06)*(10m) = 3001.2 m
  Length = 100 m + 100 m + 2*(0.59)*(10m) = 211.8 m
With the center point of the box placed mid-width, and mid-length of the turbine array.

Experiment 19 Box Model

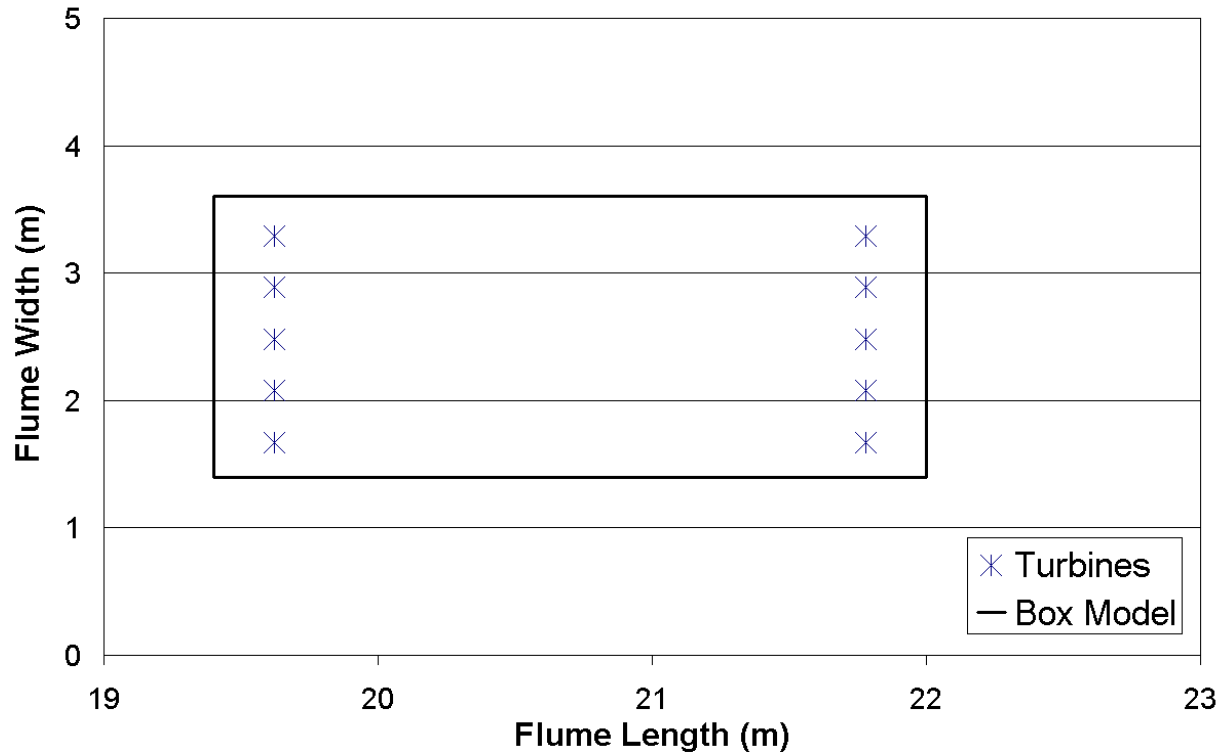**Figure 61: Non-Staggered Array Box Model Schematic.**
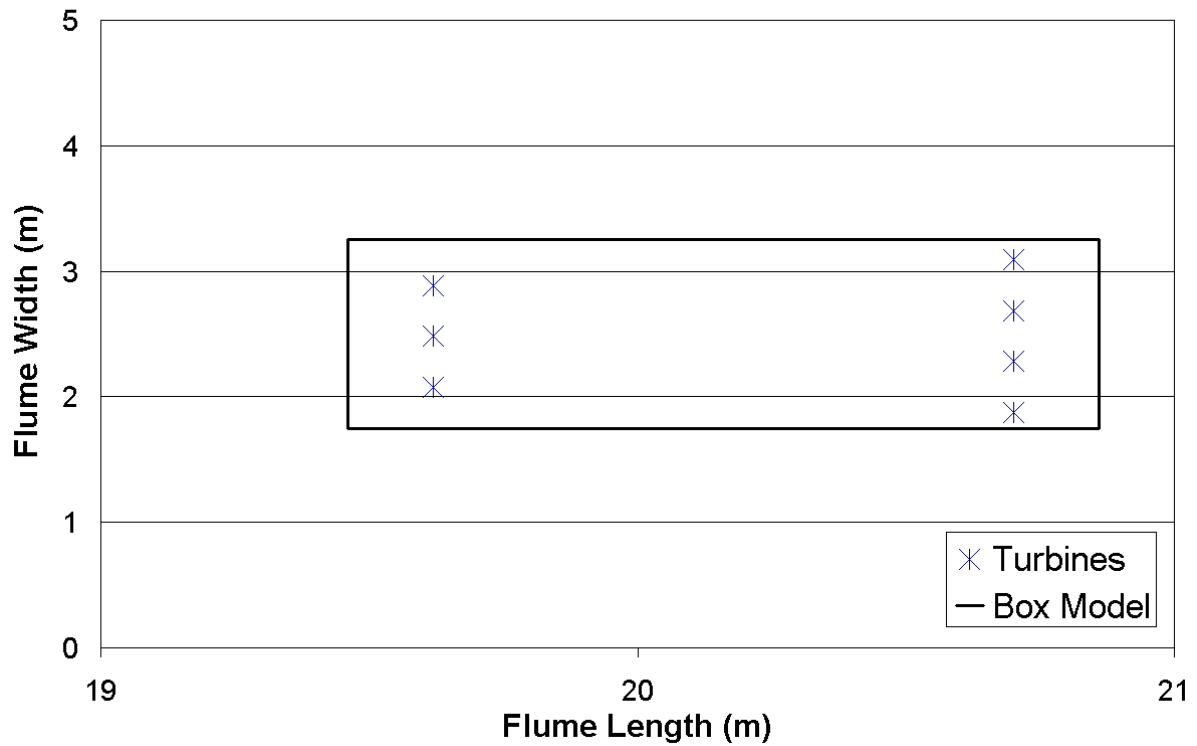
Experiment 20 Box Model

Figure 62: Staggered Array Box Model Schematic.

3.4.2.3   Scaling-up the mesh size

In order for the results to be scaled up accurately, the mesh size employed by the model must be kept the same relative to the diameter of the turbines being simulated. To translate from the UoM mesh size to a mesh size for a large-scale array, one must hold the following relationship constant:

(UoM mesh size)/(UoM diameter) = (New mesh size)/(New diameter)

Then:

(New mesh size) = (UoM mesh size)/(UoM diameter) x (New diameter)

For example, to translate the mesh size from 5cm used in the Telemac2d model of the UoM experiments with a turbine diameter of 0.27m to the 10m diameter of the same turbine considered above, we would use a mesh size of 1.85 m. The small mesh size compared to the vast tidal region should not pose a computational problem because only the applicable region will feature this refined mesh size. As a result, these calculations should be manageable as further explained in the summaries of each method below.

3.4.2.3.1 Method 1: The Brute Method

This first method is more computationally brutal, in that the computation time of each model will be extensive due to the number of points evaluated in the Pentland Firth regional model. The first step is to select the positioning of the tidal energy turbines in the ocean. Next, the mesh is refined around the array location.   The mesh refinement is performed with a growth rate of 1.2, which is an acceptable growth rate to maintain accurate Telemac2d outputs. In all tidal energy settings, the refined mesh size is expected to transition to the pre-existing mesh-size before arriving at the edges of the large modeled area.

After the mesh is refined, the model is run with the DRAGFO program with the turbines represented individually as rectangles with the same C_d value. It is important to note that this method is extremely costly, computationally speaking, and may prove outright impossible in certain situations due to an excessive number of nodes in the calculation field.

3.4.2.3.2 Method 2: Isolate and Extract

In the second method, the area immediately adjacent to the tidal array is initially completely extracted from the rest of the tidal basin for isolated modeling in order to limit computation time. In this large extracted rectangle (on the order of several square kilometers for most anticipated tidal energy projects), the mesh area is then refined to the appropriate mesh size of 1.85 m for a 10 m diameter turbine (calculation methodology described in the above section titled 'Scaling-up the Mesh Size'), and the bathymetry is interpolated.

Next, the individual turbines are placed in the extracted region to calculate the $C_{d(eq)}$ of the global box model. An inflow velocity of 2m/s is selected because this is a typical tidal velocity in the Pentland Firth and a constant velocity will aid in the calculations of the equivalent C_t to be used in the global box model of the site. The Pentland Firth tidal current model from an earlier deliverable is then consulted to impose an appropriate free surface level on the boundary layers given the imposed inflow. In a sense, the tidal array in the Pentland Firth is isolated in a giant, flume-like setting, and real tidal conditions (bathymetry, tidal current and free surface height) are imposed for a real-time simulation of 60 minutes (computational time is roughly 6 hours with 128 processors). The inflow and outflow boundary are parallel with the line of turbines, so that the flow approaches the turbines perpendicularly.

Next, the $C_{t(eq)}$ is calculated in the same general method as used in the modeling of the UoM experiments (analyzing the energy loss of the flow across the turbines). The slight difference between this basin-scale conversion and the UoM-scale conversion is the format of the results. For the Basin Scale results, it is necessary to subtract the power from the trial with the turbines from the power in the empty (no turbine) trial at each point in the length of the canal before evaluating the drop in power across the turbines. This step is necessary because the bathymetry causes the power drop across the turbines to be difficult to see in the results from the trial with the turbines alone. The $C_{t(eq)}$ is then applied to the global box, which has already been scaled up. This global box with its new $C_{t(eq)}$ is validated within the extracted, isolated model before being placed into the 'less-refined' Pentland Firth larger, regional model using the DRAGFO routine. The validation of this 'less-refined' mesh size is demonstrated below.

Passing the Global Box to a Larger Mesh Size

In order to save on calculation time, the global box representing the turbine farm is passed to a less-refined tidal region. The size of the refined region remains that same, and basin-scale region features the same 'Brute-Method' 1.2 mesh transition factor from the refined mesh area to the greater region. In order to validate this procedure, the UoM experiments were reconsidered and models were run with mesh sizes of 0.10 m (twice the original mesh size of 0.05 m), 0.27 m (1 turbine diameter), and 1 m (20x the original mesh size). The UoM flume was expanded to 67m long by 50 m wide for these simulations in order to avoid side-wall effects that became apparent when the mesh size was increased. The tidal turbines are kept in the middle of the flume, to maintain symmetry.

The following velocity profiles show the wake properties downstream of the tidal turbines at 5 cm, 10 cm, 27 cm, and 100 cm (1m) at 6D, 10D, and 15D downstream.

Figure 63 : Staggered-Alignment Tidal Turbine Wake Comparisons altering Mesh Size at 6D downstream of final row of turbines.

Figure 64 : Staggered-Alignment Tidal Turbine Wake Comparisons altering Mesh Size at 10D downstream of final row of turbines.

Figure 65 : Staggered-Alignment Tidal Turbine Wake Comparisons altering Mesh Size at 15D downstream of final row of turbines.

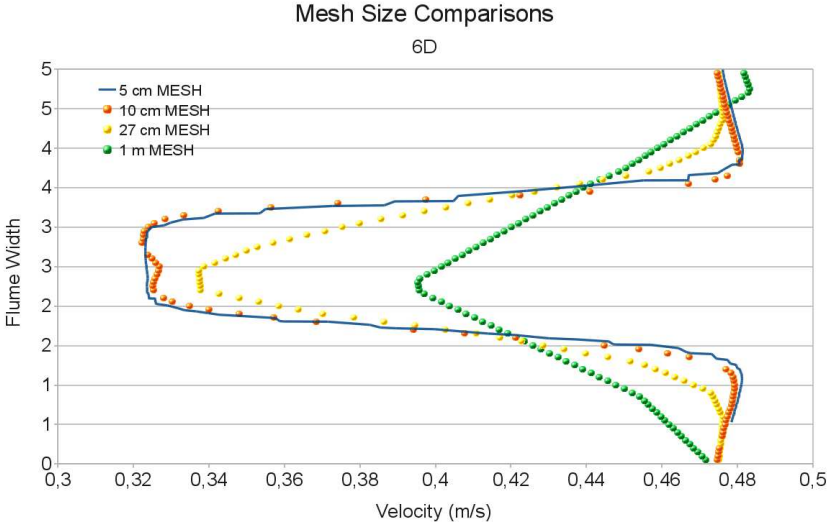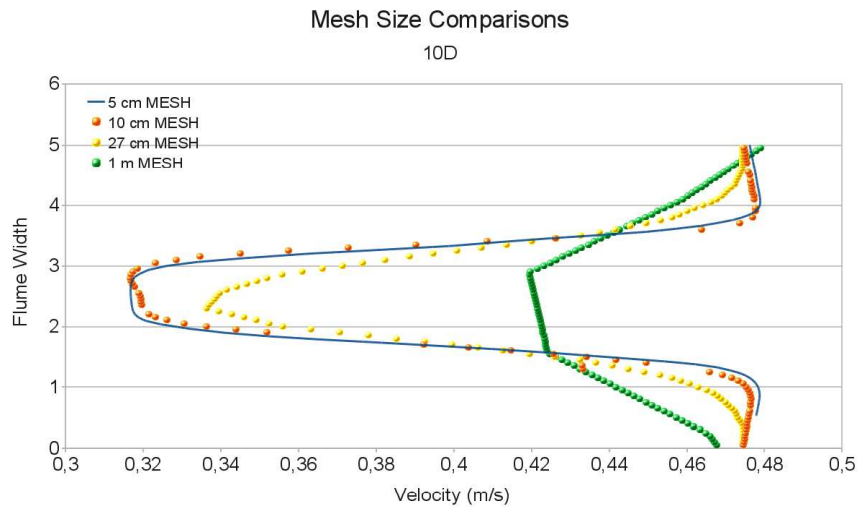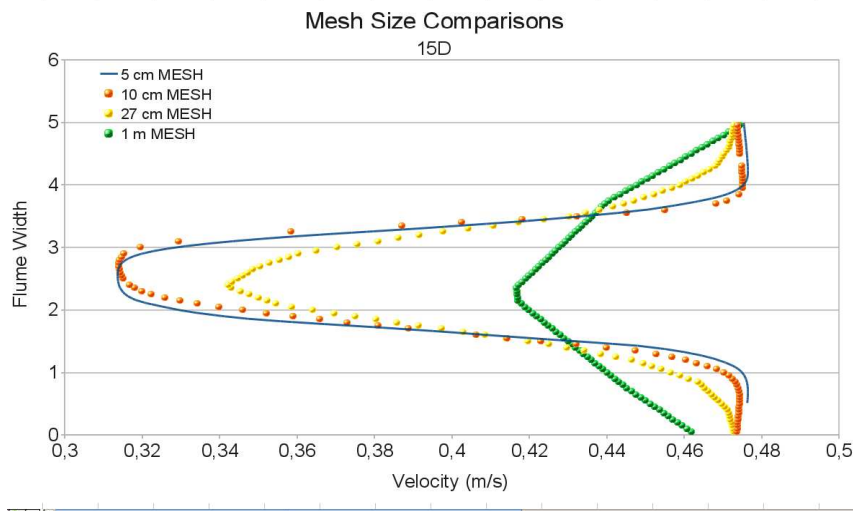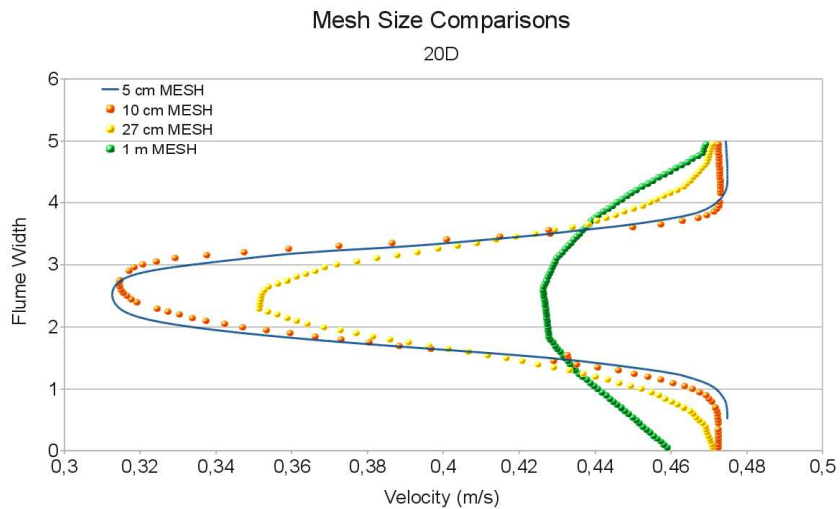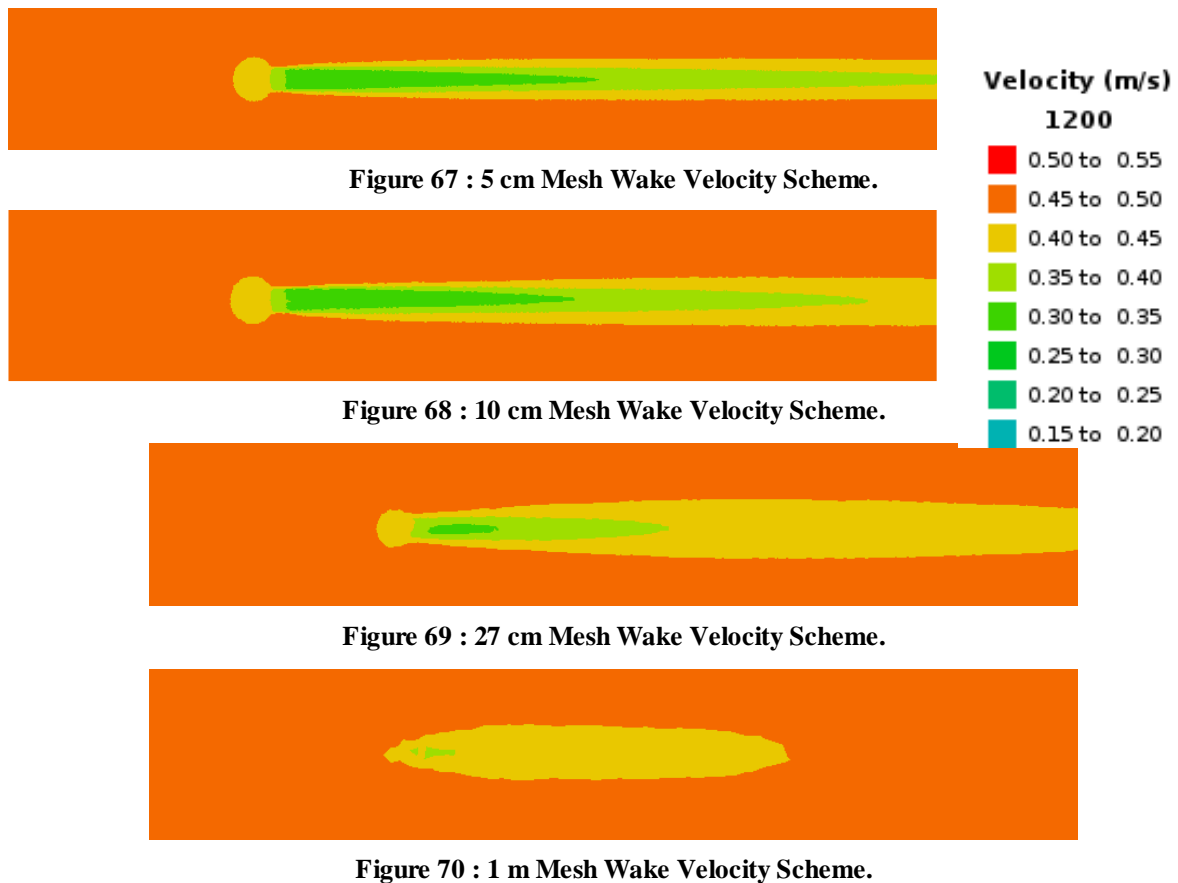**Figure 66 : Staggered-Alignment Tidal Turbine Wake Comparisons altering Mesh Size at 20D downstream of final row of turbines.**

Figure 67 : 5 cm Mesh Wake Velocity Scheme.

Figure 68 : 10 cm Mesh Wake Velocity Scheme.

Figure 69 : 27 cm Mesh Wake Velocity Scheme.

Figure 70 : 1 m Mesh Wake Velocity Scheme.

Based on the above graphs, we have determined that a 27 cm mesh size, or a mesh size equal to one turbine diameter accurately depicts the far downstream wake of a global model. Therefore, the Regional Tidal Current Model from a previous deliverable will be refined to a mesh size of 1D over the region surrounding the tidal farm and transition to the mesh of the greater region by a factor of 1.2. This process will save on calculation time and enable complex regions to be modeled.

3.4.2.4   Preview of Case Study of Basin Scale Model Implementation in Progress

First example: using the global box method

The methods presented in this study are in the process of being applied to the Pentland Firth Tidal Basin off the northern coast of Scotland. This section is not a presentation of the results of this study, as it is still in progress, but it is intended to provide a concrete example of the models described above and the results that can be expected.

The tidal region of the Pentland Firth was modeled in PerAWaT WG3 WP1 D1 to reproduce tidal currents without tidal turbines (Figure 71). This resulted in a reliable model that will be used in this study to as the numerical environment that the tidal turbines will be installed and observed. It is from this large regional model that we extract values of free-surface height, tidal current speed, and other characteristics which we use as parameters in both the brute method and isolate-and-extract method.
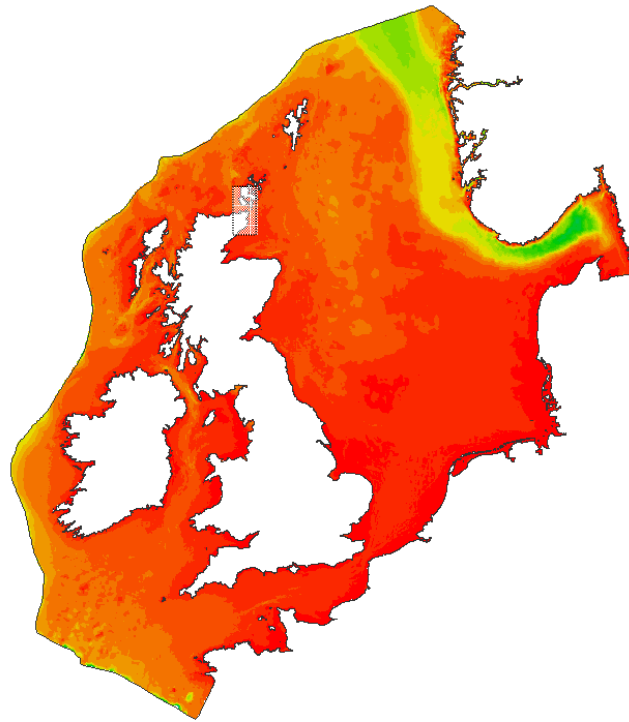
Figure 71 : Pentland Firth Region Model. The region that was modelled in WG3 WP1 D1 that will be used in this study as both a baseline comparison and a medium to install the turbines. The Pentland Firth region is marked by the semi-transparent box in the northern part of the region.

In the basin scale model, as in the laboratory-scale model, the specified Cd of the turbines have been multiplied by the same factor of 3 that was found to produce an accurate representation in the laboratory model calibrations **when using the local velocity**. Therefore, the Cd of 0.86 for the 10 m diameter turbines becomes 2.58 for the basin scale model. Figure 72 shows the isolate-and-extract method results from the early stages of the tidal study where the individual turbines are modeled individually. To benefit future model users, Table 14 specifies the aspects of the DRAGFO program that have been changed between the laboratory scale and the basin-scale models. In addition to the outlined changes in the DRAGFO code, the file specifying the locations of the turbines must also be adjusted to match the Telemac coordinate system and number and placement of the turbines as desired by the modeler.

The next step, to be shown in more detail in a separate report following the completion of the model, is to determine the $Cd_{(eq)}$ of the entire array and implement the global box geometry. As explained above, this global box will then be placed in the large, regional model of the Pentland Firth and results will be analyzed.
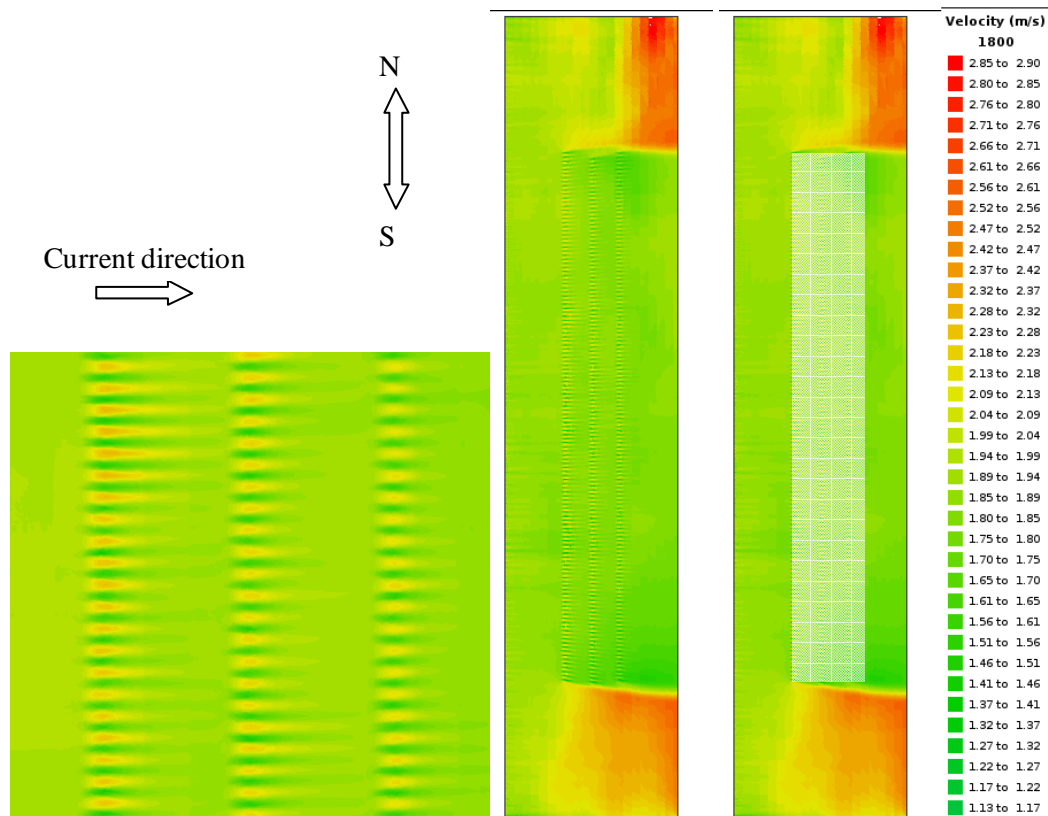
Figure 72 : Isolate and Extraction Model, Pentland Firth. The left image shows a zoomed in view of the array of individual turbines modelled in the box model. The middle images show the entire box, with the right image also portraying the general placement of the global-drag-box. Please note that the inter-row spacing is 100 m, the inter-turbine spacing (from center point to center point) is 15 m, the turbine diameter is 10 m, and there is 500 m on each side (north/south) of the array.

Variables	Description	Laboratory Scale Model	Basin Scale Model
Not in Dragfo	# of points modeled in the mesh	260000	3000000
CPOH, CDOH	The values of Cd and C_P are changed and no longer vary between turbines in the basin-scale model.	O(0.35), O(2.2)	0.53, 2.58
LMIN	The y-coordinate of the bottom boundary of the mesh.	0	1396469.1
LMAX	The y-coordinate of the top boundary of the mesh.	5	1392516.1
HDW	The half width of the drag-box in cross-sectional direction.	0.05 m	1.85 m
HDL	The half length of drag-box in current-wise direction.	0.18 m	6.67 m
EPS	Margin of error considered when placing the tidal turbines in the mesh.	0.01 m	1.0 m
RV	Radius of each turbine in reality.	0.135 m	5 m

Table 14 : DRAGFO code changes between the laboratory-scale and basin-scale models.

Second example: using the brute method

In this simulation, 28 turbines are simulated in the Pentland Firth (14 turbines in each row). The diameters of the turbine are 18 m. The far velocity is used to compute the drag force, and the Cd used

is 0.86 (the multiplication factor is equal to 1). The following figure shows the localization of the turbines (2 rows in blue):
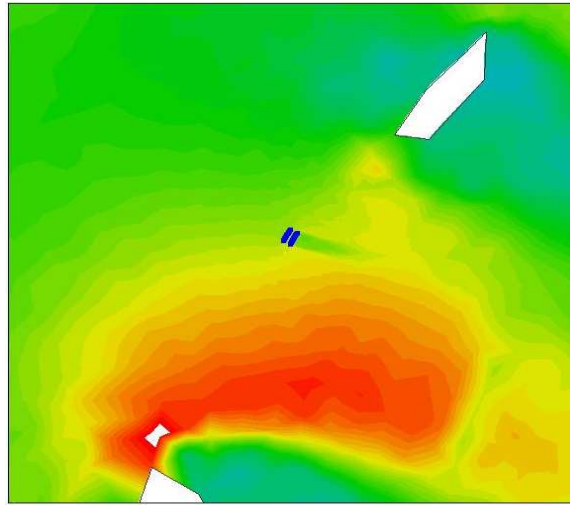
Figure 73: Localisation (in blue) of the 28 turbines between 2 islands in the Pentland Firth region.

The mesh size around the turbine is about D/5 = 3.6 m. A small mesh size is used until 25D behind and after the turbines. Then, the mesh size increases within a coefficient factor equal roughly to 1.2. The following figure shows the mesh used for the simulation.
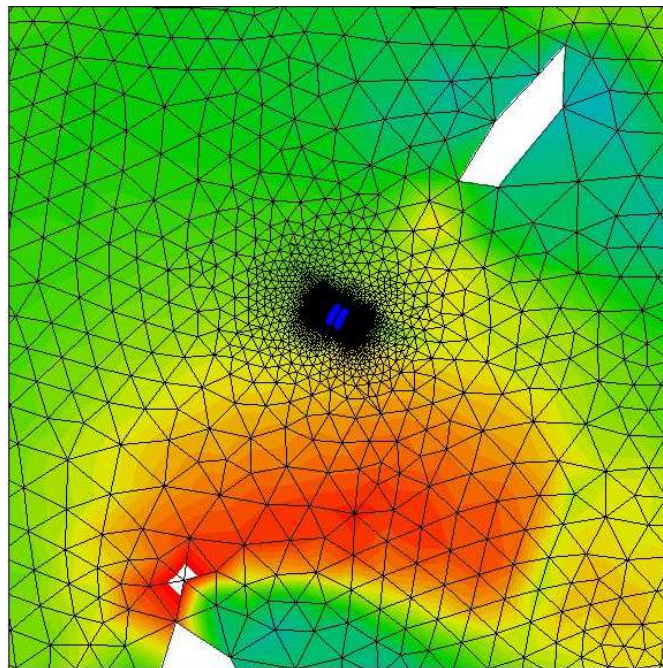
Figure 74: mesh used for the simulation: number of element: 976 844 nodes: 499 491. The mesh density is very high near the turbines.

The time simulation is 4 days. Among these 4 days, 2 days are used to install the tide flow. One week of computation time is needed with 288 processors. The time step is equal to 0.05 s, which is, as you can notice, very small. The acceleration of the flow near the turbines explains this small time step. The following figures show different results at different time step:
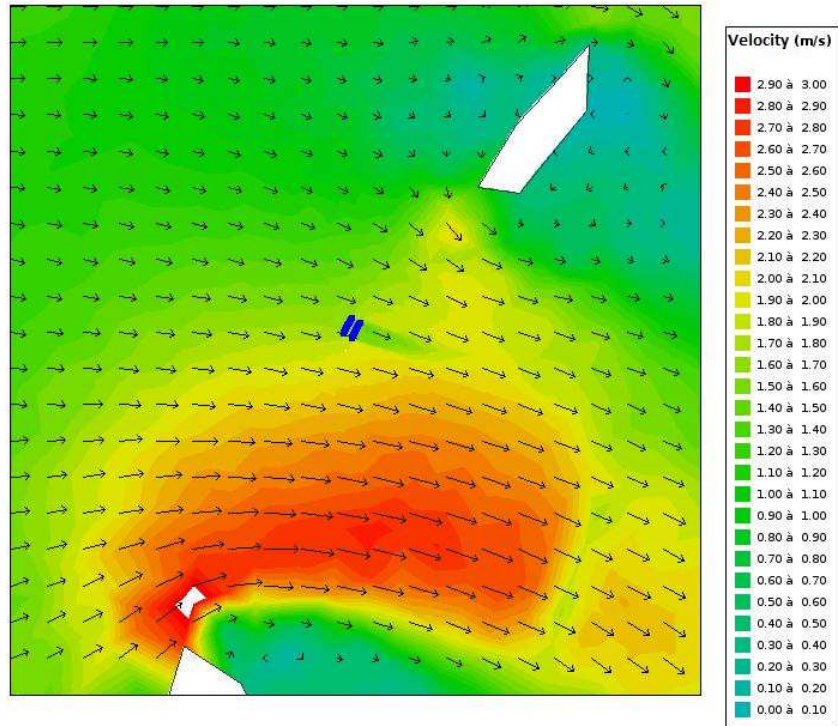
Figure 75: Velocity represented by different colours. The vectors are velocity vectors, they are not localized on each node, and they are much further apart.

The following figure shows a zoom on the turbines wake. Each wake of each turbine can be seen:
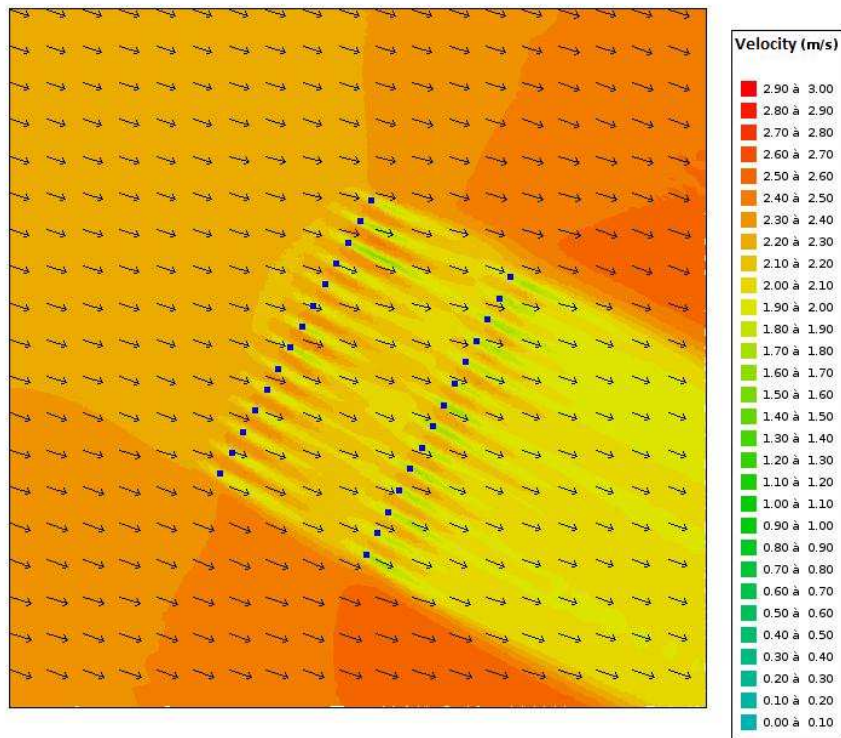
Figure 76: Zoom on the wake of the 28 turbines (in blue).

Of course, when the flow changes its direction, the wake take place on the other side. That is what we can see in the following figure:
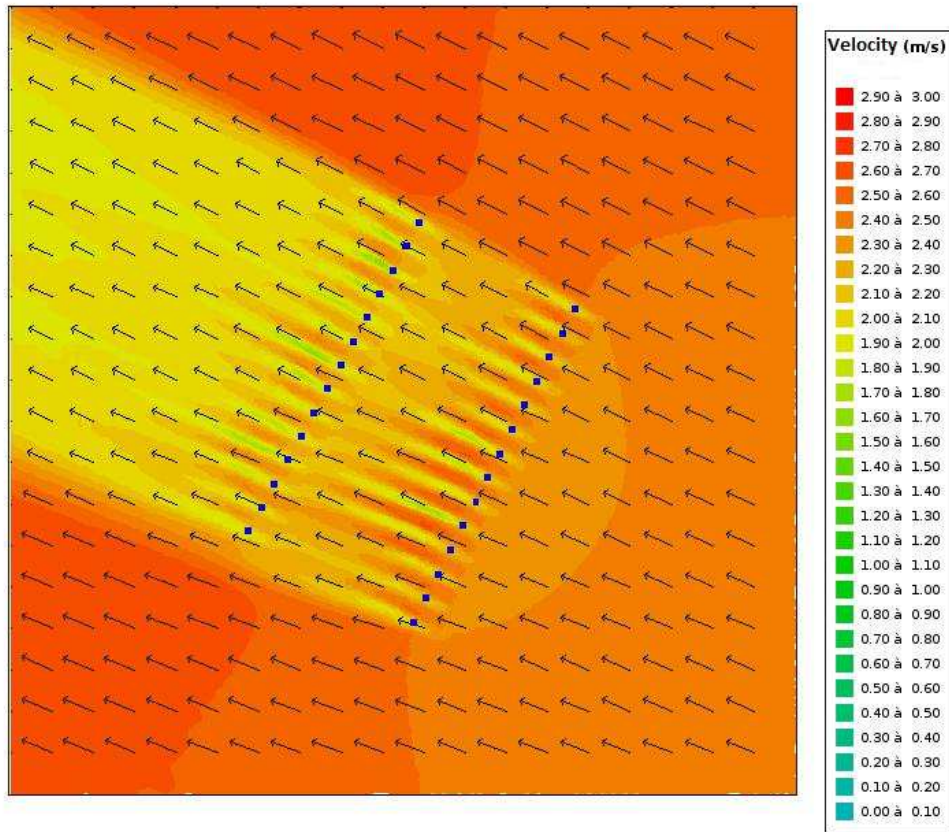
Figure 77: Zoom on the wake of the 28 turbines (in blue) when the flow changes its direction.

We can see, in figure 77, the consistency between the wake and the velocity vector.
A less zoomed view can shows the potential global impact:

Figure 78: Less zoomed view and potential global impact.

This example shows that the FORTRAN code developed can be used in a big scale simulation with several turbines and with several processors.

3.4.3   Model Limitations and Conclusions

Method 2 and method one are expected to arrive at similar results given their application to the same turbine array orientation. The main difference will lie in the CPU time, as method 1 is thought to be extremely computationally expensive.

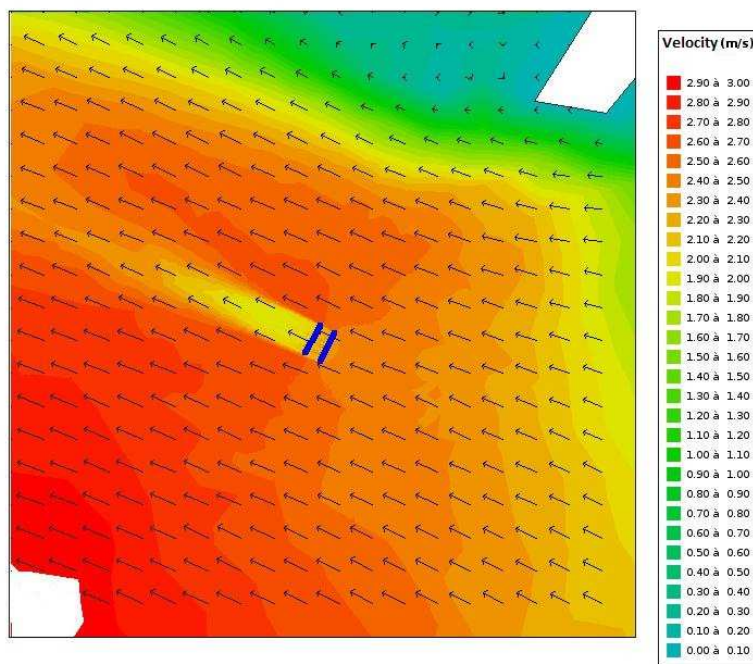As with all numerical models, it is astute to analyze the potential numerical limitations. The small mesh size is potentially a limiting factor if the region covered by the tidal farm is very large as the computational time will be great and there is a risk that too many points will be in the model.

In the UoM experiments, it was evident that the C_d values varied based on position in the array and which row the turbine is located. This will lead to a misrepresentation, but since the general scale of the C_d values do not change drastically, a single value is adequate.

Blockage ratio issue:

The blockage effect has an influence on both the performance of individual devices and on the flow through and around the array. If an array is very closely packed and placed in a blocked environment (between two islands for example), it may force the flow to divert around this densely blocked region.

- At present, there is no correction in the dragfo routine which accounts for the influence of the blockage effect on individual devices. During the validation steps, numerical models were validated against measurements of typical device locations in the water column (diameter being roughly half the water height, and the turbine placed at mid-depth) and for realistic spacing (for the Manchester experiments). Therefore, the dragfo routine and the modeling processes are valid for typical blockage ratios. One current limitations of the method is that it takes the drag coefficient as an input, and the routine does not modify its value depending on the lateral spacing between devices or its location in the water column. This could be explored for further development of the model but is out of the scope of this work.
- However, the influence of the blockage effect which is specific to the array configuration in a given environment is accounted for in the basin scale models. The flow observed with the array model reproduces the flow observed with the individual devices and is driven by both the tidal boundary conditions and the bathymetry. As a result, the model is able to reproduce the features of a flow past an array of turbines, and how this flow is affected by the presence of that array.

3.5   Conclusion for 2D simulations

To conclude the study with Telemac2D, we can say that:

- The subroutine DRAGFO has been verified with a single processor and several processors.
- The validity of DRAGFO has been checked with one and several tidal turbines.
- A methodology is defined to simulate several tidal turbines in a large scale basin.

The k-epsilon model looks more appropriate to use because no coefficient associated with the turbulence model has to be set up. Nevertheless, the constant viscosity model works also very well.

4 TELEMAC3D SIMULATIONS

In this part, simulations are launched in Telemac-3D; a simulation code for free-surface hydraulics developed by EDF (see [17] for more details). Like in 2D, the TECs (Tidal Energy Converters) will not be represented in the mesh; they will be modelled through the application of a drag force on the fluid (in a FORTRAN subroutine SOURCE). This modelling approach is already applied in Telemac-3D to simulate bridge piers; it will be necessary to adapt it to the case of tidal energy converters (TECs).

We want to emphasize that the meticulous approach in 2D is conducted beyond what is required and includes work on one cylinder, one turbine, and several turbines with two varying alignments, contains comparisons with several external experiments, checks the mesh convergence, etc. This approach was necessary to provide the ability to transpose the 2D methodology for the 3D study which can be simplified in some aspects.

4.1 Inputs

Comparisons are done in the following chapter between simulation results and several output experimental data from the following work package:

- WG4WP1: experiment done at EDF in a flume [2, 3].

4.2 Verification

The subroutine, where the drag force which can simulate the turbine effect is coded, is called: SOURCE. The verification of a subroutine can be described by the following definition:

The process of determining that a model implementation accurately represents the developer's conceptual description of the model and the solution to the model.

Therefore, a flow inside a flume was simulated, and a power deficit of 1 Watt was programmed in the subroutine "SOURCE" in a specific location in the flume. It was therefore verified that a deficit of power equal to 1 Watt was simulated at the correct location. The power deficit was located at 51.8 m from the beginning of the flume.

The following figure plots the evolution of the power in a section of the fluid along the flume:
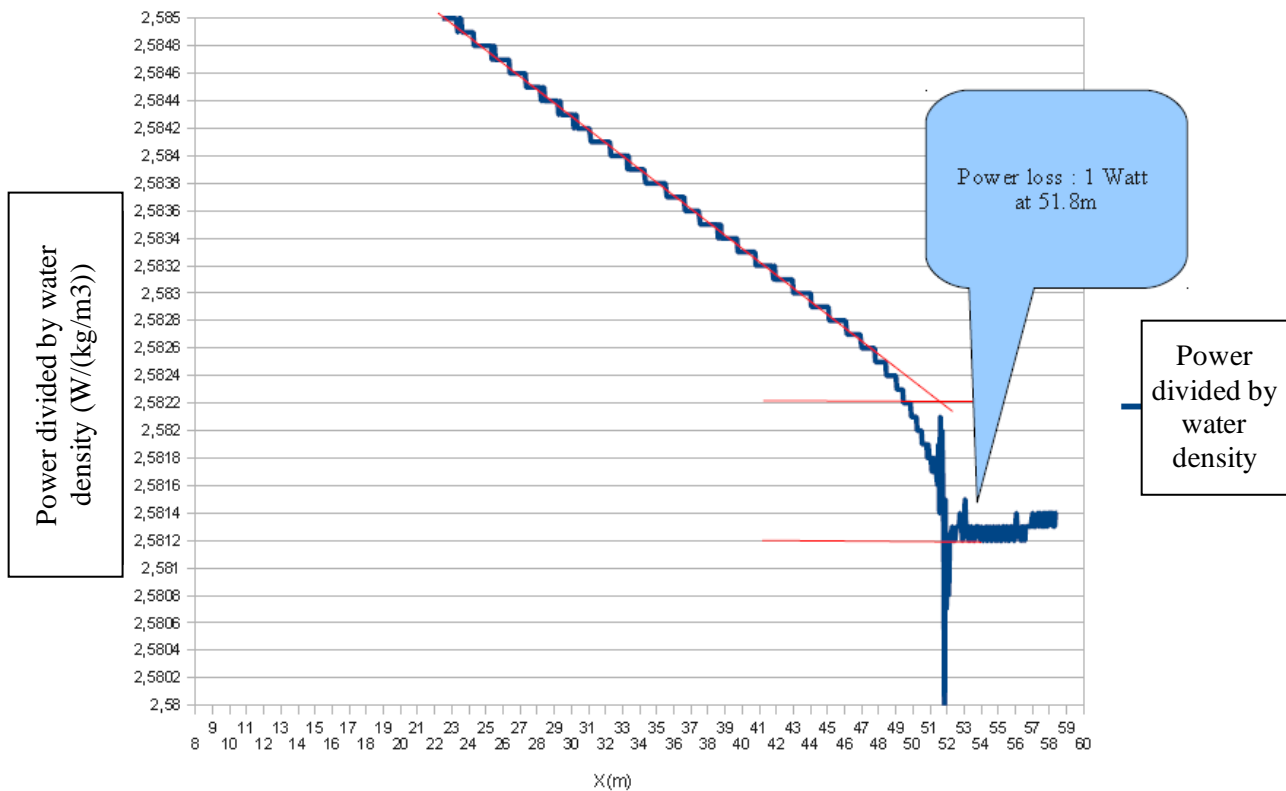
Figure 79: evolution of the power (divided by the density of water) of a section of fluid along the flume.

This simulation has been done with one processor and in parallel. In both cases, the results were the same: the deficit of power is equal to 1 watt and it occurred at the correct location. Simulations were also done for a power deficit of 2.6 Watts and the same kind of results was found. It should be noted that the value of 2.6 Watts is close to the power deficit measured in the experiment with one turbine. The conclusion of this set of simulation is that the routine has been verified with both one processor and with several processors operating in parallel.

4.3 Validation

The validation of a code can be described using the following definition:
The process of determining the degree to which a model is an accurate representation of the real world from the perspective of the intended uses of the model.

In this section, a tidal turbine is simulated in a flume and comparisons against WG4 WP1 (the experiments at EDF) experiments are done [2, 3].

Telemac3D is used to simulate the wake of one tidal turbine in a flume. The simulations will then be validated against the experimental data measured in WG4 WP1. This set of experimental data is the same as the one used to validate the Telemac2D simulations.
Unlike the study in 2D, which has been developed beyond what was required, the reproduction of the experiment for two turbulence models is the main objective of the 3D study.
To model the turbine a subroutine "SOURCE" is added to the code, where the drag force applied on the turbine is calculated (the equivalent to this subroutine in 2D is DRAGFO). The drag force modeled has the same expression as in 2D:

$$F = \frac{1}{2} \rho C_d u^2 S$$

Where C_d is the drag coefficient, calculated from the experimental data (using the speed reference taken significantly upstream from the turbine). S is the area swept by the rotating blades (S = π x (D/2)², where D is the diameter of the turbine). Unlike the study for simulating a tidal turbine in the Edf Flume in 2D (see 3.3.1.13.2), u is the velocity at significant distance upstream of the turbine, and not the velocity near the turbine (in the study in 2D with several turbines and 2 ranks the far upstream velocity is also used).

We define the volume over which the drag force is applied and distributed in order to simulate the turbine in the flow. This volume, as we will see, is roughly equal to the volume occupied by the rotating turbine (in 2D the force was applied to a surface not a volume).

Two turbulence models are investigated:

- The model with a constant turbulent viscosity.
- The k-epsilon model.

The velocity deficit from the simulation on the horizontal and axial plane of the turbine is compared to the velocity deficit of the measurements also along the horizontal and axial plane.

In addition, throughout the study 17 vertical planes will be used. Since the water level is very close to 0.8 m, each plane will be about each 5 cm high. An unstructured mesh is employed because it will be the most realistic for future studies.

Furthermore, for the rest of the report, D is the diameter of the turbine.

4.3.1 Simulation with the constant viscosity model and validation

In this section, the approach for validation is the following:

- First, the best value of the viscosity for an optimal mesh size obtained from the 2D study with one turbine (a mesh size of 5 cm) is found. A comparison between the simulations and measurements is done here in order to select this value.
- Second, the mesh size convergence for the optimal value of the viscosity found in the first part is checked. A comparison between the simulations and measurements is also done there.

4.3.1.1 First part: optimization of the viscosity coefficient

To begin analyzing the volume where the drag force is acting, a volume very close to the real volume bounded by the rotating turbine is tested. The radius is set to 0.3 m (the real radius) and the width of the volume is set to 2 x 0.05 m. The mesh size here is equal to D/12 = 5 cm. The width value is set in order to ensure that nodes are present inside the volume. This mesh size is part of the set of mesh sizes which led to good results in 2D simulations. The time step dt is 0.05 s. The Courant number condition is fulfilled since: 0.05 s = dt < (mesh size)/V ≈ 0.05/0.3 ≈ 0.16 s.

The viscosity coefficient is set to several values, and for each simulation we check that the flow reaches steady state conditions. Comparisons to measurements are provided in the figure below:
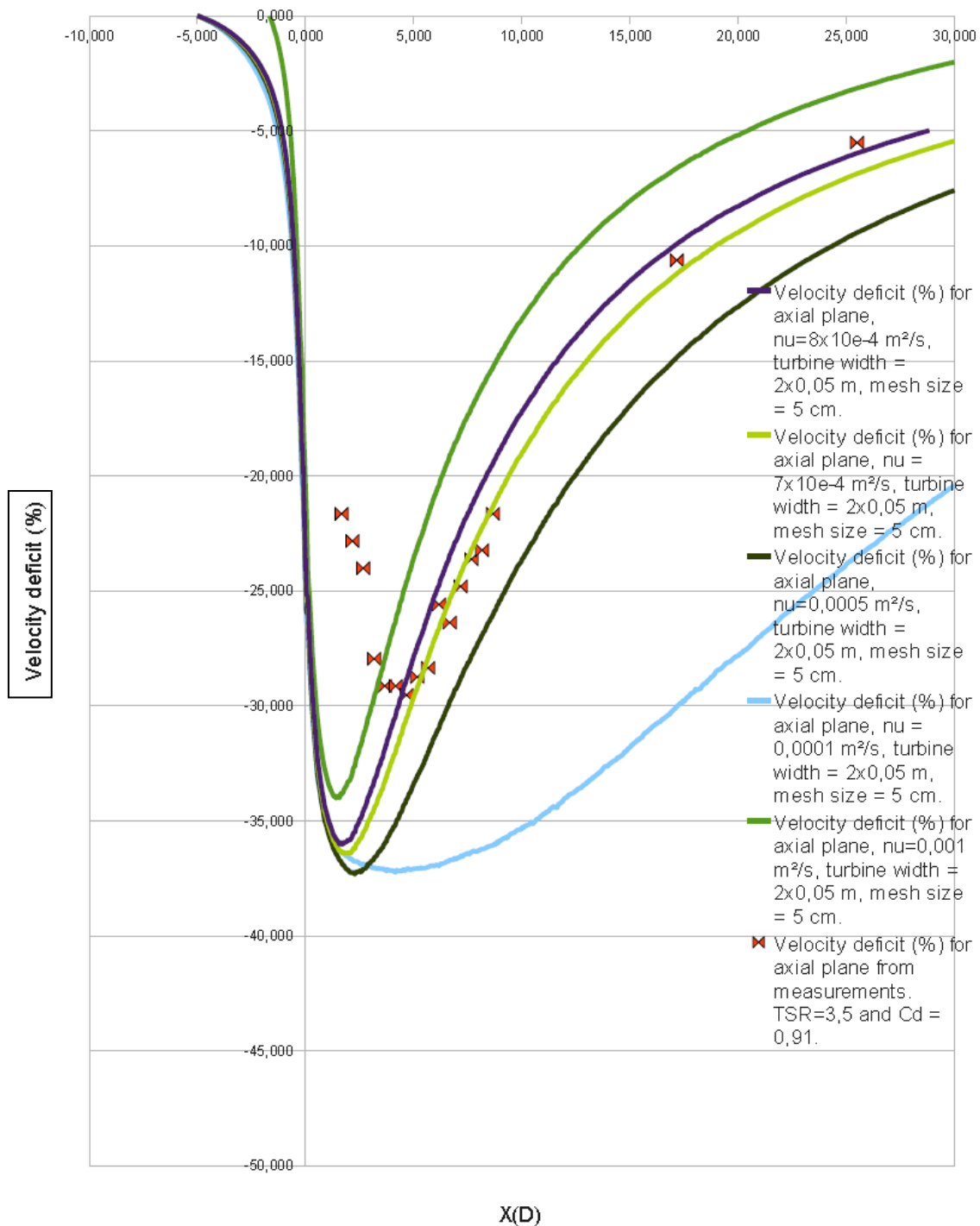
Figure 80: optimization of the viscosity value.

The graph above shows that the best value found for the viscosity constant is either 8x10e-4 m²/s or 7x10e-4 m²/s (those two value are very close). Those values lead to an axial plane velocity deficit that is very close to the measurements. In the rest of the study for this model of turbulence, the value of the viscosity is set to 8x10e-4 m²/s, which leads to the best results far from the turbines.

It can also be observed that when the viscosity decreases, the velocity deficit becomes larger (in absolute value). This behavior is less visible in the 2D simulations shown in section 3 with one turbine.

To complete the analysis of the constant viscosity turbulence model, the mesh size convergence for the selected value of the viscosity has to be checked. This is done in the following section.

4.3.1.2   Second part: mesh size convergence

In this section, the constant viscosity model with nu = 8x10e-4 m²/s is tested, for different mesh sizes: 15 cm, 10 cm and 5 cm (this last mesh size has already been tested in the previous chapter). Results can be observed in the figure below:
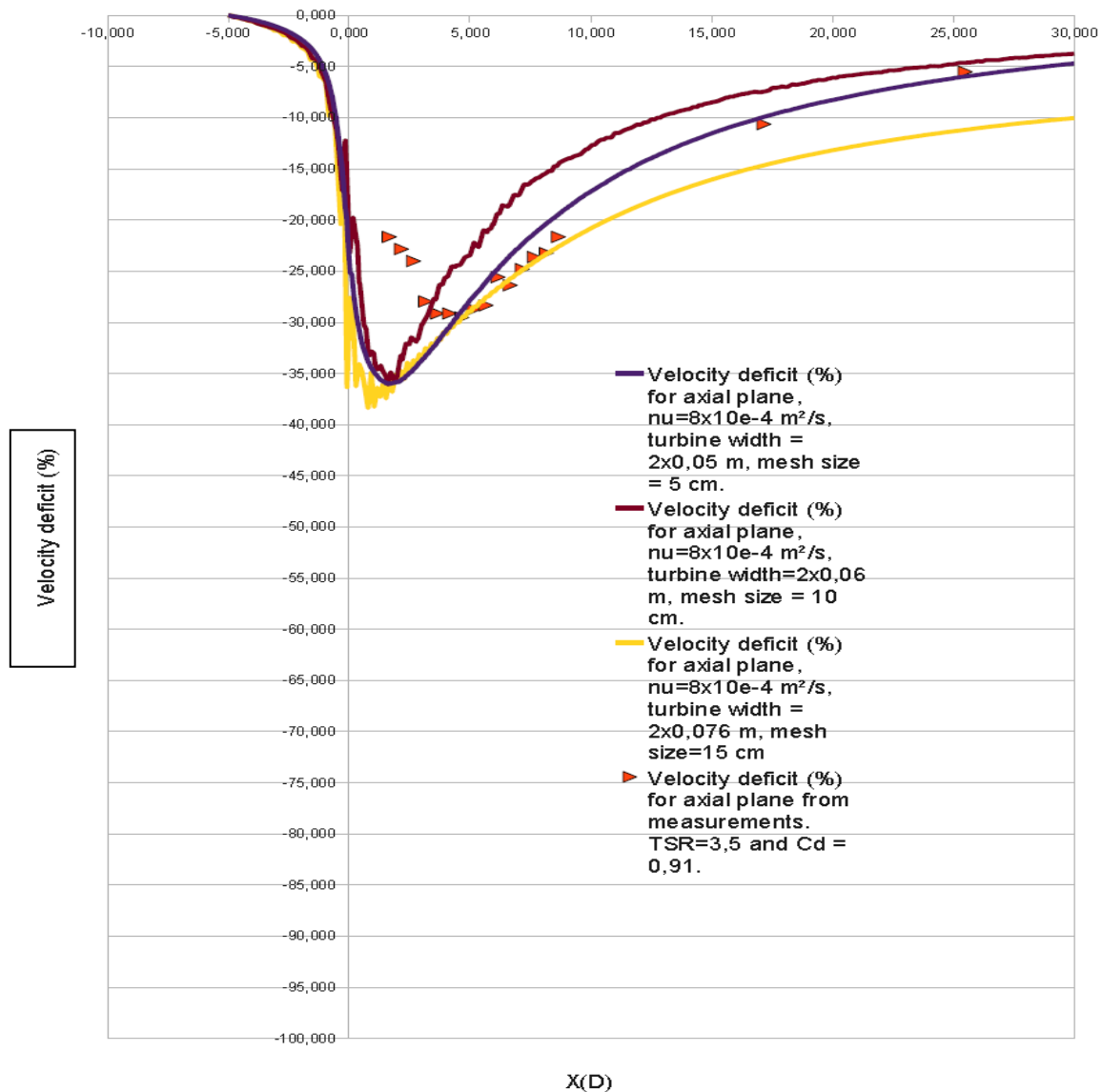
Figure 81: mesh size convergence study for constant viscosity model.

The different wakes are close to each other and the far-field wakes coming from the 5 cm and 10 cm mesh sizes converge to each other and the measurements. Thus, convergence is observed as the mesh size is reduced for the turbulence model studied.

In addition, results show that the flow is mainly in 2 dimensions for each plane since the vertical velocity is very small: about 1e-3 m/s for the maximum. Study of the convergence of the velocity deficit with the number of vertical planes will therefore not be evaluated in this case.

4.3.2 Conclusion for the constant viscosity model with Telemac3D

For the constant viscosity model, it has been verified that the velocity deficit in simulations with mesh sizes equal to D/12 and D/6 and a viscosity value equal to 8x10e-4 m²/s give less than a 5% difference when compared to the measurements.
In summary:
- The subroutine has been verified (with one processor and several processors).

- The mesh size convergence has been investigated.

- The value of the constant viscosity has been found.

- Comparison to experimental shows a good agreement.

- It is believed that the study of the convergence of the wake depending on the number of vertical planes is unnecessary as the vertical velocity is very small.

- All this shows that the SOURCE subroutine allows users to simulate accurately the wake downstream of a tidal turbine using a constant turbulent viscosity model in Telemac3D.

4.3.3 Simulation with the k-epsilon model

In this section, the following is adopted:

- First, several k-epsilon models are compared to measurements.
- Second, the mesh size convergence with the optimal k-epsilon model found in the first part is checked. A comparison between simulation and measurements is also done here.

4.3.3.1 First part: optimization of k-epsilon model

In this section, several models of k-epsilon are tested with a small mesh size (5 cm). In these simulations, since the turbine is not meshed, there is no obstacle in front of the flow, and therefore in Telemac3D turbulence cannot be generated in the flume. To overcome this problem, the following tests are performed:

- 1) A mast is added inside the flume.

- 2) Terms are added to modify the value of k and epsilon only in the volume delimited by the rotating turbine.

For the second tests the following expression is added to k:

$$\eta \times \frac{1}{2} C_d S U^2 Ul$$

The same kind of expression was also used in the Telemac2D simulations of one turbine. U is the far upstream velocity and Ul is the local velocity.
For epsilon, several expressions are tested: The equation that links k and epsilon in the k-epsilon model is the following one [2]:

$$\nu_t = C_\mu \frac{k^2}{\varepsilon}$$

Several values for ν_t are tested. In reference [15] the following relation is suggested:

$$v_t \approx \sqrt{k}\mathrm{D}$$

Where D is the diameter of the turbine. D is close to the size of large vortices.
Constant value of v_t will also be tested (only in the volume bounded by the rotating turbine).

Once v_t is defined, epsilon can be computed in Telemac3D.
The simulation without adding any term to k and epsilon gives the following results:
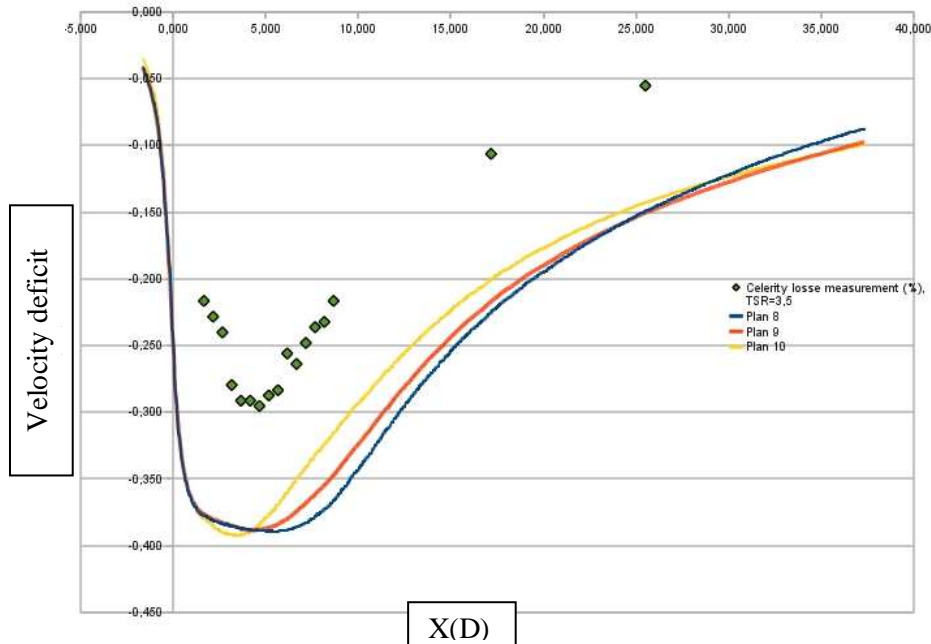
Figure 82: velocity deficit with the k-epsilon model compared to measurements.

The above results show the velocity deficit for the three planes (plane 8, 9 and 10) closest to the axial plane of the turbine.
There is no agreement between simulations and measurements (except on the location of the minimum of the velocity deficit). Further investigations are therefore needed.

In the following figure the velocity deficit on the axial plane when the mast is meshed is plotted. It should be noted that in the experiment, the mast ranges from z=0.8 m to z=0.4 m. This kind of obstacle cannot be meshed in Telemac3D, therefore, in the simulations the mast ranges from z=0 m to z=0.4 m. In addition the diameter of the mast is nearly 10 cm.
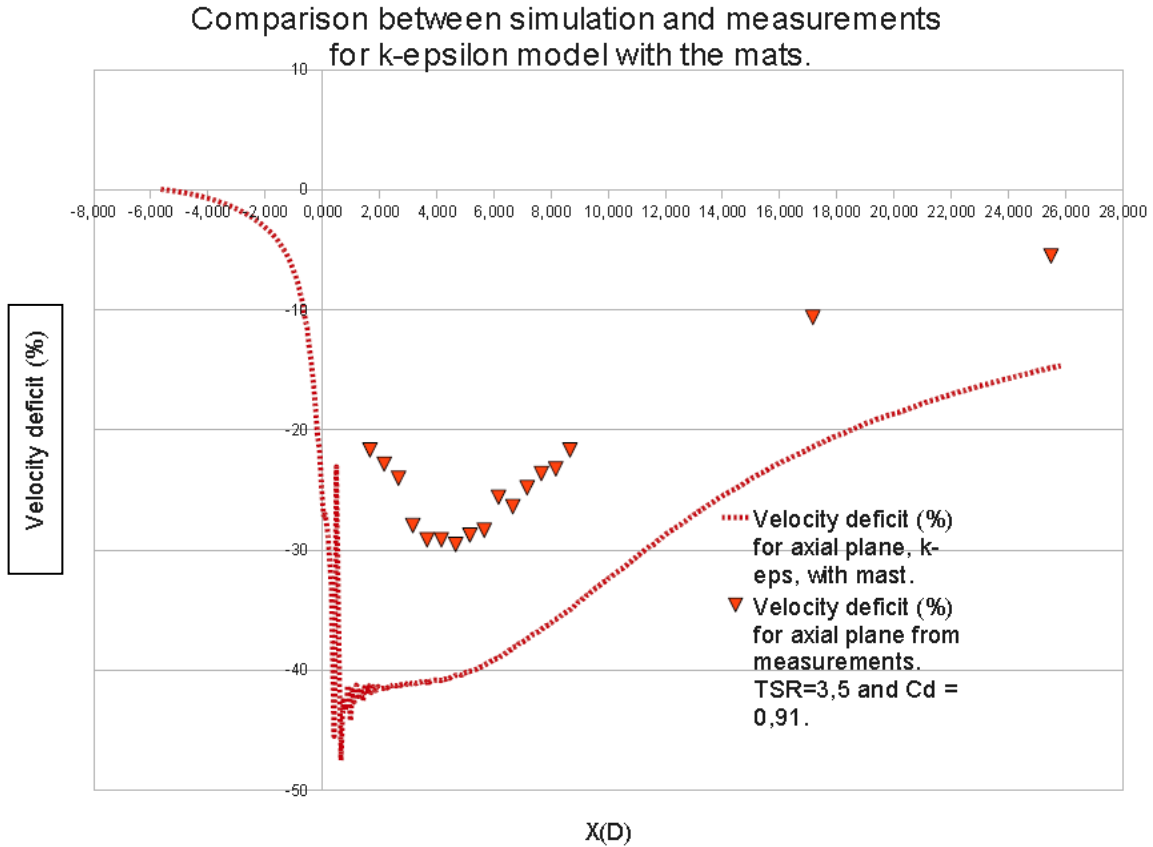
Figure 83: velocity deficit on the axial plane when the mast is meshed.

The above results are similar to the results shown in Figure 82. Oscillations coming from the mast can be seen, but the wake is still far from the experimental measurements. Moreover, the velocity deficit is greater than in the experiments. Therefore a test is performed with the drag coefficient reduced.

The following figure shows the results of reducing the drag coefficient (by 24%) in order to align the simulated velocity deficit minimum to the experiments.
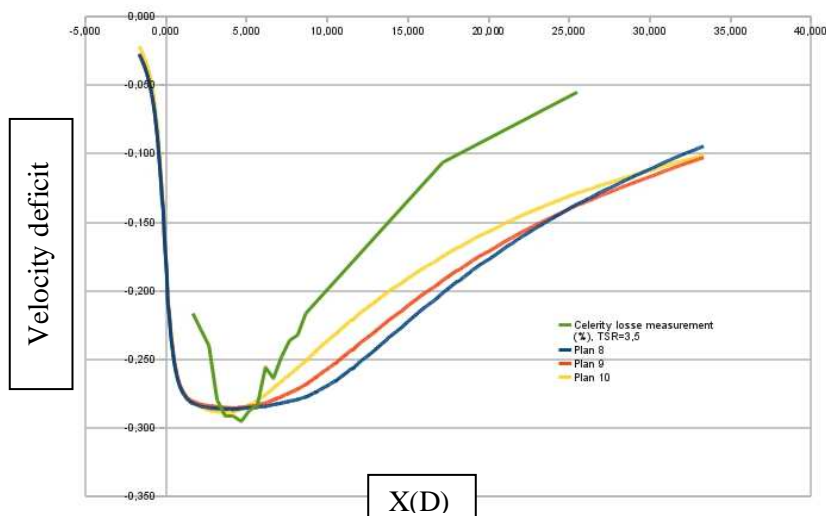
Figure 84: velocity deficit for the three planes (plane 8, 9 and 10) closest to the axis, when the drag coefficient is smaller (24% less).

The above results show a good agreement of the minimal velocity deficit, but far from the turbine the simulated wake does not converge to the measurements.

This test is therefore inconclusive, and for this reason neither the drag coefficient nor the bathymetry will be modified. Therefore only the values of k and epsilon will be modified. In Telemac3D these values are modified in the k-epsilon model through the subroutine DIFF3D.
The figure below shows the velocity deficit on the axial plane of the turbine for several k-epsilon models.

Figure 85: velocity deficit on the axial plane for several k-epsilon models.
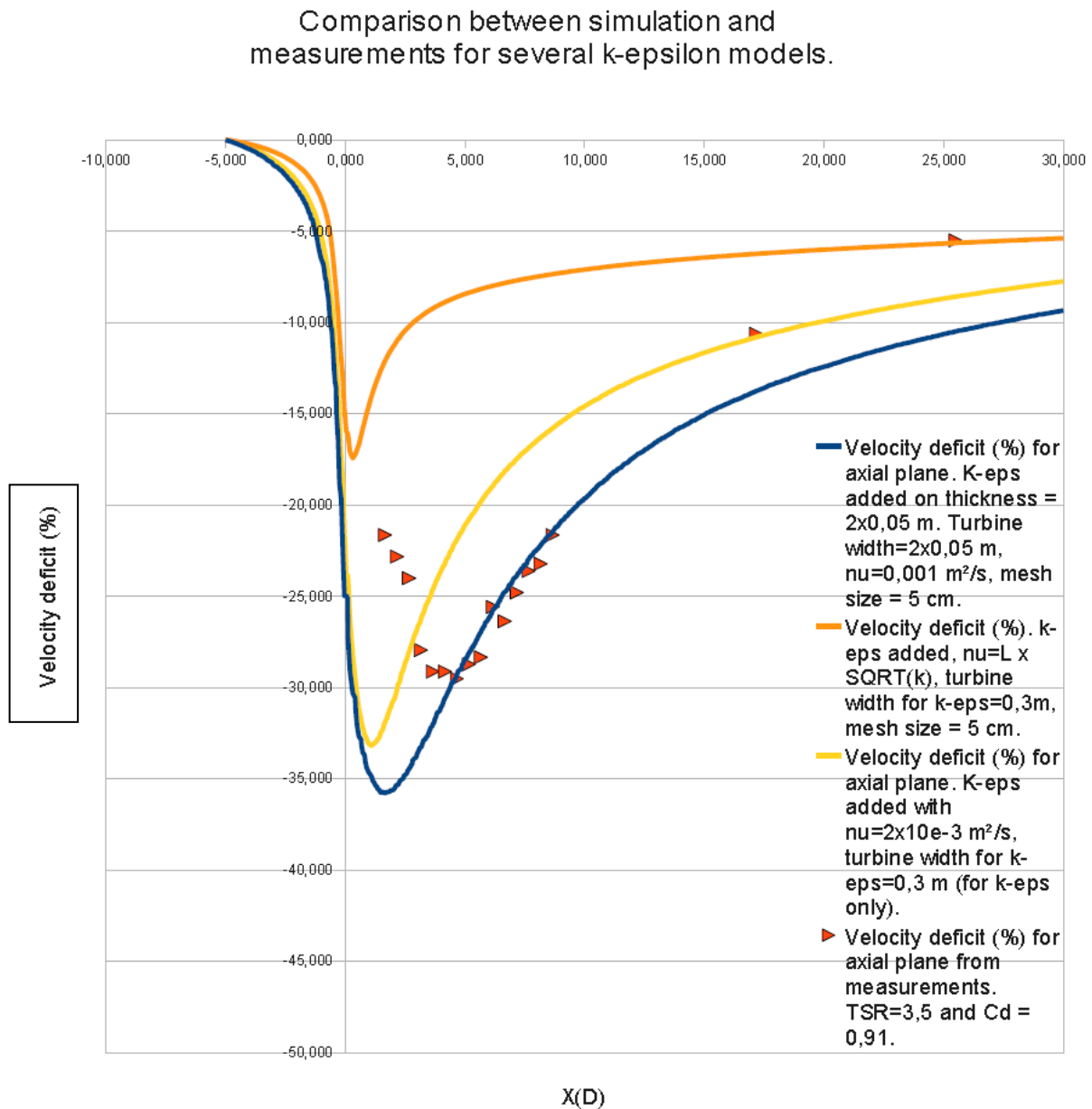
The blue line corresponds to the test where we add the following value to k:

$$\eta \times \frac{1}{2} C_d S U l^3$$

With η=0.05, this is the same coefficient as in 2D for one turbine.

The value of epsilon is then linked to to k through the following formula:

$$\nu_t = C_\mu \frac{k^2}{\varepsilon}$$

With ν_t =0.001 m²/s.

The modification of k and epsilon are done only on the volume roughly delimited by the rotating turbine (diameter D=0.6 m, width = 2 x 0.05 m).

The yellow line, is the same test but with ν_t =0.002 m²/s.

The orange line is also the same test, but the value of ν_t is:

$$\nu_t \approx \sqrt{k}.D$$

The results represented with the blue line show quite good agreement with the experiment. The difference between the minimum of this simulated and experimental velocity deficits is about 5%. Close to the turbine, the blue line goes through several experimental points. Far from the turbine, the simulated velocity deficit is also close to the measurements (less than 5% of difference). This model for k-epsilon is therefore selected. In the following chapter, the convergence with the mesh size is checked.

It can be also observed that when the viscosity is smaller inside the volume bounded by the turbine, the velocity deficit becomes larger (in absolute value).

4.3.3.2 Second part: mesh size convergence

In this section, convergence for the wake with the mesh size for the previous k-epsilon model found is checked. Comparison between wakes for three tests with three different mesh sizes, 15 cm, 10 cm and 5 cm, are made.

The figure below shows the velocity deficit on the axial plane for the three different mesh sizes in the k-epsilon model previously selected. The simulated wake is compared to the measurements.
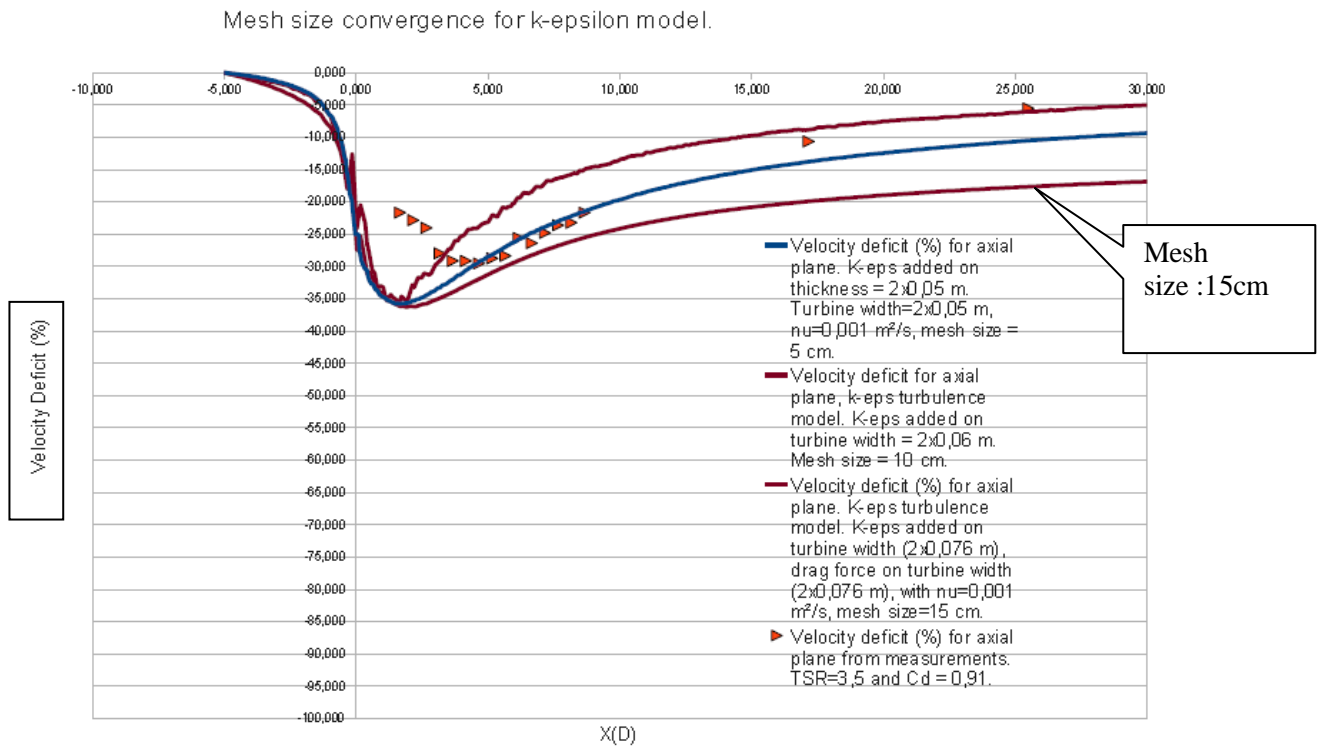
Figure 86: study of mesh size convergence for the selected k-epsilon model.

The above results show good agreement to the measurements for the smaller mesh sizes (5 cm and 10 cm). Far from the turbine, the simulated velocity deficit varies on the order of less than 5% from model for the smaller mesh sizes (5 cm and 10 cm). The simulated velocity deficit for the mesh size equal to 15 cm is non convergent far away from the turbine.

These results validate the mesh convergence for the selected k-epsilon model.

4.3.4 Conclusion for the k-epsilon model with Telemac3D

For the k-epsilon model, it has been verified that the velocity deficit in simulations with mesh sizes equal to D/12 and D/6 give less than a 5% difference when compared to the measurements.

In summary:

-   The subroutine has been verified with one processor and several processors (as it is the same subroutine used with the constant viscosity model).

-   The mesh size convergence has been investigated.

-   The modification for k and epsilon has been found.

-   Comparison to experimental data shows a good agreement.

-   It is believed that the study of the convergence of the wake depending on the number of vertical planes is unnecessary as the vertical velocity is very small.

- All this shows that the SOURCE subroutine allows users to simulate accurately the wake downstream of a tidal turbine using the k-epsilon model in Telemac3D.

4.3.5 Conclusion

Two kinds of turbulence models, with constant viscosity and k-epsilon, are tested to simulate the wake of a tidal turbine. Quite good agreement (less than 5% of difference for the velocity deficit after 5D) between the simulations and the measurements of the wake has been observed. These simulations are done without changing the drag coefficient (defined using the reference velocity far upstream of the turbine (V_{far})) or the diameter of the turbine and keeping a similar volume delimited by the rotating turbine. So, the only parameters in our simple model are the viscosity coefficient and the mesh size:
- For the constant viscosity model, the following constant is used: $\nu_t = 0.0008$ m²/s.
- For the k-epsilon model a term to k and epsilon has been added on the volume delimited by the rotating turbine. The link between k and epsilon is done with a value of $\nu_t = 0.001$ m²/s (note that this value is very close to the value used for the constant viscosity model).
- To the value of k, the following term is added:

$$\eta \times \frac{1}{2} C_d S U^2 U l$$

With η=0.05 (this is the same coefficient as in 2D simulations of one turbine).
- For epsilon, the following relation is used (this is the relation used in the k-epsilon model):

$$\nu_t = C_\mu \frac{k^2}{\varepsilon}$$

For both models, the best simulations are done with a mesh size of 5 cm (D/12). Far from the turbine, a mesh size of 10 cm (D/6) leads also to good results.

It has been observed that the 2D simulations are limited since the maximum of the velocity deficit in the axial plane is not necessarily an increasing function of Cd. This is not a big issue since the magnitude of the simulated wakes are very close to the experimental wakes (the latter being also very close to each other). In 3D, it has been found that the viscosity coefficient has an effect on the maximum of the velocity deficit in the axial plane (unlike in 2D). The viscosity coefficient could therefore be a function of the tip speed ratio. This function could help to simulate a more accurate wake and must be researched in further studies. Nevertheless, for now, the 3D simulations are accurate enough to find the magnitude of experimental wakes.

At last, it should be reemphasize that the study of the convergence of the wake depending on the number of the vertical planes is unnecessary, because the vertical velocity is very small.

4.4 Methodology for large scale simulation with Telemac3D

The methodology which has to be used in order to simulate several tidal turbines on a large basin with Telemac3D, very close to the methodology used in 2D. It is given by the following steps:

- Finding the deficit of power created by all the turbines. This means that, at first, all the turbines have to be simulated in a flume. The bathymetry is set to the true bathymetry in order to get more accuracy on the flow interactions. The SOURCE subroutine is used here, with a drag coefficient for each turbine equal to the value given by the manufacturer of the turbine or found in an experiment. The surface is equal to the surface swept by the rotating turbine and the volume over which the drag force is applied and distributed is roughly equal to the volume occupied by the rotating turbine. Then, the energy of a section of the fluid has to be calculated along the fume. It is necessary to subtract the power from the trial with the turbines from the power in the empty (no turbine) trial at each point in the length of the canal before evaluating the drop in power across the turbines. This step is necessary (like in the 2D study) because the bathymetry causes the power drop across the turbines to be difficult to see in the results from the trial with the turbines alone.

In this step, the mesh size has to be small, for example D/12 or D/6. Finally, the deficit of power ΔE/Δt created by all the turbines can be calculated. If the k-epsilon model is used, a term has to be added, in the same way as it would be done for a single turbine in a flume (the subroutine DIFF3D where k and

epsilon are modified in this case is written in the appendix 8.7). If the constant viscosity model is used, the best coefficient found is 8x10e-4 m²/s, which leads to the best results far from the turbines.

- Use this deficit of energy ΔE in order to find the global drag coefficient C_{eq} equivalent. To do this, the following formula is used:

$$(\tfrac{1}{2})\rho C_{eq}U^2 A Ul = (\Delta E/\Delta t) => C_{eq} = 2(\Delta E/\Delta t) / (U^2 A Ul \rho)$$

A is the combined areas of the turbines in the cross-section of the flume, ρ is the density of the water, and U is the far upstream velocity and Ul is the mean local velocity.

- Simulate the set of turbine with the equivalent drag coefficient C_{eq} with the subroutine SOURCE on any large basin. The mesh size used can be defined with the same methodology used with Telemac2D: the mesh is refined around the array location (a mesh size of 1 diameter can be used like in 2D) and the mesh refinement is performed with a growth rate of 1.2, which is an acceptable growth rate to maintain accurate Telemac3D outputs. The volume on which to apply the drag force can be the sum of each volume bounded by the rotating turbine. For the simulation, we use one of the two turbulence models which have been studied in this document. If the k-epsilon model is used, a term has to be added as it is explained before (the subroutine Diff3D where k and epsilon are modified in this case is written on the appendix 8.7). If the constant viscosity model is used, the best coefficient found is 8x10e-4 m²/s, which leads to the best results far from the turbines.

4.5   Limitations of the model

The main limitation is the computation time. This computation time is roughly equal to the number of planes used in the 3D simulation multiplied by the 2D computation time simulation for the same basin. For issues linked to blockage ratio, the explanations of chapter 0 are also valid for the 3D simulation.

5   GENERAL CONCLUSIONS

The DRAGFO (2D) and SOURCE (3D) routines have been developed. They have been verified with a single processor and several processors. The k-epsilon model looks more appropriate to use because no coefficient associated with the turbulence model has to be set up.
Several sets of simulations have been performed and compared to experiments in order to validate the 2D and 3D routines.

The methodology which enables the simulation of a tidal array in a coastal basin scale model has been set up for both 2D and 3D. It is built on the step-by-step process which had been used for the validation task, which increases confidence in the ability of these routines to assess large scale effects of tidal energy extraction at basin scale. It consists in running simulations at a local scale with individual devices, in extracting the equivalent array drag coefficient from these, and in inserting that piece of information in the large basin scale model.

Telemac2D and Telemac3D are now capable of assessing the impact of any array layouts on large scale hydrodynamics effects, as the software user has the opportunity of combining the use of the DRAGFO and SOURCE routines with an appropriate methodology.

6   NEXT DELIVERABLES

- D3 - Incorporating parametric characterization of an axial flow turbine array (obtained in WG3 WP2) into the 2D basin scale numerical models.
- D4 - Assessment of the effects of energy extraction at various UK sites with the 2D model: Macroscopic, but still reliable, study of the large scale impact of a tidal farm on the hydrodynamic of the area, and accurate assessment of the site tidal resource.
- D5 - Cross-comparison of 2D and 3D results, in terms of energy extraction, for the selected site.

7   BIBLIOGRAPHY

- 1. Blevins Robert D. Flow-induced vibration. Krieger publishing company, 1990, 477p.

- 2. Buvat Clément, Martin Vanessa. Identification of test requirements and physical model design. WG4 WP1 D1 deliverable for the PerAWaT project, 2010, p28.

- 3. Buvat Clément. Performance of tank tests with physical scale model of horizontal-axis turbine device installed. Analysis of results. WG4 WP1 D4 deliverable for the PerAWaT project, 2012, p39.

- 4. Hervouet Jean-Michel. Hydrodynamique des écoulements à surface libre, modélisation avec la méthode des éléments finis. Presses de l'école nationale des ponts et chaussées, 2003, 311p.

- 5. Hinze J. O. Turbulence. Mcgraw-Hill College, 1975, 790p.

- 6. Leclerq Mathilde. Estimation de l'influence sur les courants marins de l'implantation d'un parc d'hydroliennes dans la zone du Raz Blanchard. Rapport de stage de recherche à EDF, 2007, 39p.

- 7. Medici D., Alfredsson P.H. Measurements on a wind turbine wake: 3D effects and bluff body vortex shedding. Wind Energy, vol.9, 2006, p219-236.

- 8. Negretti M. E., Vignoli G., Tubino M., Brocchini M. On shallow-water wakes: an analytical study. Journal of Fluid Mechanics, 2006, vol 567, p457-475.

- 9. Nieviadomy Constance. Influence du maillage sur les résultats des simulations sous Telemac-2D. Rapport de stage à EDF, 2009, p28.

- 10. Nishino Takafumi, Willden Richard H.J. Low-order modelling of blade induced turbulence for RANS actuator disk computations of wind and tidal turbines. EUROMECH Colloquium 528: Wind Energy and the Impact of Turbulence on the Conversion Process, Oldenburg, Germany, 2012, p6.

- 11. Norberg C. Fluctuating lift on a circular cylinder: review and new measurements. Journal of Fluids and Structures 17, 2003, p57-96.

- 12. Peyrard Christophe, Buvat Clément. Approche numérique de l'influence des effets de sillage sur la puissance extractible d'un parc d'hydroliennes. Rapport de stage de fin d'étude à EDF, 2006, p77.

- 13. Sumer B. Mutlu, Fresoe Jorgen. Hydrodynamics around cylindrical structures. World Scientific, Advanced series on Ocean Engineering – vol 12, 1999, 530p.

- 14. Violeau Damien. Les fondements de la turbulence. Cours LNHE, 167p.

- 15. Viollet Pierre-Louis, Chabard Jean-Paul, Esposito Pascal, Laurence Dominique. Mécanique des fluides appliquée, écoulements incompressibles dans les circuits, canaux et rivières autour de structures et dans l'environnement. Presses de l'école nationale des ponts et chaussées, 2002, 367p.

- 16. Yulistiyanto Bambang. Flow around a cylinder installed in fixed-bed open channel. Thesis presented to the Ecole Polytechnique Fédérale de Lausanne, 1997, 229p.

- 17. Systeme de modelisation TELEMAC TELEMAC3D/ Manuel Utilisateur.

8 APPENDICES:

8.1 Brief description of Telemac-2D

The Telemac-2D code is based on the two-dimensional Saint Venant equations, well suited to the study of free surface flows in shallow waters and thus to fluvial and marine hydraulics. These equations are obtained by depth-averaging the Navier-Stokes equations and making the following assumptions:

Pressure is assumed to be hydrostatic.
The wave-length of the phenomena being studied must be much larger than the water height.
The vertical component of velocity is ignored.
The bottom and the free surface are impermeable.

The continuity equation and the two equations for the quantity of motion are then written:

$$\frac{\partial h}{\partial t} + \operatorname{div}(h\vec{u}) = 0$$

$$\frac{\partial(hu)}{\partial t} + \frac{\partial(huu)}{\partial x} + \frac{\partial(huv)}{\partial y} = -gh\frac{\partial Z_s}{\partial x} + hF_x + \operatorname{div}\left(hv_e \overline{\operatorname{grad}(u)}\right)$$

$$\frac{\partial(hv)}{\partial t} + \frac{\partial(huv)}{\partial x} + \frac{\partial(hvv)}{\partial y} = -gh\frac{\partial Z_s}{\partial y} + hF_y + \operatorname{div}\left(hv_e \overline{\operatorname{grad}(v)}\right)$$

where h is the water height, u and v the two horizontal components of the velocity, Zs the free surface elevation and v_e an effective diffusion that takes into account the turbulent viscosity and the dispersion terms [4].

8.2 Calculation and validation of the Strouhal number for the meshed cylinder case

For the simulations involving vortex shedding, the shedding frequency can be obtained by performing a Fourier transform of the temporal variations of velocity at a point in the wake. The Strouhal number can then be calculated easily and plotted in Figure 87:

$$St = \frac{fD}{U}$$

The relationship between Strouhal and Reynolds numbers is also well described in the literature. Figure 87 presents the Strouhal as a function of Reynolds noted during the experiments together with a line obtained with empirical formulae [11].
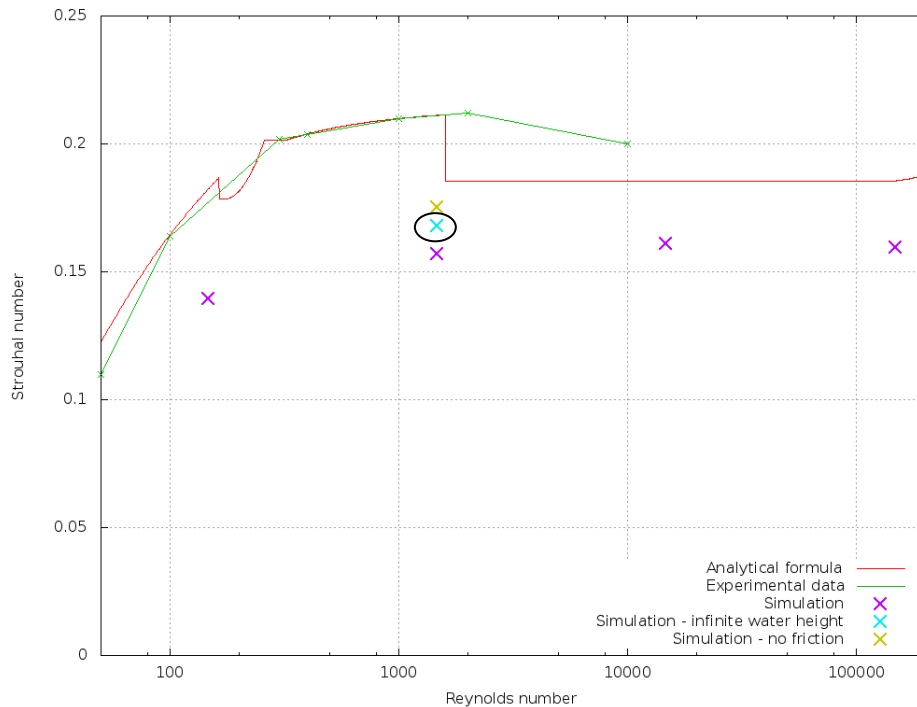
Figure 87: Strouhal number as a function of the Reynolds number. The circled examples show good agreement theory-measurement.

The simulations give a good order of magnitude of the Strouhal number even the resting slightly below the values obtained through experimental measurements.

The Strouhal number is, in principle, defined for unbounded flow (i.e. unrestricted by channel walls) and non-dimensional (infinite) depth; thus bottom friction plays no role in the parameters of the theoretic system. However, the flow is simulated in a flume with a width only 10 times larger than the cylinder, in shallow water (less than 1 diameter) and bottom friction is considered non-negligible. This could explain the lower values obtained in the simulations for the Strouhal number.

The simulations confirm that depth has an influence on the Strouhal number, as the former increases, so does the latter (Figure 88). The role played by friction is also be seen in this figure: in shallow water, the presence of friction corresponds to a decrease in Strouhal number. Taking account of these factors enables to obtain better values for the Strouhal number (circled points in Figure 87). The Strouhal value is still lower than the values described in the literature. It seems reasonable to infer that this is due to the effect of the sidewalls of the flume [13].
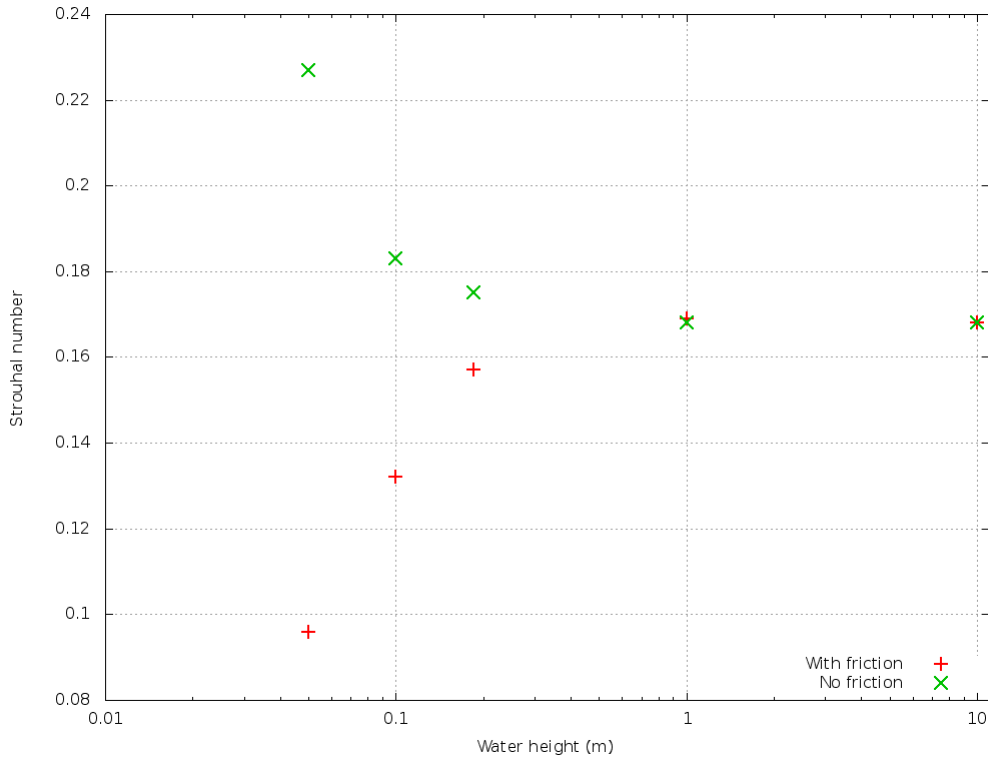
Figure 88: Strouhal number as a function of the water height in the flume, with and without friction, for the constant viscosity model with v=10^{-4} (Re=1474).

8.3   Verification of the self-similarity in the wake of the meshed cylinder

Using a number of assumptions, Hinze [5] proposes the following formula for the velocity deficit for the transverse dimension of the wake of a cylinder:

$$\frac{\overline{U_1}}{\overline{U_{1,max}}} = \exp\left[-\left(\frac{\xi_2}{C}\right)^2\right]$$

For a given x, $\overline{U_1}$ is the velocity deficit defined as: $\overline{U_1}(x, y) - U_0 - \overline{U}(x, y)$

U_0 is the upstream velocity, where the obstacle produces no effect.

$\xi_2 = \frac{y}{\sqrt{D_{Px}}}$ describes the transverse and $C = \sqrt{\frac{U_0 D}{4(\varepsilon_m)_{11}}}$, where $(\varepsilon_m)_{11}$ is the turbulent viscosity (or eddy-diffusion) component [5]. Hinze proposes 0.256 as the value for C. In the present case, this coefficient is changed to 0.275.

For the simulations using the k-ε model, self-similarity is clearly verified (cf. Figure 13). On the other hand, for the constant viscosity model, the formula proposed by Hinze does not allow retracing the line plotted with the simulated data, as shown by Figure 89. This is notably due to the fact that, with the constant viscosity model, strong velocity acceleration occurs at the flume sidewalls (Figure 88), whereas the formula merely provides for an increase in the velocity from the centreline to the sides only to the point where it reaches its reference value.
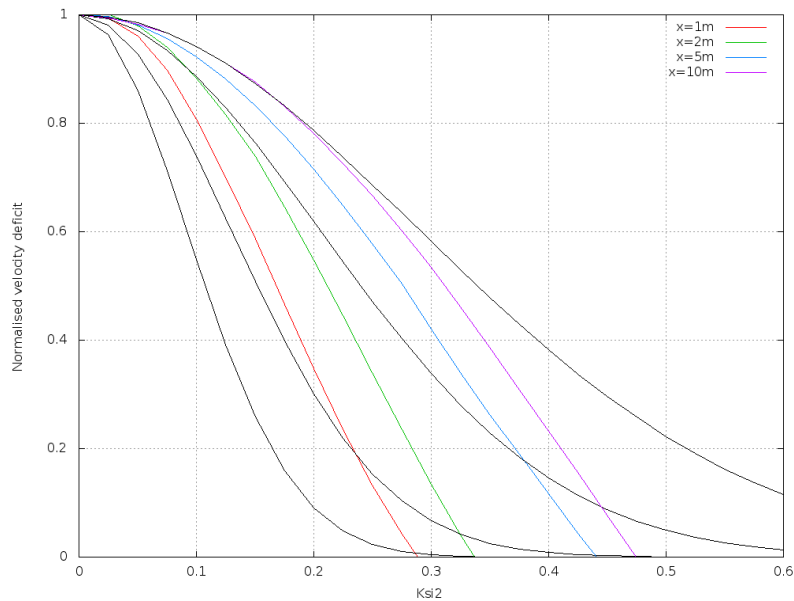
Figure 89: Normalised velocity deficit as a function of ξ2, at different distances downstream of the cylinder, obtained through simulation (coloured lines) or with the analytical formula [5] (black lines) – constant viscosity model.
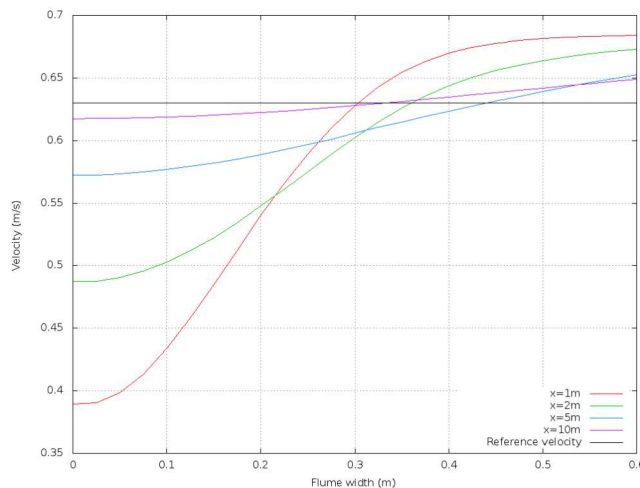

Figure 90: Transverse velocity profiles at different downstream distances from the cylinder for the constant viscosity model. The black line represents the reference velocity, relative to which the deficit is calculated.

This problem was resolved by turning to the formula proposed by Negretti [8], which is valid for shallow water flow in open channels.

The indices ∞ correspond to the far-upstream or reference velocity values. The velocity deficit is then defined as:

$$u_{def} = u_{\infty} \quad u(x,y) = u_{def}\,\varphi(\zeta)$$

The function φ represents the normalised velocity deficit relative to ζ, which describes the transverse direction according to y:

$$\zeta = \frac{y}{l(x)}$$

$l(x)$ corresponds, for a given x, to the y-value for which the velocity deficit equals 61% of the centreline velocity.

Also defined is:

$$l_* = \frac{Eh_\infty}{f} = l4$$

L being the boundary between the near wake and the far-wake. f is the friction coefficient, determined using the Manning coefficient m, the hydraulic radius R_H, and the following formula [4]:

$$f = 4\frac{^{1}\!/_{0}\, g m^{2}}{R_{H}^{1/3}} = 0,02$$

L being equal to 74 m, the case remains that $x \ll L$. In this case, based on the assumption $h \ll l \ll L$, with x being given, the function φ can be calculation using the following formula:

$$\varphi(\zeta) = \exp\left(\frac{1}{2}\zeta^{2}\right)$$

The plot of this function using the above formula and the values obtained from the simulations under Telemac-2D enables to check whether the latter verify adequately the self-similarity condition. On the following figures, it is observed that self-similarity is respected for both turbulence models.
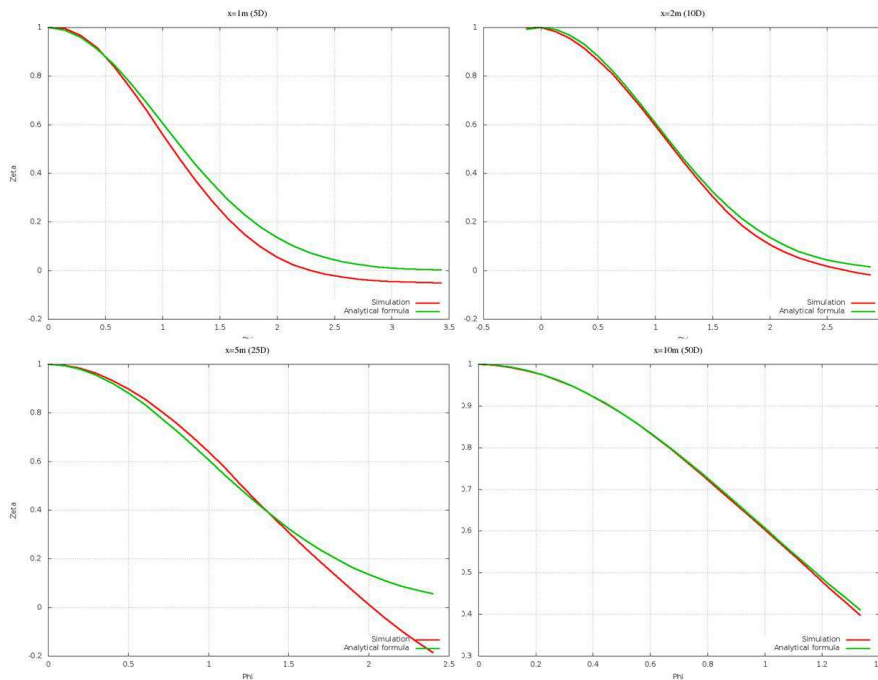

Figure 91: $\varphi(\zeta)$ resulting from the simulations (red curve) and the analytical formula (green curve), for x=1m, 2m, 5m and 10m, for the constant viscosity model.
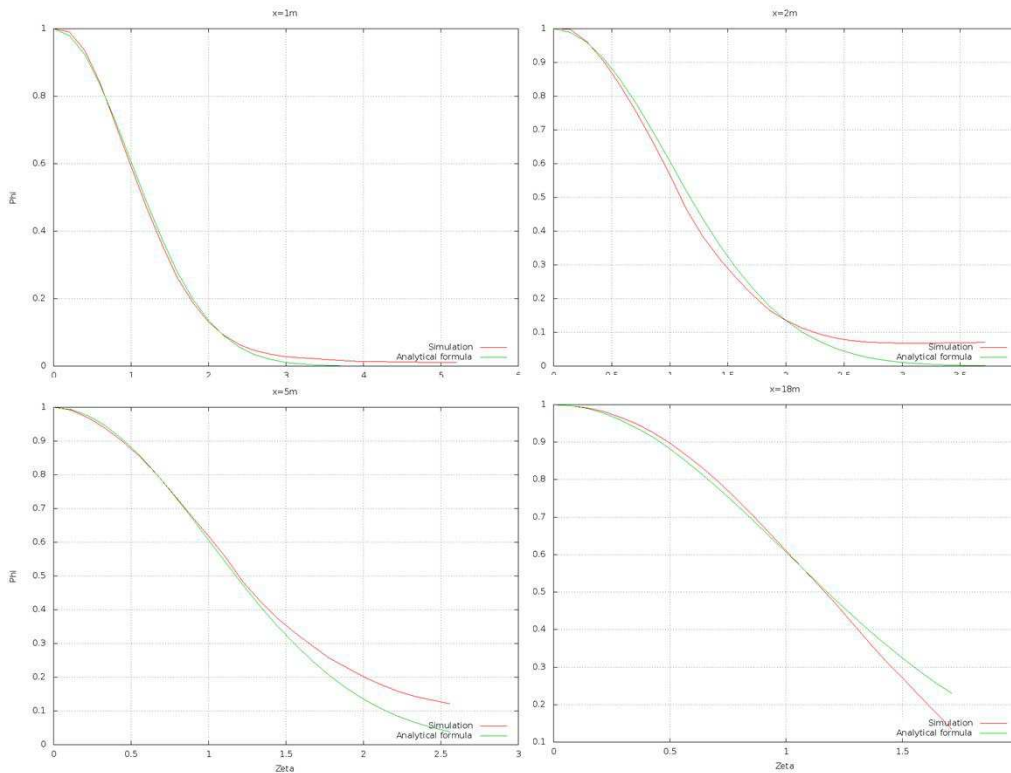
Figure 92: $\varphi(\zeta)$ resulting from the simulations (red curve) and the analytical formula (green curve), for x=1m, 2m, 5m and 10m, for the k-ε model.

8.4 Summary of the parameters used for modelling the tidal energy converter in a flume

Test	Test n°1					Test n°2 (high turbulent intensity)					Test n°3 (high velocity)	
Operating regime	w1	w2	w3	w4	w5	w1	w2	w3	w4	w5	w0	w1
TSR	1.5	2.5	3.5	4.5	5.5	1.5	2.5	3.5	4.5	5.5	3.5	4.5
Δx (D equivalent)						D/12 / D/24						
Δx (cm)						5 cm / 2.5 cm						
Δt (s)		0.1					0.1 / 0.01					0.1
Q (m3/s)						0.281 / 0.278					0.625 / 0.61	
Cf (Strickler coefficient) (-)		80 / 140				80 (impossible to adjust for the k-ε model)					80 / 140	
vt (constant viscosity) (m²/s)						5.10^{-5}						
η (k-ε model) (-)						0.05						
L (m)						1						
D (m)						0.15						
Position / flume inlet (m)						52.3						
Cd experiment (-)	0.78	0.88	0.91	0.97	0.77	0.5	0.53	0.62	0.66	0.55	0.68	0.7
Cd simulation (-)	0.7	0.9	1.05	0.9	0.9	(too much variation of velocity)					0.73	0.83 / 0.88

For data given in the form • / •, the left-hand term corresponds to constant viscosity and the right-hand term to k-ε. D is equal to 0.6 m for the EDF experiment.

8.5 Simulations for the test at high velocity (test n°3)

The following part describes results found when testing the turbine model in the EDF flume for different cases: test at high velocity and low turbulent intensity and test at law velocity and high turbulent intensity.

8.5.1 Experimental results

This test at high velocity ($U \approx 0.55 m/s$) and low turbulent intensity (5%), is only carried out for two operating regimes:

Operating regime	W0	W1
TSR	3.5	4.5
Ct	0.68	0.70
Cp	0.40	0.35

Table 15: Details of operating regimes studied – w0 and w1

The lines representing the drag coefficient and the power coefficient are not the same as those obtained with the low velocity test; the same operating regime corresponds in this case to different values of Cd and Cp. It is also noted that even though the drag coefficients are nearly equal for the two operating regimes, the velocity deficit varies by 1cm/s (cf. black crosses on Figure 93 or Figure 94). This is probably due to effects induced by the rotational speed of the turbine rotor.
The wake is longer than in the previous test, but there is not necessarily a greater maximum velocity deficit [3]. This is due to the fact that the Cd is lower and the velocity is higher than in test n°1; on the other hand, the drag force is proportional to Cd and to U².
A noteworthy point is the appearance of a flat plateau of constant deficit in the wake velocity, as can be seen in Figure 93 or Figure 94 (black points). A similar plateau is observed in the wake of wind turbines; it is certainly due to the presence of two types of vortices [7, 10]:
- Those generated by the solid disc that the rotor forms (rotor vortices)
- Those generated by the rotor blade tips (tip vortices)

The rapid disappearance of small vortices generated by the blades is probably at the source of the plateau observed during velocity recovery. It is clear that this type of phenomenon cannot be reproduced by using the model based on the DRAGFO routine.

8.5.2 Simulation parameters

As the only difference between tests n°1 and n°3 is the velocity, it was considered worthwhile to simulate the wake observed in test n°3 of the experiment, by adapting the following parameters:
- The flow, which is adjusted in order to obtain the correct velocity upstream of the TEC
- The value of the drag coefficient, as this is different
- The value of the coefficient η8

On the other hand, care is taken to not alter any of the other parameters; that is, the constant viscosity, the area 'A' on which DRAGFO is applied and the position of the TEC.
Velocity being higher, a quick convergence study is conducted. A time-step of 0.1s corresponding to 1000 iterations, a mesh size of 5 cm for the constant viscosity model and 2.5 cm for the k-ε model enable to ensure convergence is achieved.

---

[8] At present, whenever the k-ε model is used, production of k and of ε is systematically taken into account by means of the enhanced KEPSIL routine.

In the case of the k-ε model, the value of the friction coefficient is adjusted, with the help of turbulent kinetic energy data, to Cf=100 (cf. Figure 95).

8.5.3   Simulation results

As discussed previously, the velocity deficit plateau present in the wake cannot be simulated with the simplified model being used. It is possible however to reproduce the correct velocity deficit, the initial slope of velocity recovery and the far velocity.

8.5.4   Constant viscosity model

Velocity measurements taken during the experiment and results of the simulations for different values of drag coefficients are presented in Figure 93. By adjusting the drag coefficient adequately it is effectively possible to numerically reproduce the velocity deficit and the initial slope of recovery to the uniform upstream velocity. The correct order of magnitude is also achieved for the far velocity.
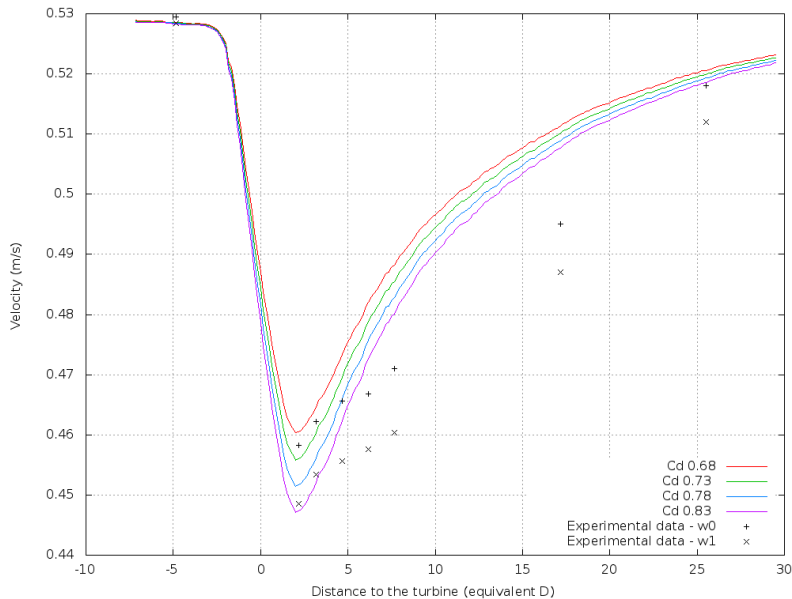

Figure 93: TEC wake for constant viscosity model and different drag coefficient values

After 15D, the error between simulation and measurement is less than 5%.

8.5.5   The k-ε model

Figure 94 is the same graph as above but for the k-ε model. The same observations can also be made. The only difference is that the velocity deficit predicted by the simulations is located slightly further downstream than observed during the experiment.
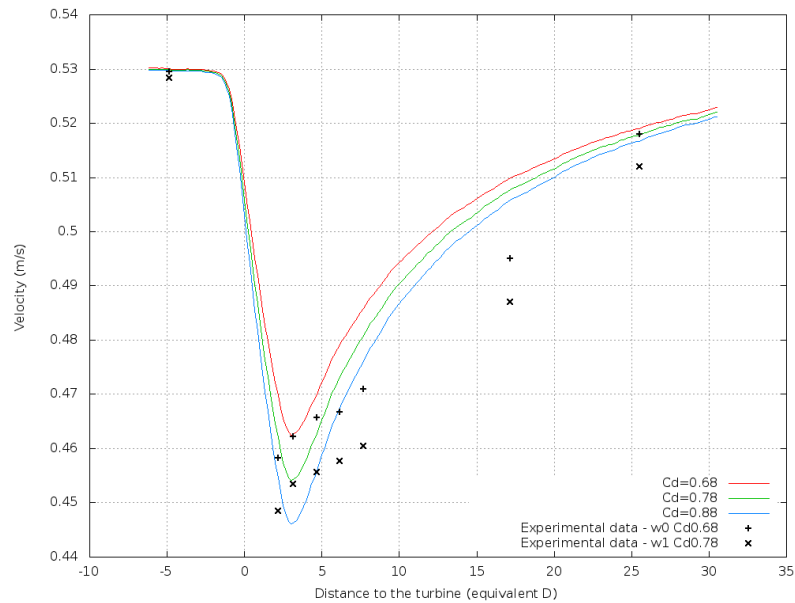
Figure 94: TEC wake for k-ε model and different drag coefficient values

Figure 94 shows that after 15D, the error between simulation and measurement is also less than 5%. Figure 95 illustrates kinetic energy variations along the flume. The measured values of k are higher than in test n°1, which is explained by the increase in velocity between the two tests. The variations in turbulent kinetic energy are reproduced well, with η=0.05.

It is noticeable in the simulations that when the drag coefficient is increased, more turbulent kinetic energy is generated. This is also the case for the experimental results, which is positive for validation of the TEC model in terms of production of k.
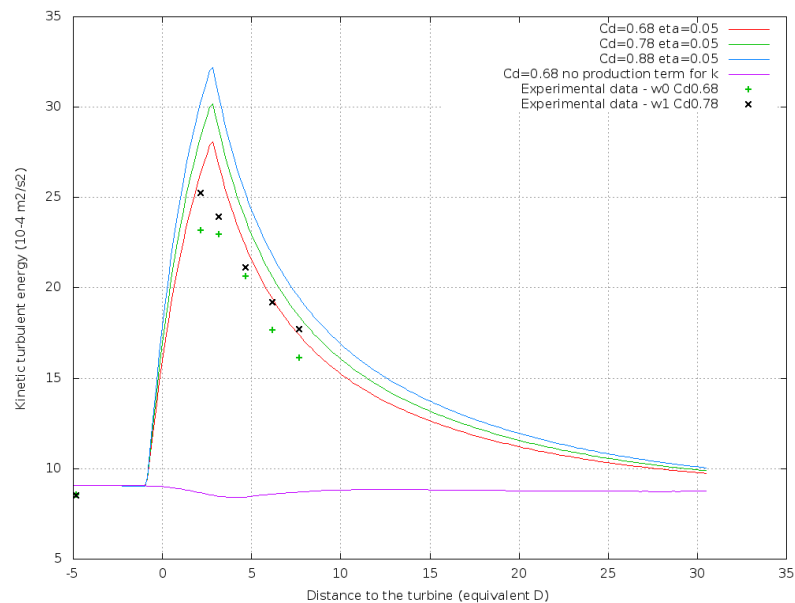

Figure 95: Turbulent kinetic energy along the flume for Cd=0.68 and different values of η. Simulations for the test at high turbulent intensity (test n°2)

8.5.6   Experimental data

Test n°2 is performed with low velocity ($U = 0.2\,m/s$). The high turbulent intensity – 15% rather than the 5% in previous tests, is obtained as a result of the presence of breeze blocks laid out along the flume floor both in front of and behind the TEC.

The effects of this configuration on the wake structure are as follows:

- Recovery to the upstream flow velocity occurs more rapidly due to the greater level of mixing phenomena; the wake is therefore systematically shorter [3].

- The variations of velocity due to the breeze blocks are cumulative with the velocity variations due to the TEC and to friction. Despite being limited to the flume floor, the influence of the breeze blocks on the wake is visible as it is depth-averaged velocity that is considered (cf. black points on Figure 97).

This test is carried out for 5 turbine operating regimes. The power and drag curves differ from previous cases. The measured values are summarised in Table 16.

Operating regime	W1	W2	W3	W4	W5
TSR	1.5	2.5	3.5	4.5	5.5
Ct	0.50	0.53	0.62	0.66	0.55
Cp	0.10	0.26	0.34	0.29	0.15

Table 16: Details of operating regimes studied in test n°2

8.5.7   Numerical aspects

The influence of the breeze blocks being visible on the velocity measurements, it was decided to simulate their presence by modifying the bathymetry through the CORFON routine (cf. Figure 96).
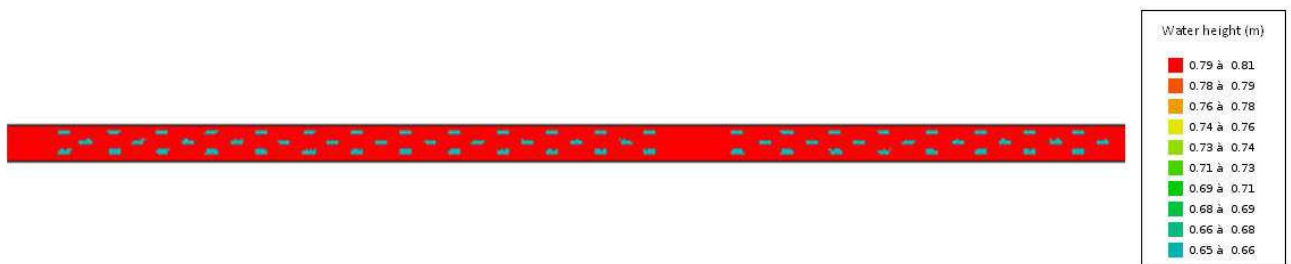

Figure 96: Water height in the flume with addition of bathymetry corresponding to breeze blocks presence

Note that, the breeze blocks should create strong flow effects that cannot be well modelled using Telemac2D.

8.5.8   Simulation results

A quick convergence study is performed. For the k-ε model, a small time-step is necessary because of the significant variations induced by the bathymetry.
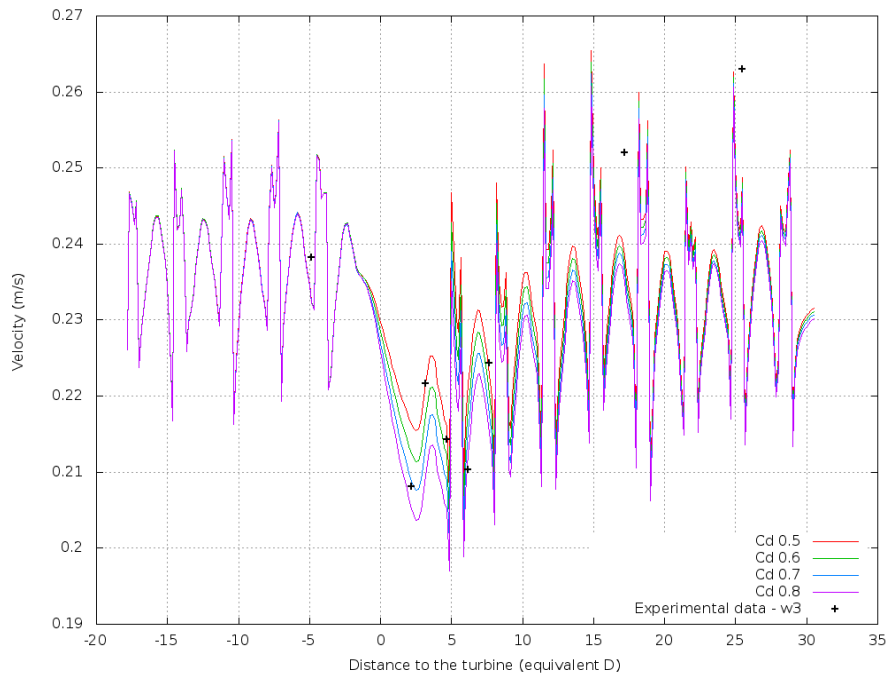
Figure 97: Vertically-averaged velocity along turbine axis (m/s), for constant viscosity model, different values of Cd and a TSR of 3.5

Figure 97 presents simulation results for the constant viscosity model and different values of the drag coefficient. The black points correspond to experimental results for a given operating regime (TSR=3.5). The order of magnitude of the velocity deficit is roughly reproduced (between -5D and +5D). The simulation results demonstrate that wake velocity variations observed during the experiment are clearly due to the breeze block presence. However, no conclusion can be made as to the best Cd value since the velocity variations due to the breeze blocks are too large in comparison to those caused by the presence of the TEC.

The same type of result is obtained with the k-ε model. The study is not carried further however as the turbulence being strong, the phenomena involved are clearly three-dimensional and thus poorly reproduced with Telemac-2D.

8.6   Code of the subroutine "DRAGFO"

Only available to PerAWaT participants.

8.7   Code of the subroutine "SOURCE"

Only available to PerAWaT participants.